universität wien

Microbial C_1-Fixation

Dr. Simon K.-M. R. Rittmann

Global carbon cycle

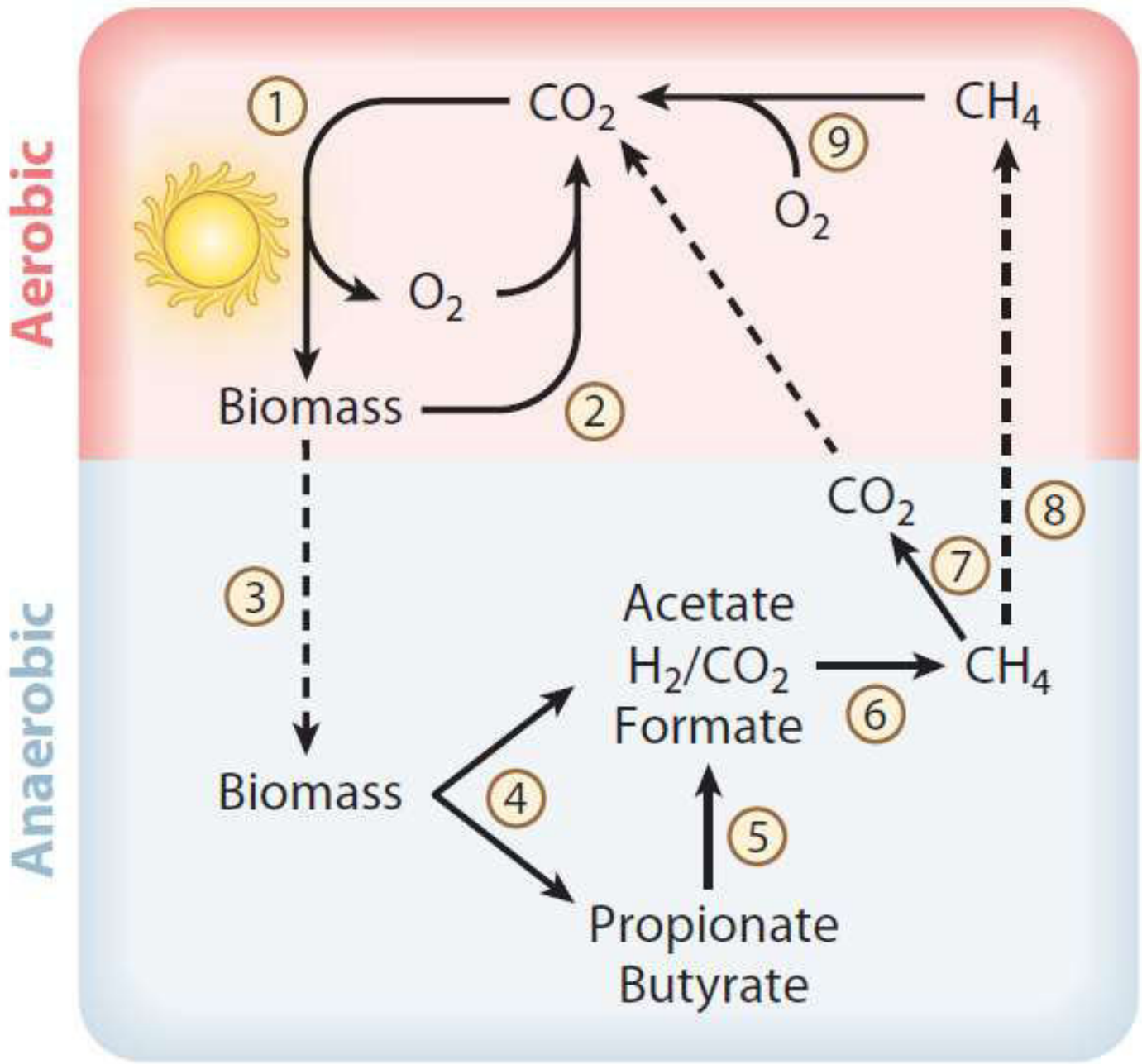

The global carbon cycle. Aerobic O_2-requiring conversions are shown in the top panel and anaerobic conversions in the bottom panel. **Step 1**: Fixation of CO_2 into organic matter. **Step 2**: Decomposition of organic matter to CO_2 by O_2-requiring microbes. **Step 3**: Deposition of organic matter into anaerobic environments. **Step 4**: Decomposition of complex biomass by fermentative microbes. **Step 5**: Conversion of volatile fatty acids by obligate H_2- and formate-producing syntrophic acetogens. **Step 6**: H_2- and formate-dependent reduction of CO_2 to CH_4 and conversion of the methyl group of acetate to CH_4 by methanogens. **Step 7**: Anaerobic oxidation of CH_4. **Step 8**: Diffusion of CH_4 into aerobic zones. **Step 9**: Aerobic oxidation of CH_4 by O_2-requiring methylotrophs.

Ferry, 2010

C_1 species

- (Dissolved) carbon dioxide (CO_2),

  also in the form of bicarbonate (HCO_3^-)
- Carbon monoxide (CO)
- Formate ($HCOO^-$)
- Methane (CH_4)
- Methanol (CH_3OH)
- Mono-, di-, trimethylamine
- Methanethiole (CH_3SH)

CO_2 equilibrium in aqueous solution

$$CO_2(aq) + H_2O \underset{k_{-1}}{\overset{k_1}{\rightleftharpoons}} H_2CO_3$$

$$CO_2(aq) + OH^- \underset{k_{-2}}{\overset{k_2}{\rightleftharpoons}} HCO_3^-$$

$$CO_3^{2-} + H^+ \overset{K_{a1}}{\rightleftharpoons} HCO_3^-$$

$$HCO_3^- + H^+ \overset{K_{a2}}{\rightleftharpoons} H_2CO_3$$

$$OH^- + H^+ \overset{K_W}{\rightleftharpoons} H_2O$$

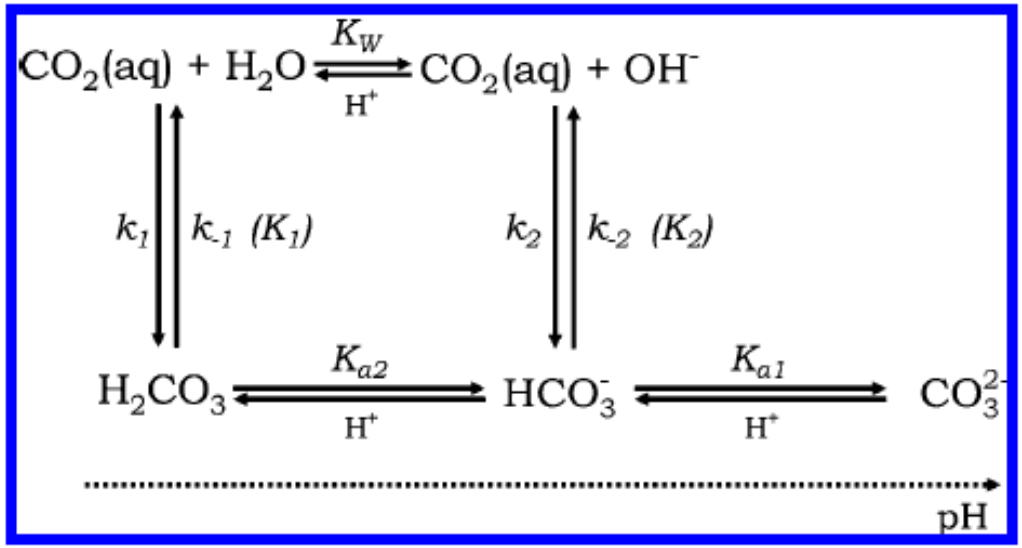

Figure 1. Reaction scheme of CO_2(aq) in aqueous solution.

Wang et al., 2010

CO_2 fixation pathways

Currently six CO_2 fixation pathways are known:

- Calvin–Benson–Bassham cycle
- reductive tricarboxylic acid cycle
- reductive acetyl-CoA pathway – Wood-Ljungdahl pathway
- 3-hydroxypropionate bicycle
- 3-hydroxypropionate/4-hydroxybutyrate cycle
- dicarboxylate/4-hydroxybutyrate cycle
- (reductive hexulose-phosphate pathway) *proposed*
- [reductive glycine pathway] *metagenome*
- [Crotonyl-CoA/ethylmalonyl-CoA/hydroxybutyryl-CoA cycle] *synthetic*

Calvin–Benson–Bassham cycle

- In the **Calvin–Benson–Bassham** cycle, which was discovered about 50 years ago, CO_2 reacts with the five-carbon sugar ribulose 1,5-bisphosphate to yield two carboxylic acids, 3-phosphoglycerate, from which the sugar is regenerated.
- This cycle operates in plants, algae, cyanobacteria, some aerobic or facultative anaerobic Proteobacteria, CO-oxidizing mycobacteria and representatives of the genera *Sulfobacillus* (iron- and sulphur-oxidizing Firmicutes) and *Oscillochloris* (green sulphur bacteria).
- An autotrophic symbiotic cyanobacterium conferred the CO_2 fixation machinery on a eukaryotic cell giving rise to the chloroplasts of plant cells. The presence of the **key enzyme, ribulose 1,5-bisphosphate carboxylase–oxygenase (RubisCO)**, is often considered to be synonymous with autotrophy.
- Phylogenetic analysis and general considerations denote the Calvin cycle as a late innovation.

Berg et al., 2010

universität wien

Calvin–Benson–Bassham cycle

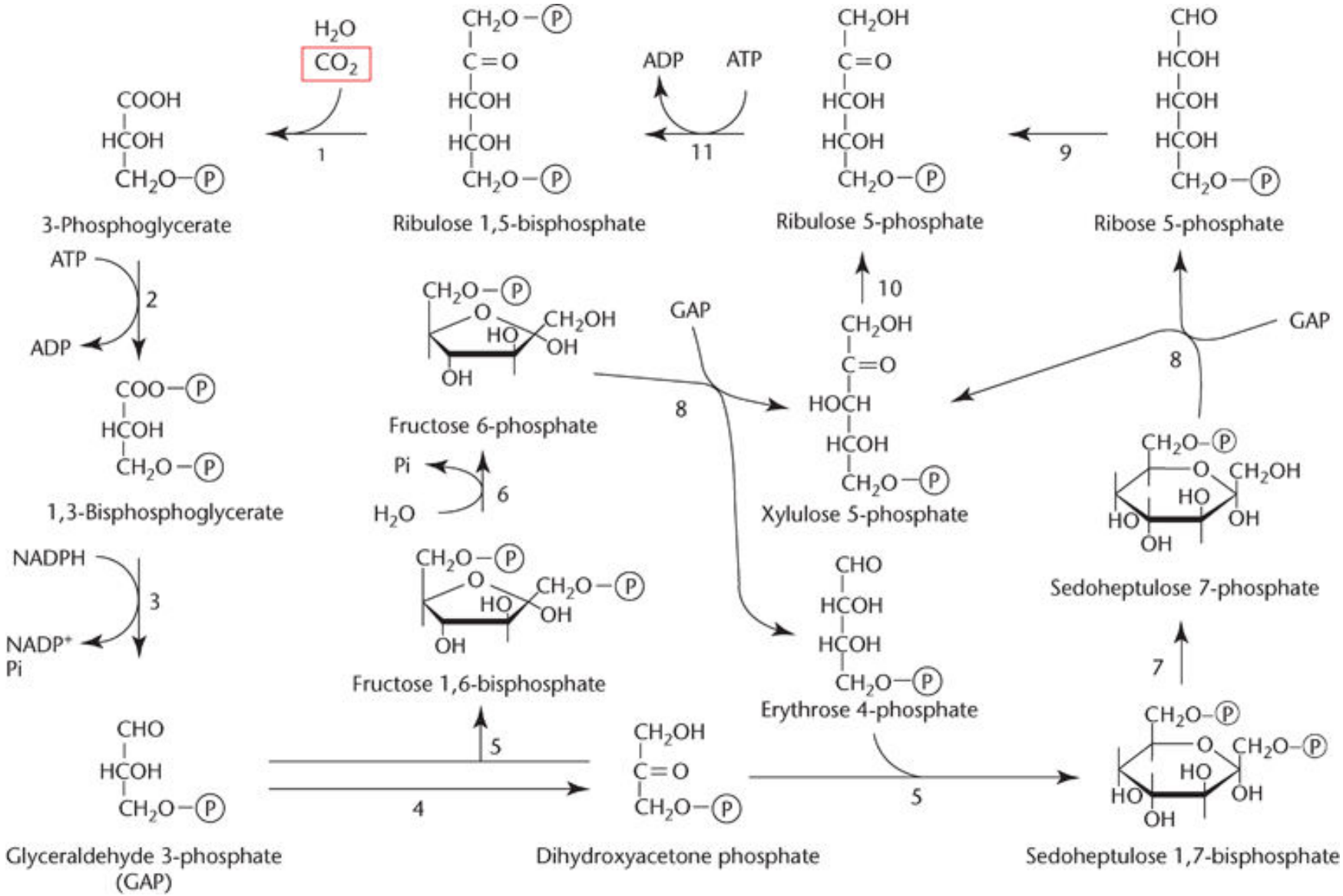

Diagram illustrating the reactions of the Calvin–Benson–Bassham cycle. The corresponding enzymes are: 1: ribulose-1,5-bisphosphate carboxylase/oxygenase, 2: phosphoglycerate kinase, 3: glyceraldehyde-3-phosphate dehydrogenase, 4: triose phosphate isomerase, 5: fructose-bisphosphate aldolase, 6: fructose-1,6-bisphosphatase, 7: sedoheptulose bisphosphatase, 8: transketolase, 9: ribose-5-phosphate isomerase, 10: ribulose-5-phosphate 3-epimerase and 11: phosphoribulokinase. The directions of the arrows represent the direction of the pathway, and do not indicate that the enzyme reactions are irreversible.

Sato & Atomi , 2010

reductive tricarboxylic acid cycle

- In 1966, Arnon, Buchanan and co-workers proposed another autotrophic cycle for the green sulphur bacterium *Chlorobium limicola*, the **reductive citric acid cycle** (also known as the **Arnon–Buchanan cycle**).
- This cycle is less energy-consuming than the Calvin cycle, involves enzymes that are sensitive to oxygen and is therefore found only in anaerobes or in aerobes growing at low oxygen tensions.
- These include some Proteobacteria, green sulphur bacteria and microaerophilic bacteria of the early bacterial phylum Aquificae.
- Initially, the reductive citric acid cycle was also proposed to operate in certain archaea (notably *Thermoproteus neutrophilus*), but recent findings refute this proposal.

Berg et al., 2010

reductive tricarboxylic acid cycle

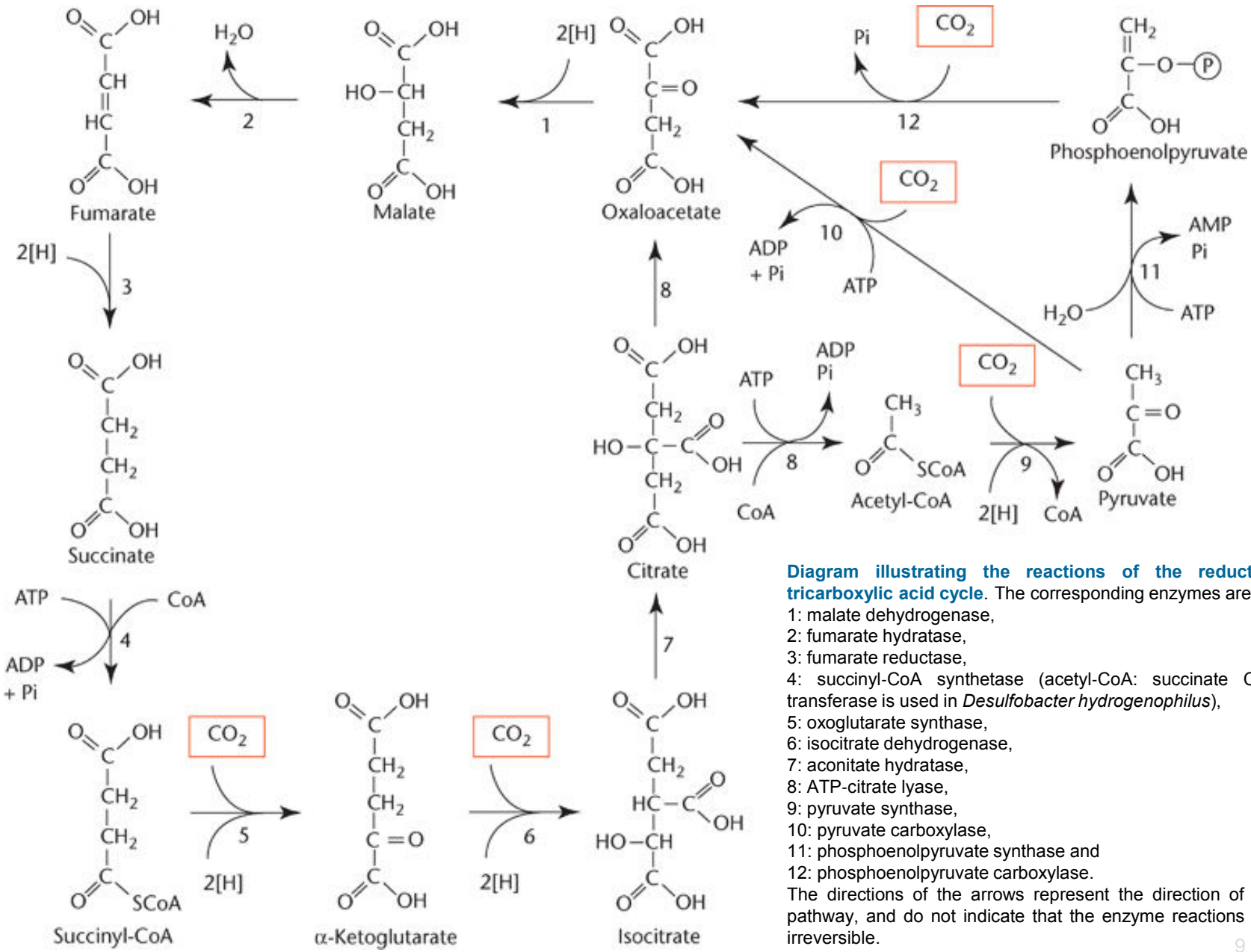

Diagram illustrating the reactions of the reductive tricarboxylic acid cycle. The corresponding enzymes are:
1: malate dehydrogenase,
2: fumarate hydratase,
3: fumarate reductase,
4: succinyl-CoA synthetase (acetyl-CoA: succinate CoA transferase is used in *Desulfobacter hydrogenophilus*),
5: oxoglutarate synthase,
6: isocitrate dehydrogenase,
7: aconitate hydratase,
8: ATP-citrate lyase,
9: pyruvate synthase,
10: pyruvate carboxylase,
11: phosphoenolpyruvate synthase and
12: phosphoenolpyruvate carboxylase.
The directions of the arrows represent the direction of the pathway, and do not indicate that the enzyme reactions are irreversible.

Sato & Atomi , 2010

reductive acetyl-CoA pathway

- At the start of the 1980s, a third autotrophic pathway was found in certain Gram-positive bacteria and methane-forming archaea, the reductive acetyl-coenzyme A (acetyl-CoA) or Wood–Ljungdahl pathway.
- In these strict anaerobic organisms that now also include some Proteobacteria, Planctomycetes, spirochaetes and Euryarchaeota, one CO_2 molecule is reduced to CO and one to a methyl group (bound to a carrier); subsequently, acetyl-CoA is synthesized from CO and the methyl group.
- Although this pathway is the most energetically favourable autotrophic carbon fixation pathway, it is restricted to strictly anaerobic organisms.
- Use of the acetyl-CoA pathway as an autotrophic, terminal electron-accepting process is the hallmark of acetogens. Other obligate anaerobic bacteriological groups, including methanogens and sulfate-reducing bacteria, also utilize the acetyl-CoA pathway for either catabolic or anabolic purposes.

Berg et al., 2010; Drake et al., 1997

reductive acetyl-CoA pathway

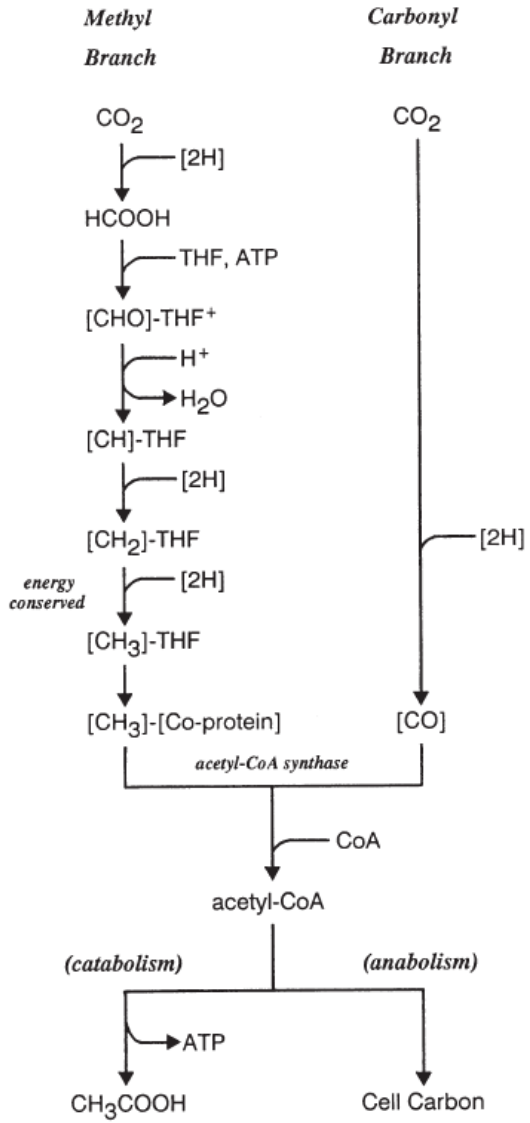

During the reductive synthesis of acetate via the acetyl-CoA pathway, six reducing equivalents are required for the fixation of CO_2 to the methyl level, and two reducing equivalents are required for the fixation of CO_2 to the carbonyl level.

The overall conversion of substrate to product can be divided into oxidative and reductive processes. For example, the glycolytic utilization of glucose yields eight reducing equivalents per glucose consumed that are routed towards the reductive synthesis of acetate.

oxidation: $C_6H_{12}O_6 + 2\ H_2O \rightarrow 2\ CH_3COOH + 2\ CO_2 + 8\ H$

reduction: $2\ CO_2 + 8\ H \rightarrow CH_3COOH + 2\ H_2O$

net reaction: $C_6H_{12}O_6 \rightarrow 3\ CH_3COOH$

Fig. 1. Pathway for the autotrophic synthesis of acetate and biomass via the acetyl-CoA 'Wood/Ljungdahl' pathway (modified from [12]). Abbreviations: THF: tetrahydrofolate; [Co-protein]: corrinoid protein. Brackets indicate that a particular C_1 unit is bound to a cofactor or an enyzme.

Drake et al., 1997

reductive acetyl-CoA pathway

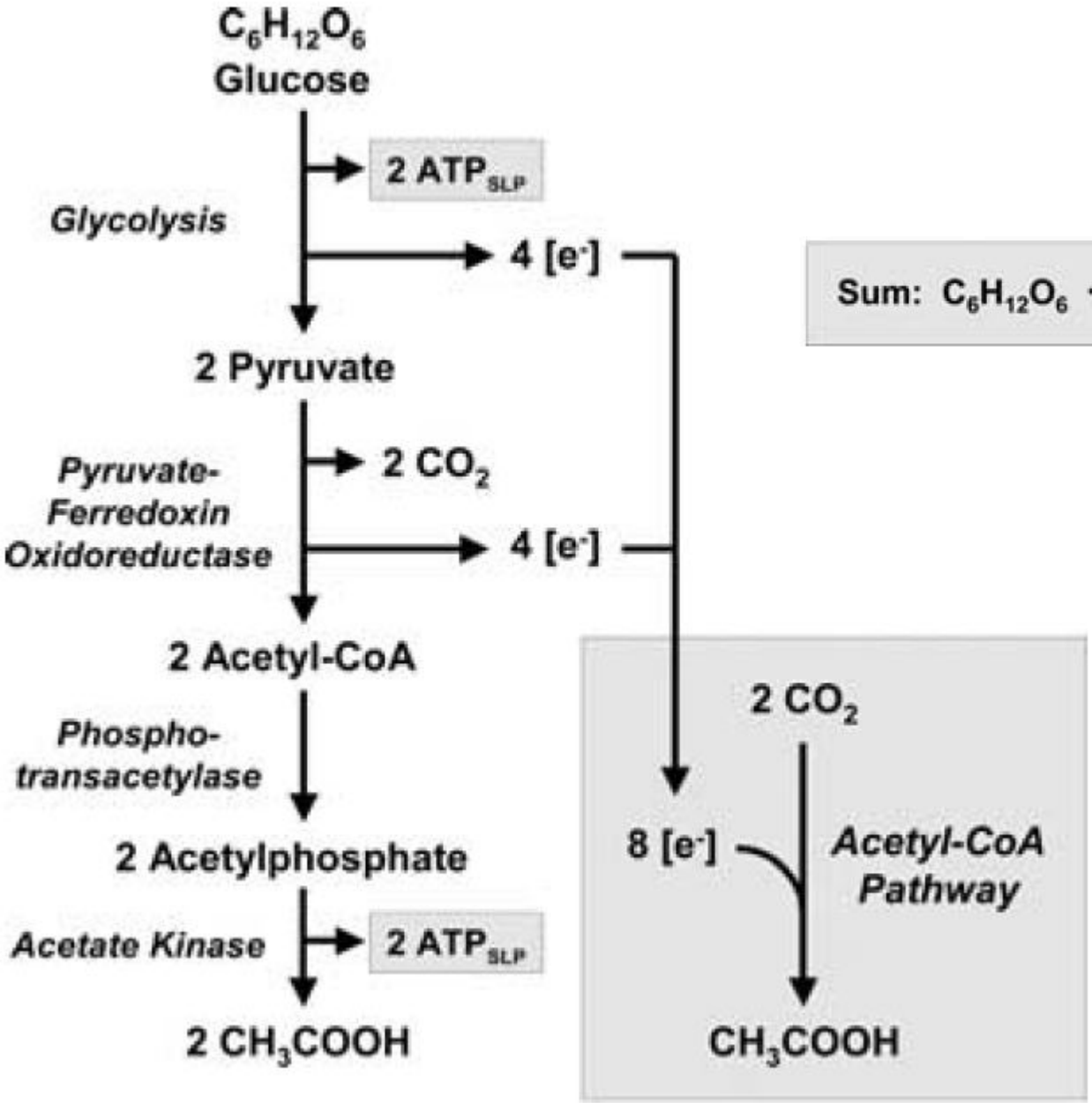

Sum: $C_6H_{12}O_6 \rightarrow 3\ CH_3COOH + 4\ ATP_{SLP}$

Homoacetogenic conversion of glucose to acetate.
The two molecules of CO_2 that are reduced to acetate in the acetyl-CoA pathway can be derived from exogenous CO_2 rather than the CO_2 that is produced via the decarboxylation of pyruvate (see text). ABBREVIATIONS: ATPSLP = ATP that is produced by substrate-level phosphorylation; [e−], reducing equivalent.

Drake et al., 2008

reductive acetyl-CoA pathway

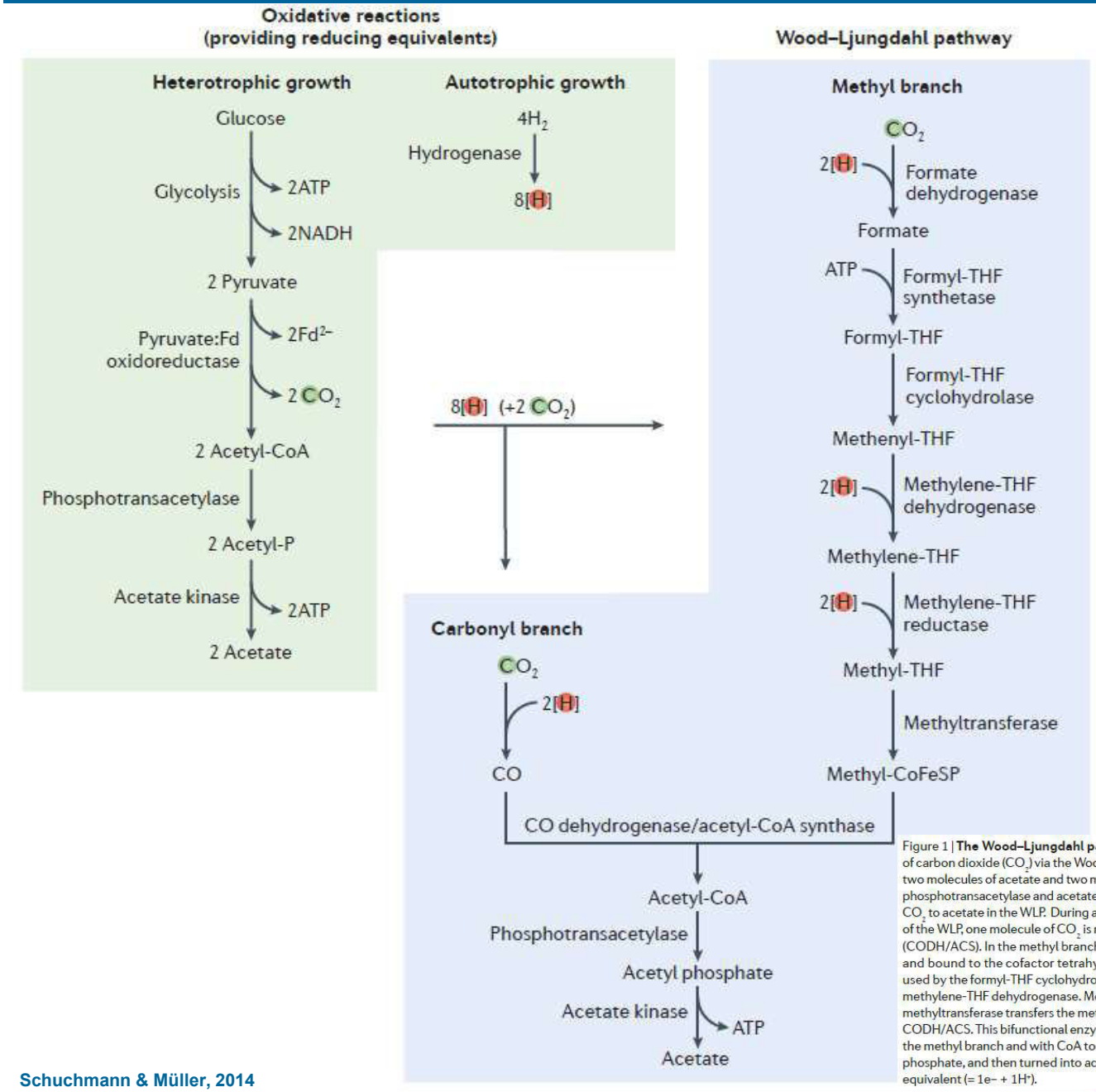

Figure 1 | **The Wood–Ljungdahl pathway of acetogenesis.** Acetogenic bacteria produce acetate from two molecules of carbon dioxide (CO_2) via the Wood–Ljungdahl pathway (WLP). During heterotrophic acetogenesis, glucose is oxidized to two molecules of acetate and two molecules of CO_2 via a combination of glycolysis, pyruvate:ferredoxin oxidoreductase, phosphotransacetylase and acetate kinase. The reducing equivalents are reoxidized by the reduction of the two molecules of CO_2 to acetate in the WLP. During autotrophic acetogenesis, acetate is formed from $4H_2$ and $2CO_2$. In the carbonyl branch of the WLP, one molecule of CO_2 is reduced to CO via the carbon monoxide (CO) dehydrogenase/acetyl-CoA synthase (CODH/ACS). In the methyl branch of the WLP, one molecule of CO_2 is reduced to formate via a formate dehydrogenase and bound to the cofactor tetrahydrofolate (THF), yielding formyl-THF via the formyl-THF synthetase. Formyl-THF is used by the formyl-THF cyclohydrolase to generate methenyl-THF, which in turn is reduced to methylene-THF via the methylene-THF dehydrogenase. Methylene-THF is reduced to methyl-THF via the methylene-THF reductase. Finally, a methyltransferase transfers the methyl group from methyl-THF via a corrinoid iron-sulphur protein (CoFeSP) to the CODH/ACS. This bifunctional enzyme reduces CO_2 to CO in the carbonyl branch and fuses it with the methyl group from the methyl branch and with CoA to form acetyl-CoA, which is then used by a phosphotransacetylase to generate acetyl phosphate, and then turned into acetate via an acetate kinase. Fd, ferredoxin; Fd^{2-}, reduced ferredoxin; [H], reducing equivalent (= $1e^- + 1H^+$).

Schuchmann & Müller, 2014

Excursion: flavin-based electron bifuraction

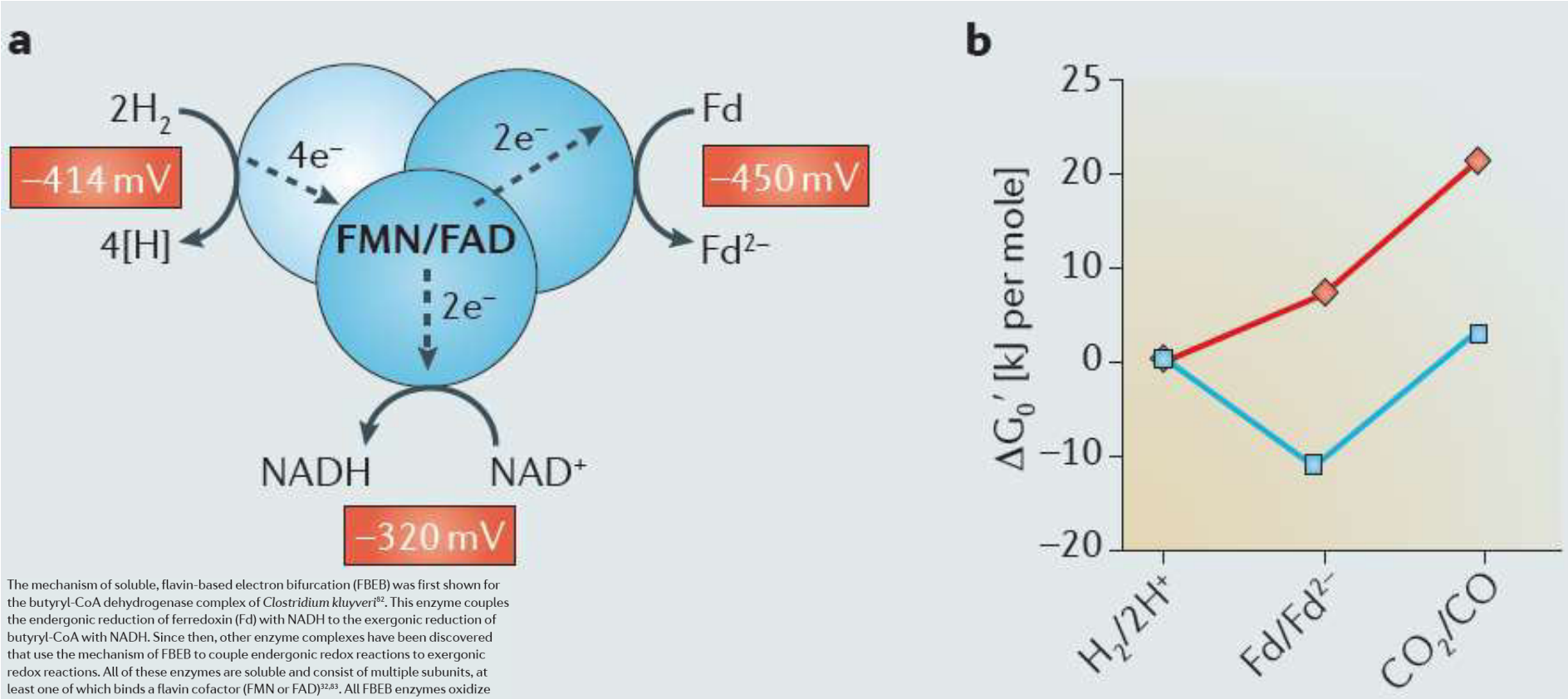

The mechanism of soluble, flavin-based electron bifurcation (FBEB) was first shown for the butyryl-CoA dehydrogenase complex of *Clostridium kluyveri*[82]. This enzyme couples the endergonic reduction of ferredoxin (Fd) with NADH to the exergonic reduction of butyryl-CoA with NADH. Since then, other enzyme complexes have been discovered that use the mechanism of FBEB to couple endergonic redox reactions to exergonic redox reactions. All of these enzymes are soluble and consist of multiple subunits, at least one of which binds a flavin cofactor (FMN or FAD)[32,83]. All FBEB enzymes oxidize one electron donor and deliver the electrons simultaneously and tightly coupled to two different electron acceptors. The reduction of one acceptor is always exergonic, which drives the endergonic reduction of the second acceptor. In the case of the acetogenic bifurcating hydrogenases, the reduction of NAD drives the reduction of ferredoxin (see the figure, part **a**). FBEB is essential to drive the overall electron transfer from H_2 ($[H^+/H_2]$ $E_0' = -414$ mV) to the CO_2/CO couple (standard redox potential (E_0') = −520 mV). Under physiological conditions, the redox potential of the CO_2/CO couple might be more positive[80]. As the exact redox potential of the ferredoxin is not known, we use the E_0' value ($[Fd/Fd^{2-}]$ $E_0' = -450$ mV) for simplicity in our discussion (BOX 1), as the redox potential of the electron donor H_2 is shifted under physiological conditions to more positive values at comparable magnitudes, thus leaving the same energetic problems. In both cases, it is obvious that the cells must have coupling mechanisms to catalyse the endergonic reaction of ferredoxin reduction with H_2 as the electron donor. Part **b** of the figure shows the energy profile of the electron transfer first from hydrogen to ferredoxin, which is catalysed by the hydrogenase ($\Delta G_0' = +6.9$ kJ per mole), followed by the electron transfer from ferredoxin to CO_2, which is reduced to CO, catalysed by the CO dehydrogenase/acetyl-CoA synthase (CODH/ACS) ($\Delta G_0' = +13.5$ kJ per mole). Without FBEB, the sum of both electron-transfer reactions is highly endergonic (red line, $\Delta G_0' = +20.4$ kJ per mole). By coupling the hydrogen oxidation to NAD reduction with FBEB, the reaction sequence is close to the equilibrium (blue line, $\Delta G_0' = +2.3$ kJ per mole; $\Delta G_0'$ of electron transfer from H_2 to ferredoxin and NAD = −11.2 kJ per mole and $\Delta G_0'$ of electron transfer from ferredoxin to CO_2/CO = +13.5 kJ per mole).

reductive acetyl-CoA pathway

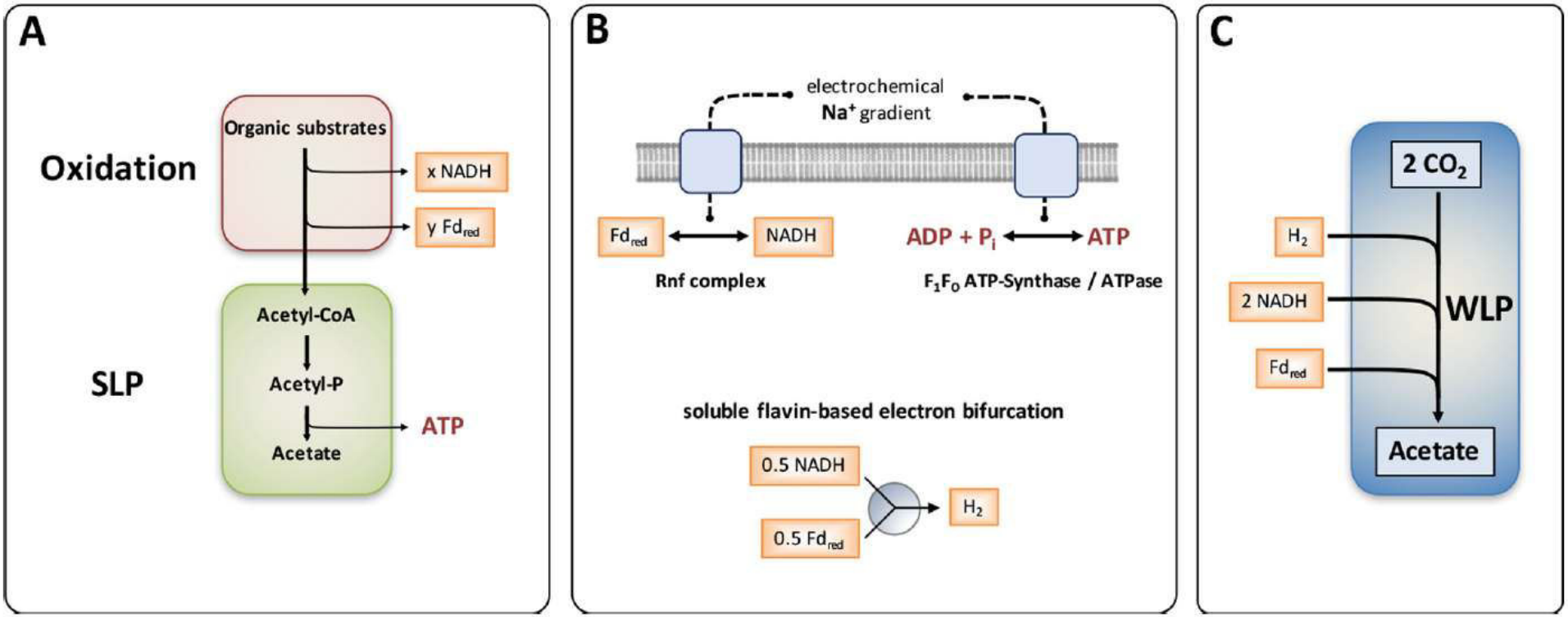

FIG 2 The heterotrophic metabolism of *A. woodii*, the model organism of the Rnf-dependent acetogens, is composed of well-defined modules. (A) Most heterotrophic substrates (e.g., glucose, lactate, ethanol) are oxidized to the level of acetyl-CoA by transferring the electrons to NAD^+ and ferredoxin. Acetyl-CoA is converted to acetate, generating 1 ATP by SLP. (B) The module responsible for redox balancing between modules A and C. This is achieved either by a soluble hydrogenase using flavin-based electron bifurcation or by a membrane-bound Rnf complex. The latter is coupled to ATP synthesis via an electrochemical sodium ion gradient and a Na^+-dependent F_1F_O ATP synthase/ATPase. Note that some acetogens have Ech instead of Rnf, and in both, Ech- and Rnf-containing species, the coupling ion may be Na^+ or H^+. (C) The WLP functions as an electron sink to reoxidize the electron carriers by reducing CO_2 to acetate. Fd_{red}, reduced ferredoxin (reduced by 2 electrons).

Schuchmann & Müller, 2016

reductive acetyl-CoA pathway

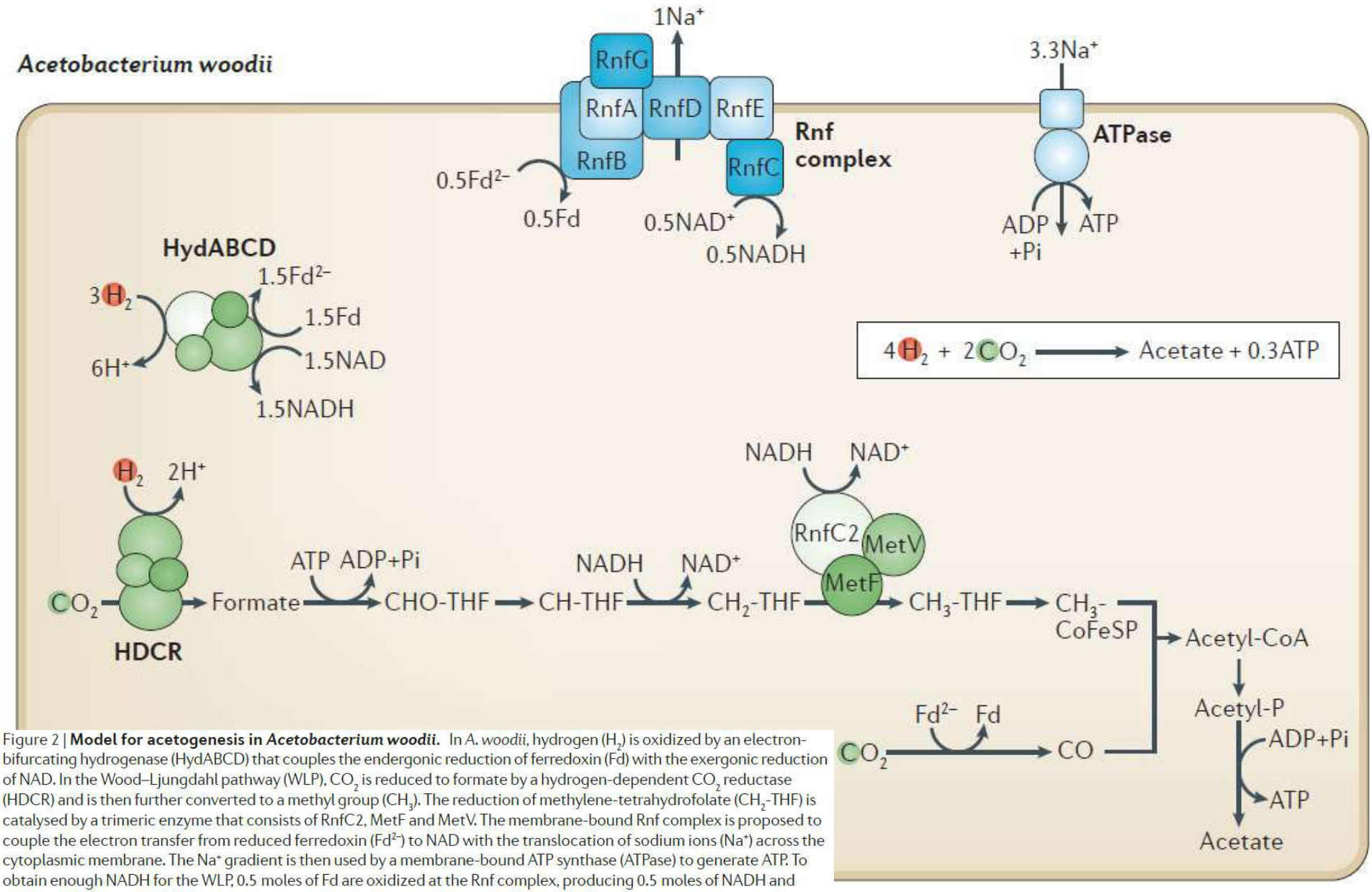

Figure 2 | **Model for acetogenesis in *Acetobacterium woodii*.** In *A. woodii*, hydrogen (H_2) is oxidized by an electron-bifurcating hydrogenase (HydABCD) that couples the endergonic reduction of ferredoxin (Fd) with the exergonic reduction of NAD. In the Wood–Ljungdahl pathway (WLP), CO_2 is reduced to formate by a hydrogen-dependent CO_2 reductase (HDCR) and is then further converted to a methyl group (CH_3). The reduction of methylene-tetrahydrofolate (CH_2-THF) is catalysed by a trimeric enzyme that consists of RnfC2, MetF and MetV. The membrane-bound Rnf complex is proposed to couple the electron transfer from reduced ferredoxin (Fd^{2-}) to NAD with the translocation of sodium ions (Na^+) across the cytoplasmic membrane. The Na^+ gradient is then used by a membrane-bound ATP synthase (ATPase) to generate ATP. To obtain enough NADH for the WLP, 0.5 moles of Fd are oxidized at the Rnf complex, producing 0.5 moles of NADH and translocating 1 mole of Na^+, which is enough for the phosphorylation of 0.3 moles of ADP by the ATP synthase. CH-THF, methenyl-THF; CH_3-THF, methyl-THF; CHO-THF, formyl-THF; CoFeSP, corrinoid iron–sulphur protein, Pi, inorganic phosphate.

Schuchmann & Müller, 2014

universität wien

reductive acetyl-CoA pathway

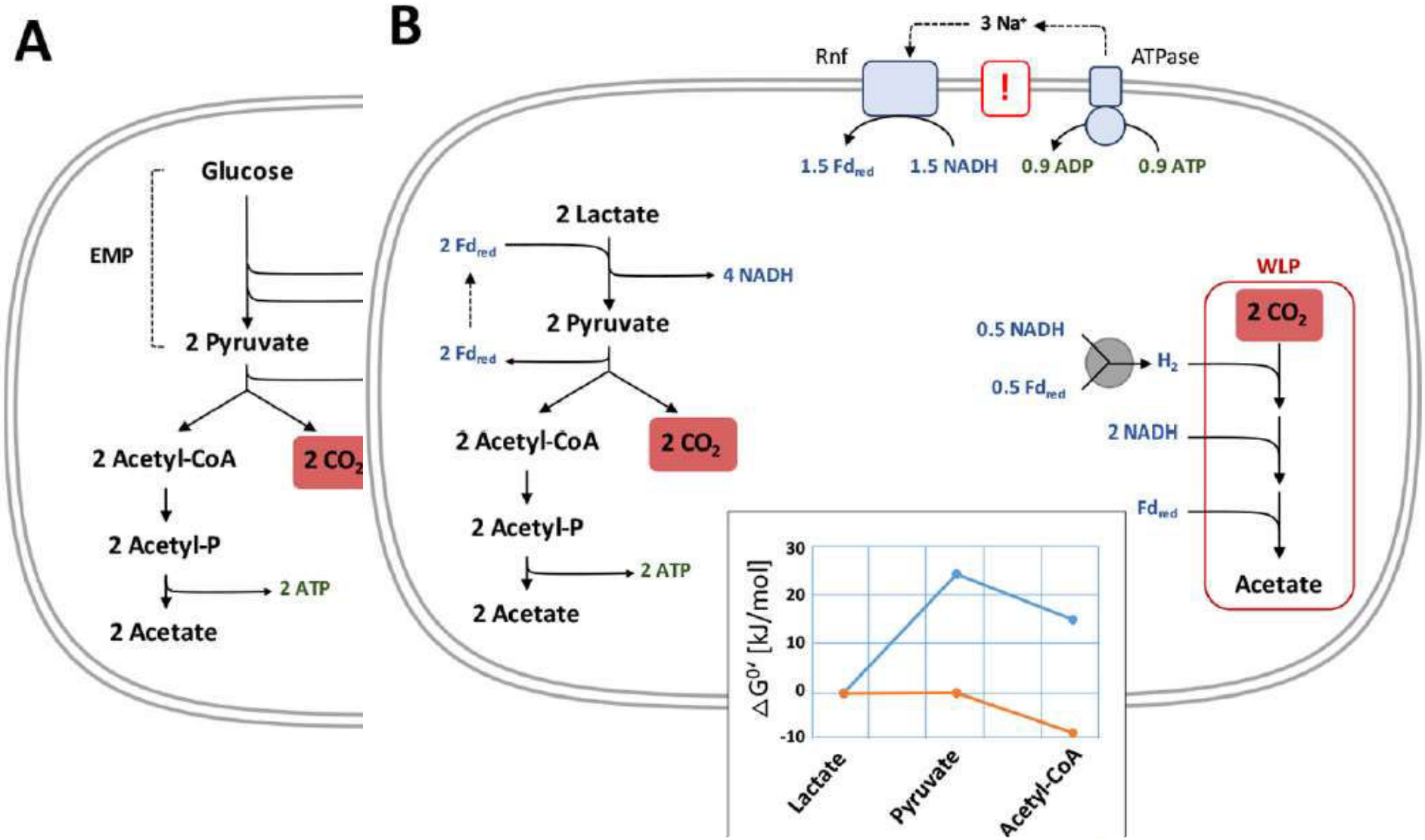

FIG 3 Carbohydrate (A) and lactate (B) metabolism of *A. woodii*. The inset in panel B represents the energetics ($\Delta G^{0'}$ profile for the conversion of the corresponding substrates to the products/intermediates) of the oxidation of lactate to acetyl-CoA not coupled (blue) or coupled (orange) to flavin-based electron bifurcation. Blue line, lactate is oxidized with NAD^+ as the electron acceptor, followed by ferredoxin-dependent oxidation of pyruvate. Orange line, lactate is oxidized with NAD^+ as the electron acceptor, coupled to NAD^+ reduction by reduced ferredoxin by electron bifurcation, and pyruvate is oxidized with ferredoxin as the electron acceptor. EMP, Embden-Meyerhof-Parnas pathway (glycolysis); Fd_{red}, reduced ferredoxin (reduced by 2 electrons).

reductive acetyl-CoA pathway

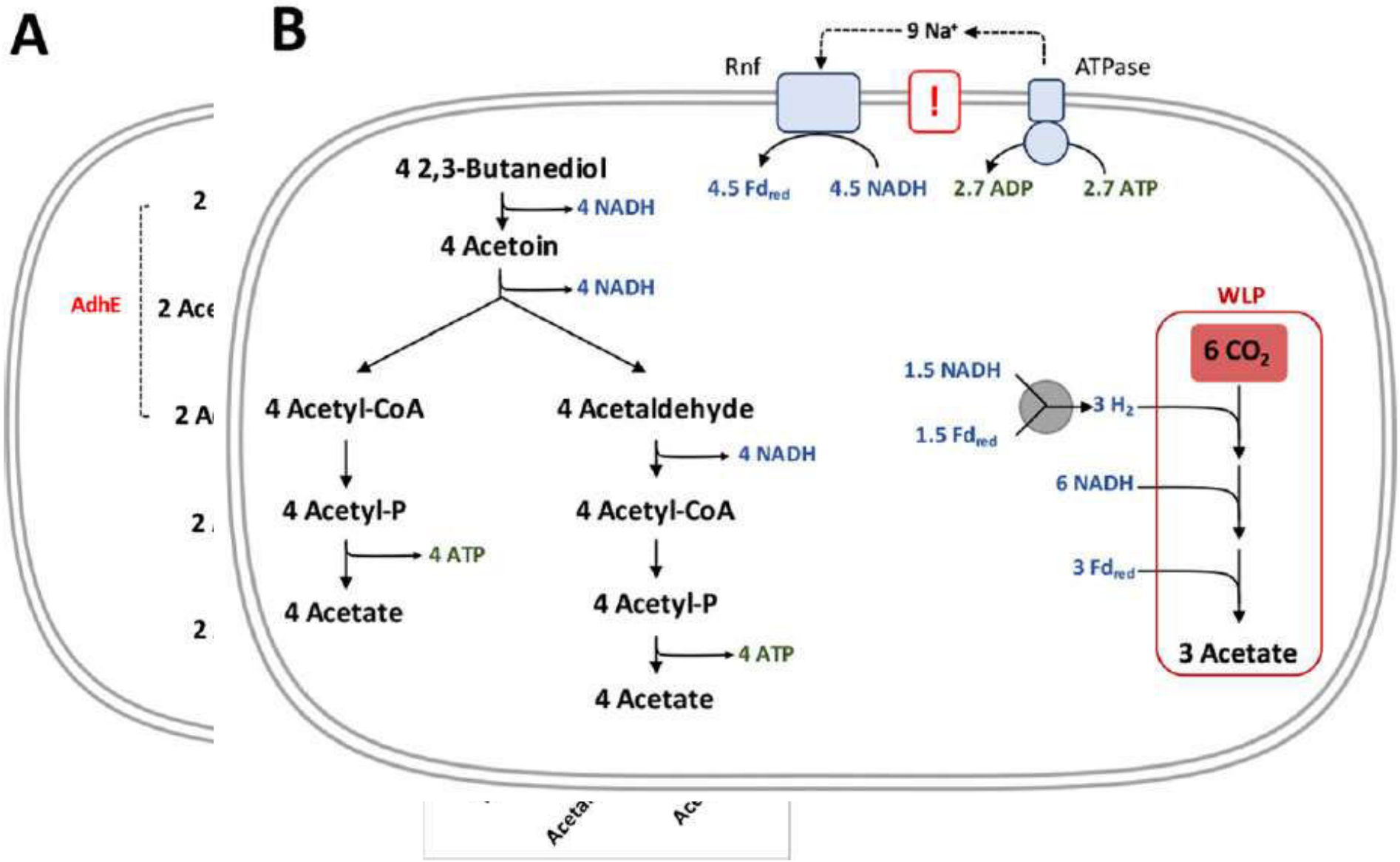

FIG 4 Ethanol (A) and 2,3-butanediol (B) metabolism of *A. woodii*. The inset in panel A represents the energetics ($\Delta G^{0'}$ profile for the conversion of the corresponding substrates to the products/intermediates) of the oxidation of ethanol to acetyl-CoA. Both ethanol and acetaldehyde are oxidized with NAD^+ as the electron acceptor. AdhE, bifunctional acetaldehyde/ethanol dehydrogenase; Fd_{red}, reduced ferredoxin (reduced by 2 electrons).

reductive acetyl-CoA pathway

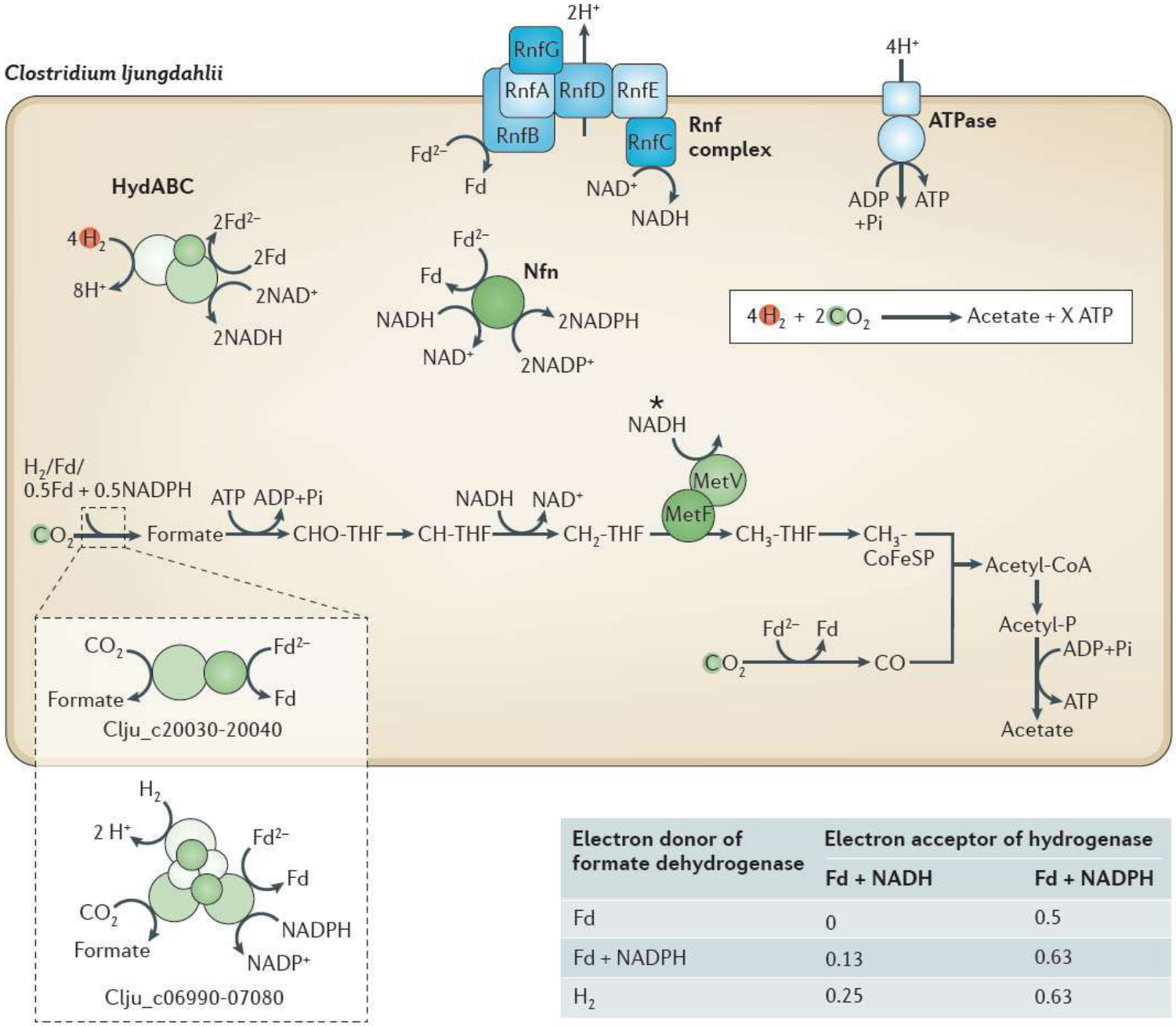

Electron donor of formate dehydrogenase	Electron acceptor of hydrogenase	
	Fd + NADH	Fd + NADPH
Fd	0	0.5
Fd + NADPH	0.13	0.63
H_2	0.25	0.63

Figure 3 | **Model for acetogenesis in *Clostridium ljungdahlii*.** *C. ljungdahlii* oxidizes hydrogen either by an electron-bifurcating hydrogenase (HydABC), as described for *Acetobacterium woodii*, or by an enzyme complex of hydrogenase and formate dehydrogenase (Clju_c06990–07080), resulting in the reduction of ferredoxin (Fd) and NAD or NADP (the model of the enzyme represents all possible electron donors and acceptors, but the physiological electron transfer is unknown). The electron-bifurcating enzyme Nfn catalyses the interconversion of Fd, NADH and NADPH. In the Wood–Ljungdahl pathway (WLP), CO_2 is reduced to formate, with electrons provided either by Fd (Clju_c20030–20040) or either by hydrogen or by Fd and NADPH (Clju_c06990–07080). Reduction of methylene-THF (CH_2-THF) is catalysed by a dimeric enzyme (MetF and MetV). The membrane-bound Rnf complex in *C. ljungdahlii* is proposed to couple the electron transfer from reduced ferredoxin (Fd^{2-}) to NAD with the translocation of protons (H^+) across the cytoplasmic membrane. The H^+ gradient is then used by a membrane-bound ATP synthase (ATPase) to generate ATP (assuming four H^+ to phosphorylate one ADP). In the different proposed models for acetogenesis in *C. ljungdahlii*, the total amount of conserved energy in the form of ATP is variable owing to differences in the enzymes that are proposed to be involved. The table provides the ATP gain per mole of acetate, depending on the different enzyme combinations (mole ATP/mole acetate). *The electron donor for MetFV is not known but is assumed to be equivalent to the redox potential range of NADH. CH-THF, methenyl-THF; CH_3-THF, methyl-THF; CHO-THF, formyl-THF; CoFeSP, corrinoid iron–sulphur protein, Pi, inorganic phosphate.

Schuchmann & Müller, 2014

reductive acetyl-CoA pathway

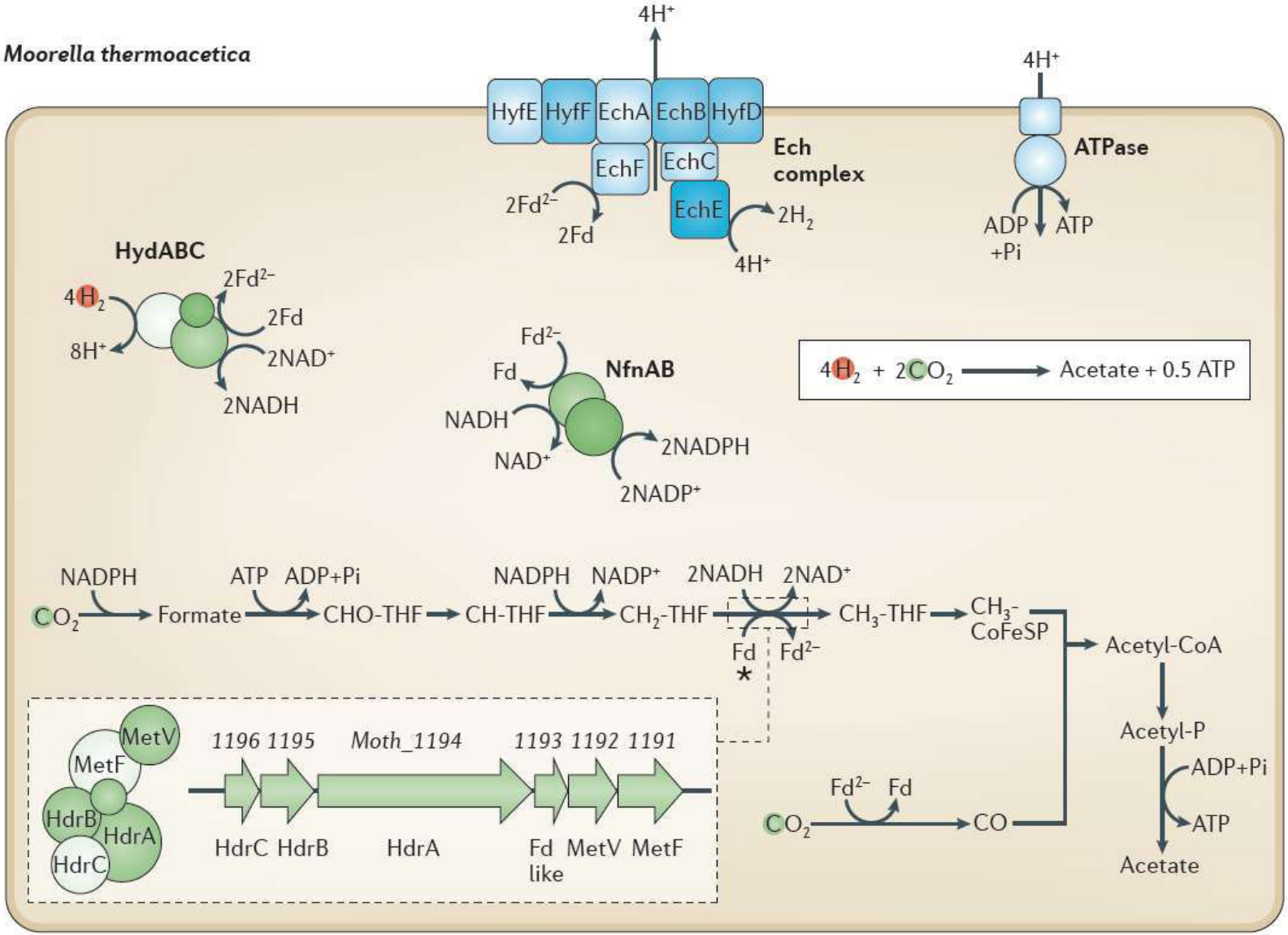

Figure 4 | **Model for acetogenesis in *Moorella thermoacetica*.** In *M. thermoacetica*, hydrogen (H_2) is oxidized by an electron-bifurcating hydrogenase, HydABC, which reduces ferredoxin (Fd) and NAD. NADP is reduced by an electron-bifurcating transhydrogenase, NfnAB, with Fd and NADH as the electron donor. These two enzymes in combination catalyse the same reaction as the NADP-dependent hydrogenase alone (Moth_1883–1885) (not shown). In the Wood–Ljungdahl pathway (WLP), methylene-THF (CH_2-THF) is reduced by an electron-bifurcating enzyme that couples the exergonic electron transfer from NADH to CH_2-THF with the reduction of an energetic equivalent of ferredoxin (Fd). The genetic organization for this enzyme is shown in the inset. The proposed enzyme complex is composed of the subunits MetF and MetV of CH_2-THF reductases and subunits that are similar to the electron-bifurcating Hdr complex of *Methanothermobacter marburgensis*. To balance the electron flow, two molecules of Fd need to be oxidized at the Ech complex that translocates protons (H^+) across the cytoplasmic membrane. The H^+ gradient is then used by a membrane-bound ATP synthase (ATPase) to generate ATP. *The second electron acceptor for the CH_2-THF reductase is not known but for simplicity is assumed to be an energetic equivalent of Fd. CH-THF, methenyl-THF; CH_3-THF, methyl-THF; CHO-THF, formyl-THF; CoFeSP, corrinoid iron–sulphur protein; Fd^{2-}, reduced ferredoxin; Pi, inorganic phosphate.

Schuchmann & Müller, 2014

reductive acetyl-CoA pathway

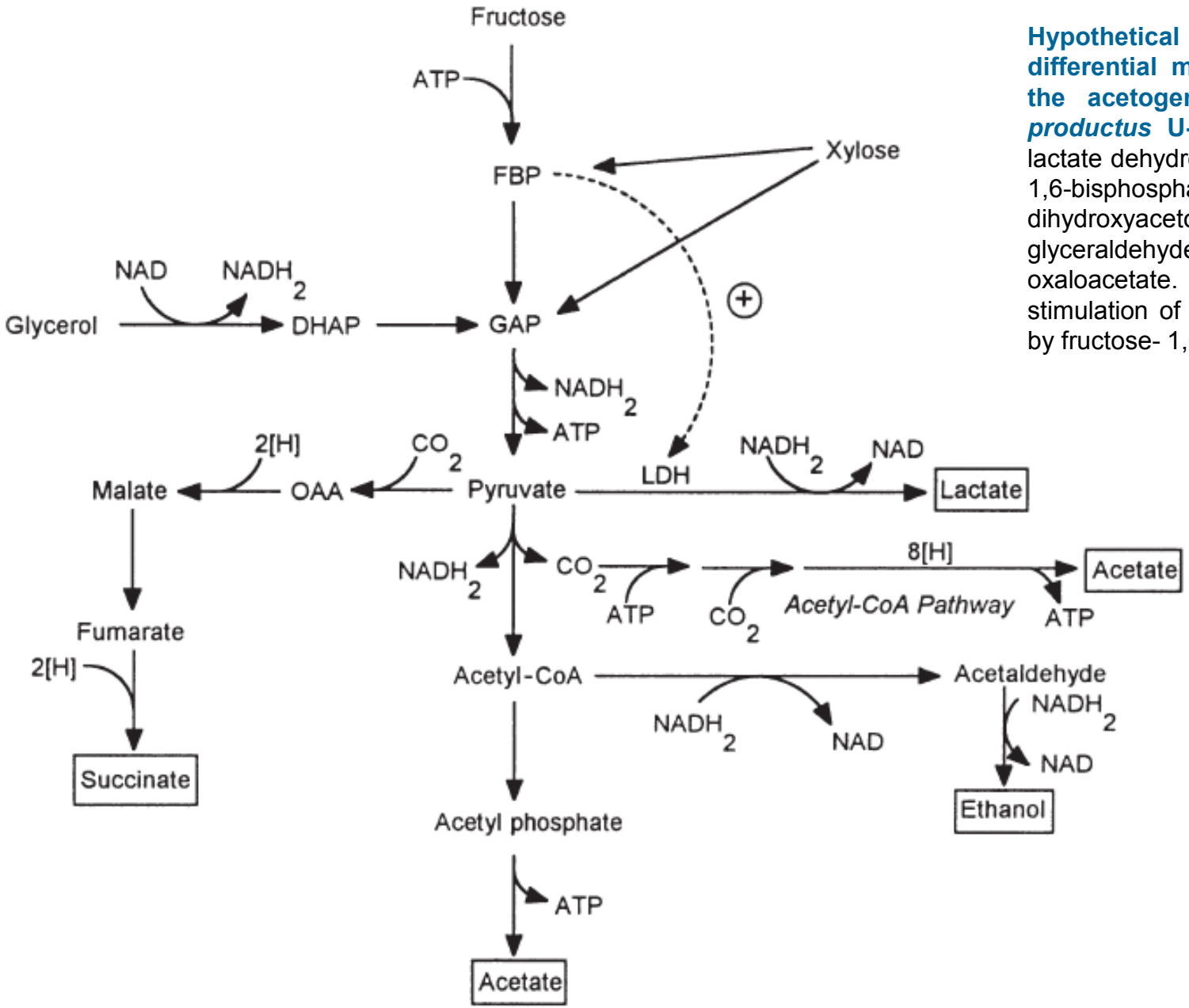

Hypothetical scheme for the differential metabolic capacities of the acetogen *Peptostreptococcus productus* U-1. Abbreviations: LDH: lactate dehydrogenase; FBP: fructose-1,6-bisphosphate; DHAP: dihydroxyacetone phosphate; GAP: glyceraldehyde-3-phosphate; OAA: oxaloacetate. Broken line indicates stimulation of lactacte dehydrogenase by fructose- 1,6-bisphosphate.

Drake et al., 1997

reductive acetyl-CoA pathway

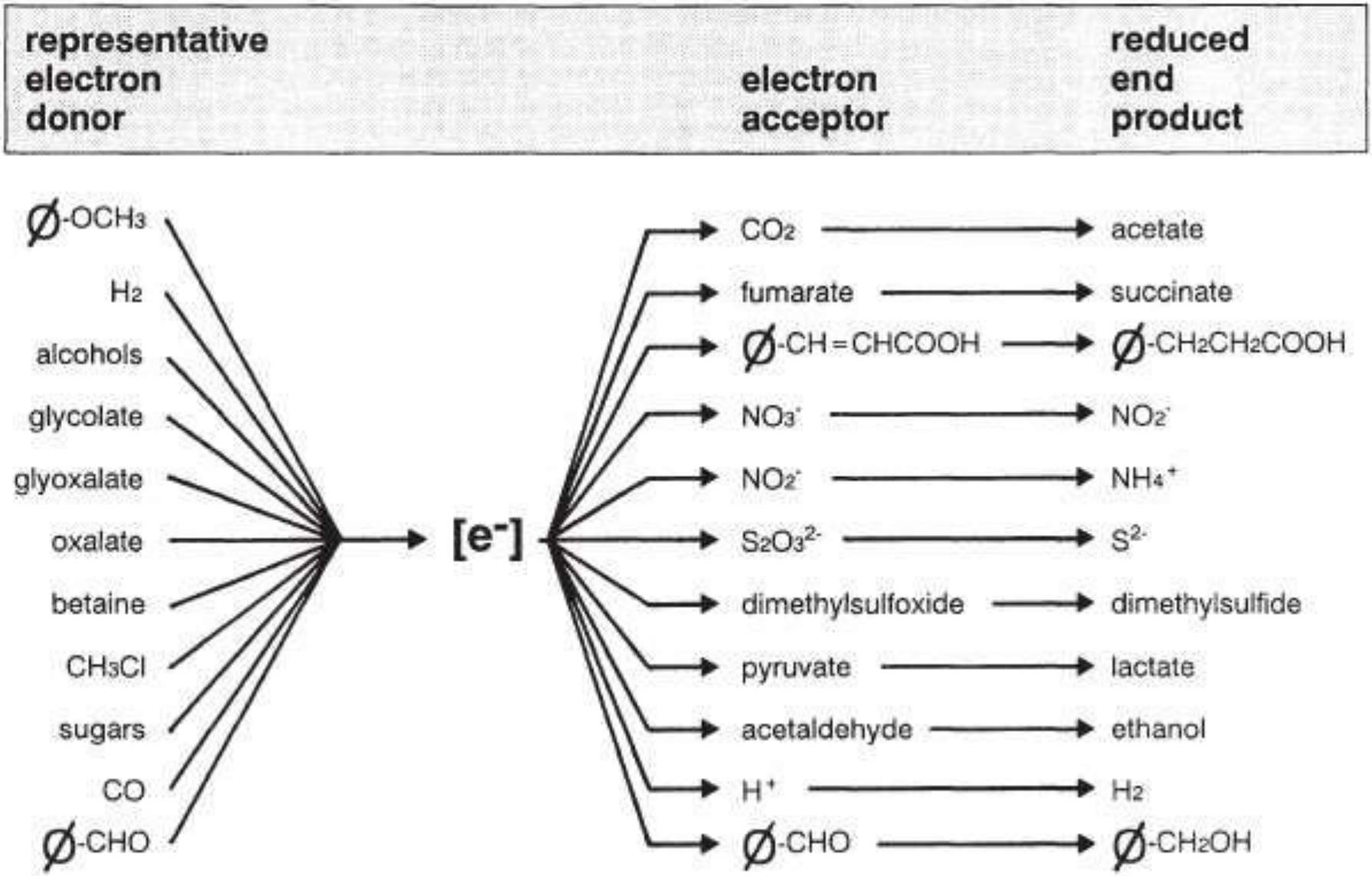

Fig. 5. Composite illustrating the diverse flow of electrons by acetogens.

Drake et al., 1997, 2008

reductive acetyl-CoA pathway

Substrate	Overall stoichiometry	Representative acetogen
acetoin	$2\ CH_3COCHOHCH_3 + 2\ CO_2 + 2\ H_2O \rightarrow 5\ CH_3COOH$	*Acetobacterium carbinolicum*
2,3-butanediol	$4\ CH_3CHOHCHOHCH_3 + 6\ CO_2 + 2\ H_2O \rightarrow 11\ CH_3COOH$	*Clostridium magnum*
carbon monoxide	$4\ CO + 2\ H_2O \rightarrow CH_3COOH + 2\ CO_2$	*Clostridium thermoaceticum*
citrate	$4\ C_6H_8O_7 + 2\ H_2O \rightarrow 9\ CH_3COOH + 6\ CO_2$	*Clostridium magnum*
cellobiose	$C_{12}H_{22}O_{11} + H_2O \rightarrow 6\ CH_3COOH$	*Peptostreptococcus productus*
ethanol	$2\ CH_3CH_2OH + 2\ CO_2 \rightarrow 3\ CH_3COOH$	*Clostridium formicoaceticum*
formate	$4\ HCOOH \rightarrow CH_3COOH + 2\ CO_2 + 2\ H_2O$	*Clostridium thermoaceticum*
glucose	$C_6H_{12}O_6 \rightarrow 3\ CH_3COOH$	*Clostridium thermoaceticum*
glycerol	$4\ CH_2OHCHOHCH_2OH + 2\ CO_2 \rightarrow 7\ CH_3COOH + 2\ H_2O$	*Acetobacterium carbinolicum*
glycolate	$4\ CH_2OHCOOH \rightarrow 3\ CH_3COOH + 2\ CO_2 + 2\ H_2O$	*Clostridium thermoaceticum*
glyoxylate	$2\ COHCOOH \rightarrow CH_3COOH + 2\ CO_2$	*Clostridium thermoaceticum*
hydrogen	$4\ H_2 + 2\ CO_2 \rightarrow CH_3COOH + 2\ H_2O$	*Clostridium aceticum*
4-hydroxybenzaldehyde	4 4-hydroxybenzaldehyde + $2\ CO_2 + 2\ H_2O \rightarrow CH_3COOH$ + 4-hydroxybenzoate	*Clostridium formicoaceticum*
malate	$2\ COOHCHOHCH_2COOH \rightarrow 3\ CH_3COOH + 2\ CO_2$	*Clostridium magnum*
methanol	$4\ CH_3OH + 2\ CO_2 \rightarrow 3\ CH_3COOH + 2\ H_2O$	*Clostridium thermoaceticum*
methoxyacetate	$4\ CH_3OCH_2COOH + 2\ CO_2 + 2\ H_2O \rightarrow 3\ CH_3COOH$ + $4\ HOCH_2COOH$	strain RMMac1
2-methoxyethanol	$4\ CH_3OCH_2CH_2OH + 2\ CO_2 + 2\ H_2O \rightarrow 4\ CH_3OH + 5\ CH_3COOH$	*Acetobacterium malicum*
methyl chloride	$4\ CH_3Cl + 2\ CO_2 + 2\ H_2O \rightarrow 3\ CH_3COOH + 4\ HCl$	strain MC
oxalate	$4\ COOHCOOH \rightarrow CH_3COOH + 6\ CO_2 + 2\ H_2O$	*Clostridium thermoaceticum*
pyruvate	$4\ CH_3COCOOH + 2\ H_2O \rightarrow 5\ CH_3COOH + 2\ CO_2$	*Clostridium thermoaceticum*
vanillate	4 vanillate[-OCH_3] + $2\ CO_2 + 2\ H_2O \rightarrow$ 4 protocatechuate[-OH] + $3\ CH_3COOH$	*Acetobacterium woodii*
xylose	$2\ C_5H_{10}O_5 \rightarrow 5\ CH_3COOH$	*Clostridium thermoaceticum*

Representative oxidizeable substrates that can be used for the reductive synthesis of acetate via the acetyl-CoA 'Wood/Ljungdahl' pathway

Drake et al., 1997

reductive acetyl-CoA pathway

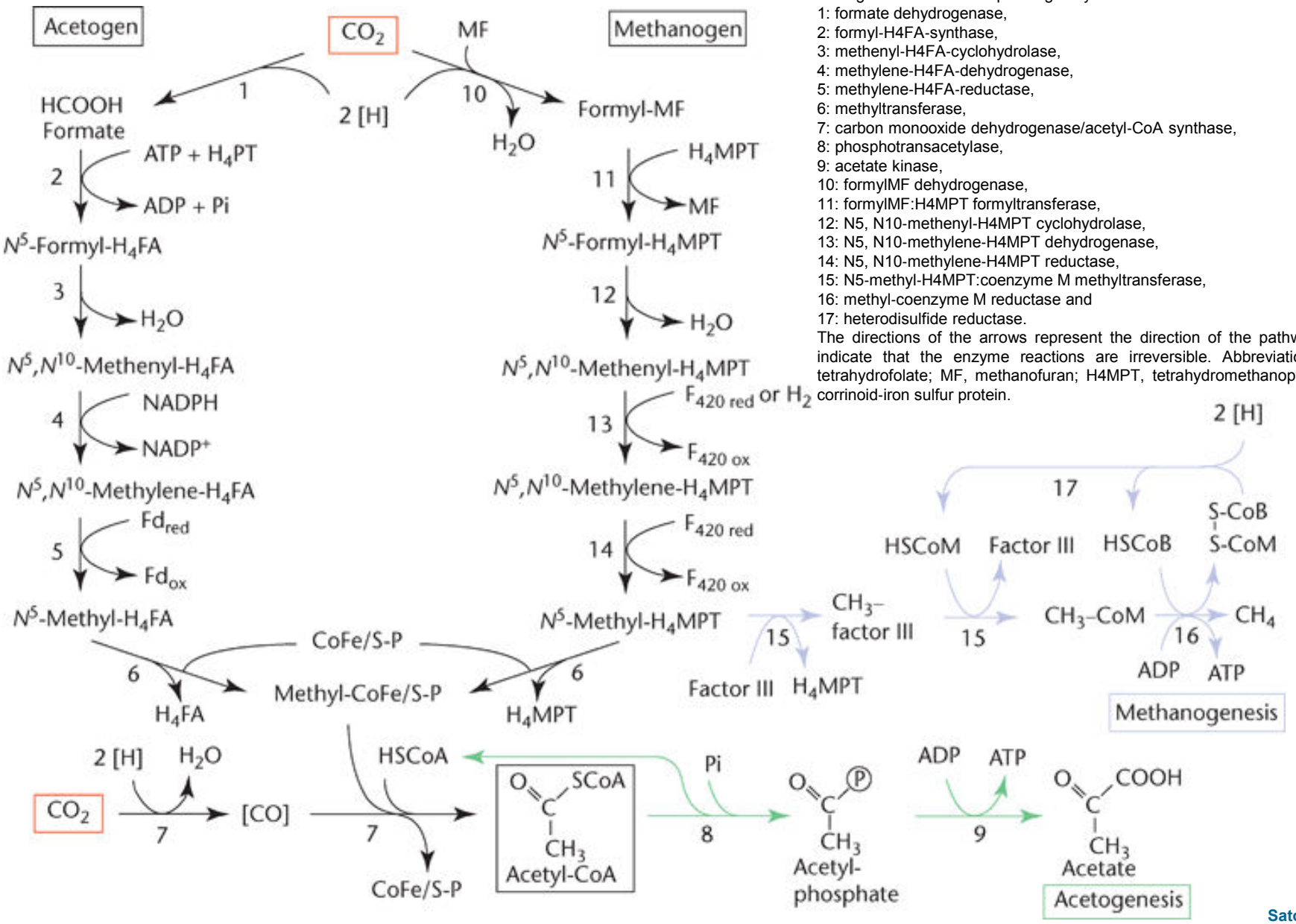

Diagram illustrating the reactions of the reductive acetyl-CoA pathway. Coloured pathways indicate related enzymes involved in methanogenesis and acetogenesis. The corresponding enzymes are:
1: formate dehydrogenase,
2: formyl-H4FA-synthase,
3: methenyl-H4FA-cyclohydrolase,
4: methylene-H4FA-dehydrogenase,
5: methylene-H4FA-reductase,
6: methyltransferase,
7: carbon monooxide dehydrogenase/acetyl-CoA synthase,
8: phosphotransacetylase,
9: acetate kinase,
10: formylMF dehydrogenase,
11: formylMF:H4MPT formyltransferase,
12: N5, N10-methenyl-H4MPT cyclohydrolase,
13: N5, N10-methylene-H4MPT dehydrogenase,
14: N5, N10-methylene-H4MPT reductase,
15: N5-methyl-H4MPT:coenzyme M methyltransferase,
16: methyl-coenzyme M reductase and
17: heterodisulfide reductase.
The directions of the arrows represent the direction of the pathway, and do not indicate that the enzyme reactions are irreversible. Abbreviations are: H4FA, tetrahydrofolate; MF, methanofuran; H4MPT, tetrahydromethanopterin; CoFe/S-P, corrinoid-iron sulfur protein.

Sato & Atomi , 2010

reductive acetyl-coenzyme A pathway

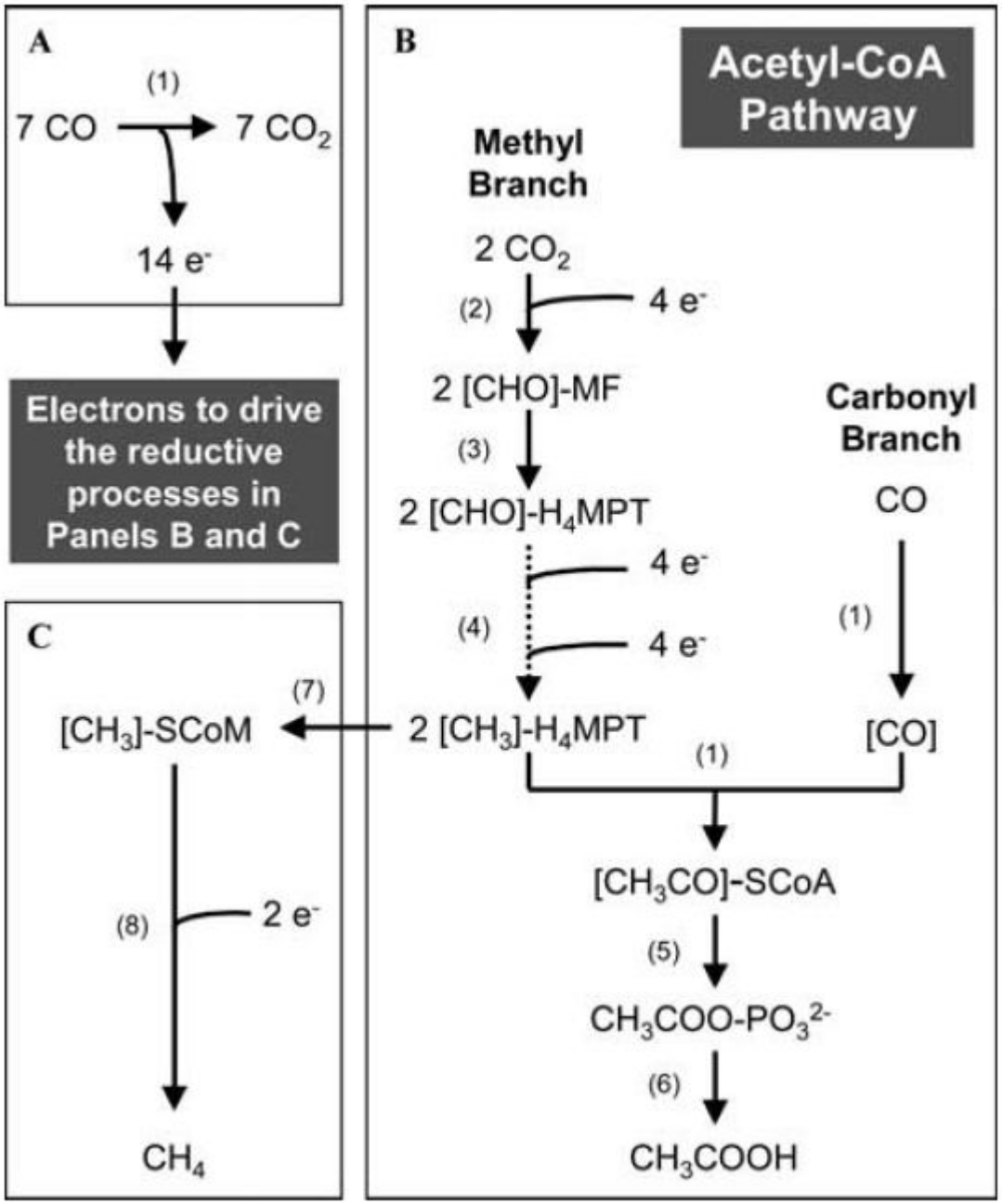

Metabolic processes by which carbon monoxide is utilized by *Methanosarcina acetivorans*.
(**A**) Oxidation of carbon monoxide;
(**B**) reductive synthesis of acetate via the acetyl-CoA pathway;
(**C**) production of methane.

Parenthetical numbers identify enzymes that catalyze the indicated reactions:
1, CO dehydrogenase/acetyl-CoA synthetase;
2, formyl-methanofuran dehydrogenase;
3, formyl-methanofuran:H4MPT formyltransferase;
4, combined activities of methenyl-H4MPT cyclohydrolase, methylene-H4MPT dehydrogenase; methylene-H4MPT reductase;
5, phosphotransacetylase;
6, acetate kinase;
7, methyl-H4MPT:CoM methyltransferase;
8, combined activities of methyl-CoM reductase, membranous heterodisulfide reductase, and membranous F420H2 dehydrogenase complex (F420, coenzyme F420).

ABBREVIATIONS: MF = methanofuran; H4MPT = tetrahydromethanopterin; HSCoM = coenzyme M. [The figure is based on information in Lessner *et al*. (further details on how these processes are coupled to the chemiosmotic conservation of energy can be found in this reference).]

reductive acetyl-coenzyme A pathway

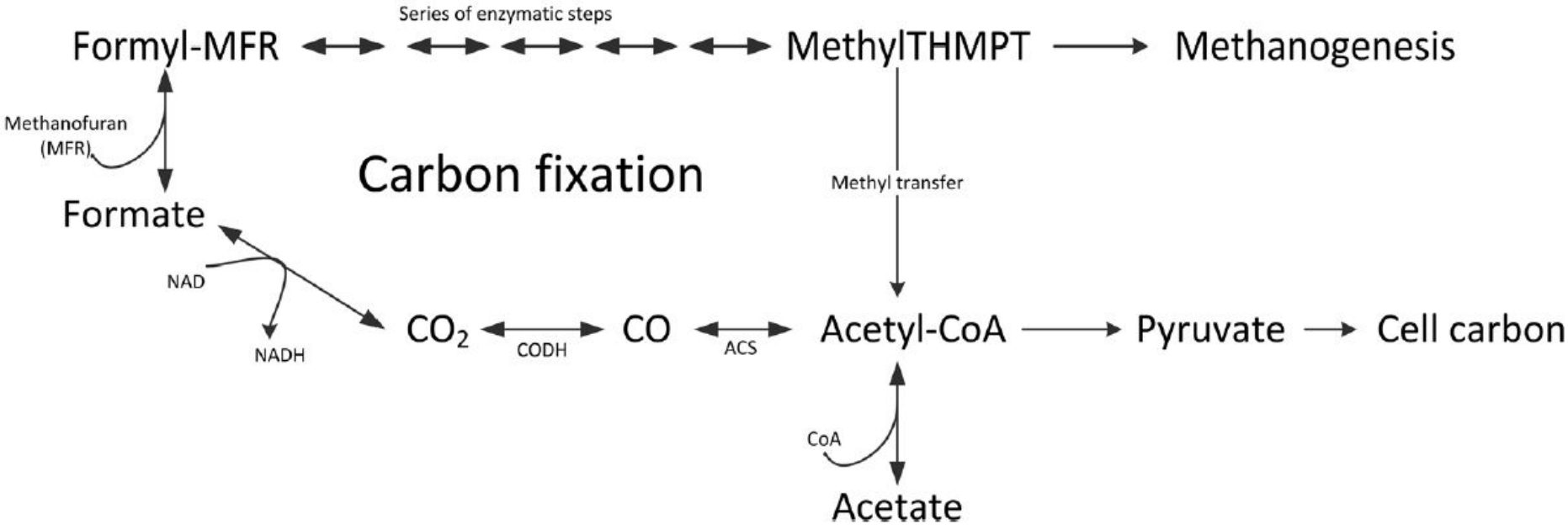

Fig. 1 Wood–Ljungdahl pathway for CO_2 fixation occurring in *M. maripaludis*. One CO_2 molecule is reduced to CO and the other CO_2 molecule is reduced to a methyl group bound to carrier methylTHMPT; subsequent methyl transfer to CO in the presence of CoA leads to acetyl-CoA synthesis. Formyl-MFR, formyl-methanofuran; methylTHMPT, methyltetrahydromethanopterin, acetyl-CoA, acetyl-coenzyme A; CODH, carbon monoxide dehydrogenase; ACS, acetyl-CoA synthase.

Goyal *et al.*, 2014

reductive acetyl-CoA pathway

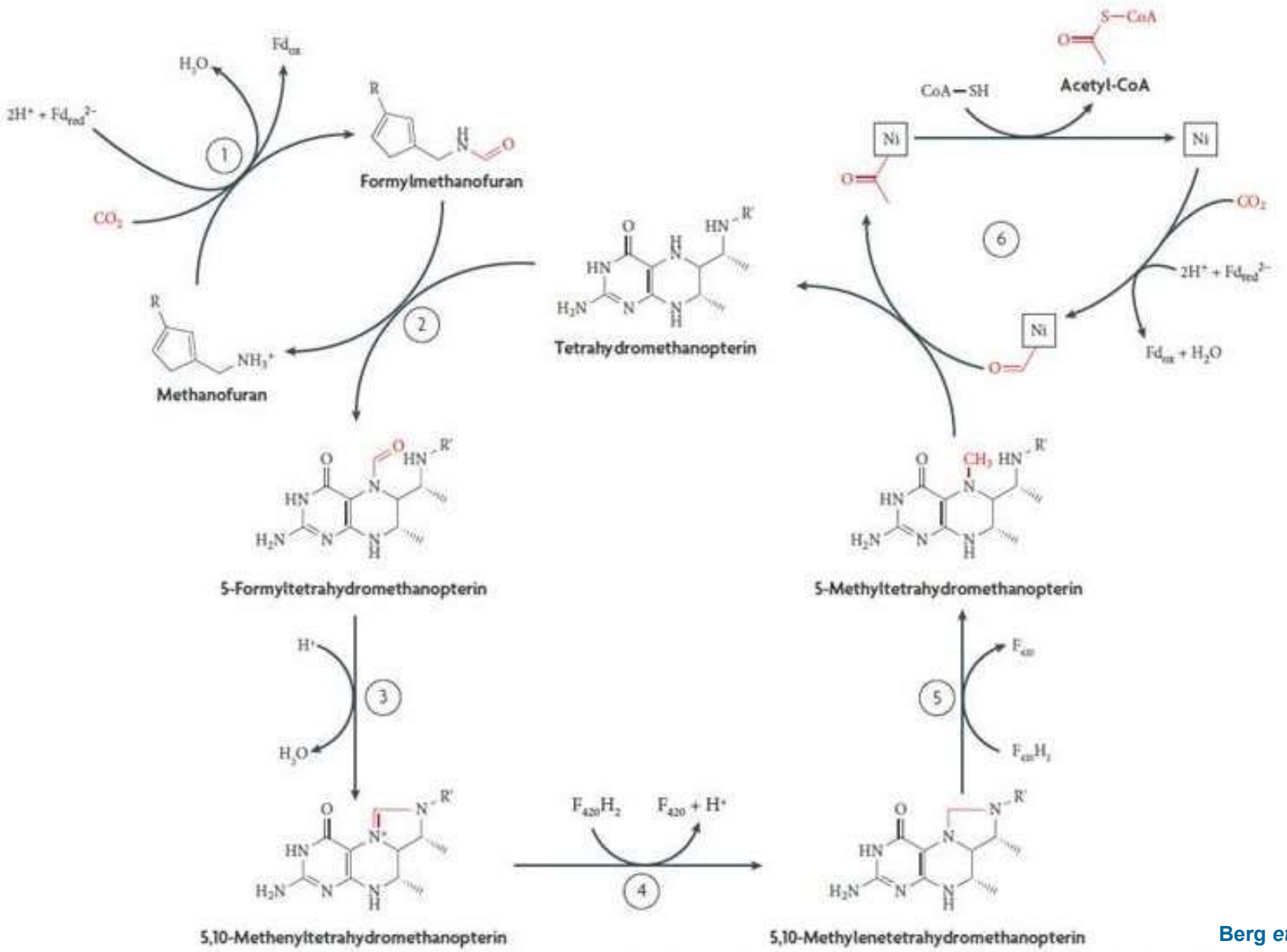

Berg *et al.*, 2010

(1) Formylmethanofuran dehydrogenase (Fmd); (2) Formylmethanofuran:tetramethanopterin formyltransferase (Ftr), (3) methenyl-tetrahydromethanopterin cyclohydrolase (Mch), (4) methylene-tetrahydromethanopterin dehydrogenase (Hmd), (5) methylene-tetrahydromethanopterin reductase (Mer), (6) CO dehydrogenase-acetyl-CoA synthase

reductive acetyl-coenzyme A pathway

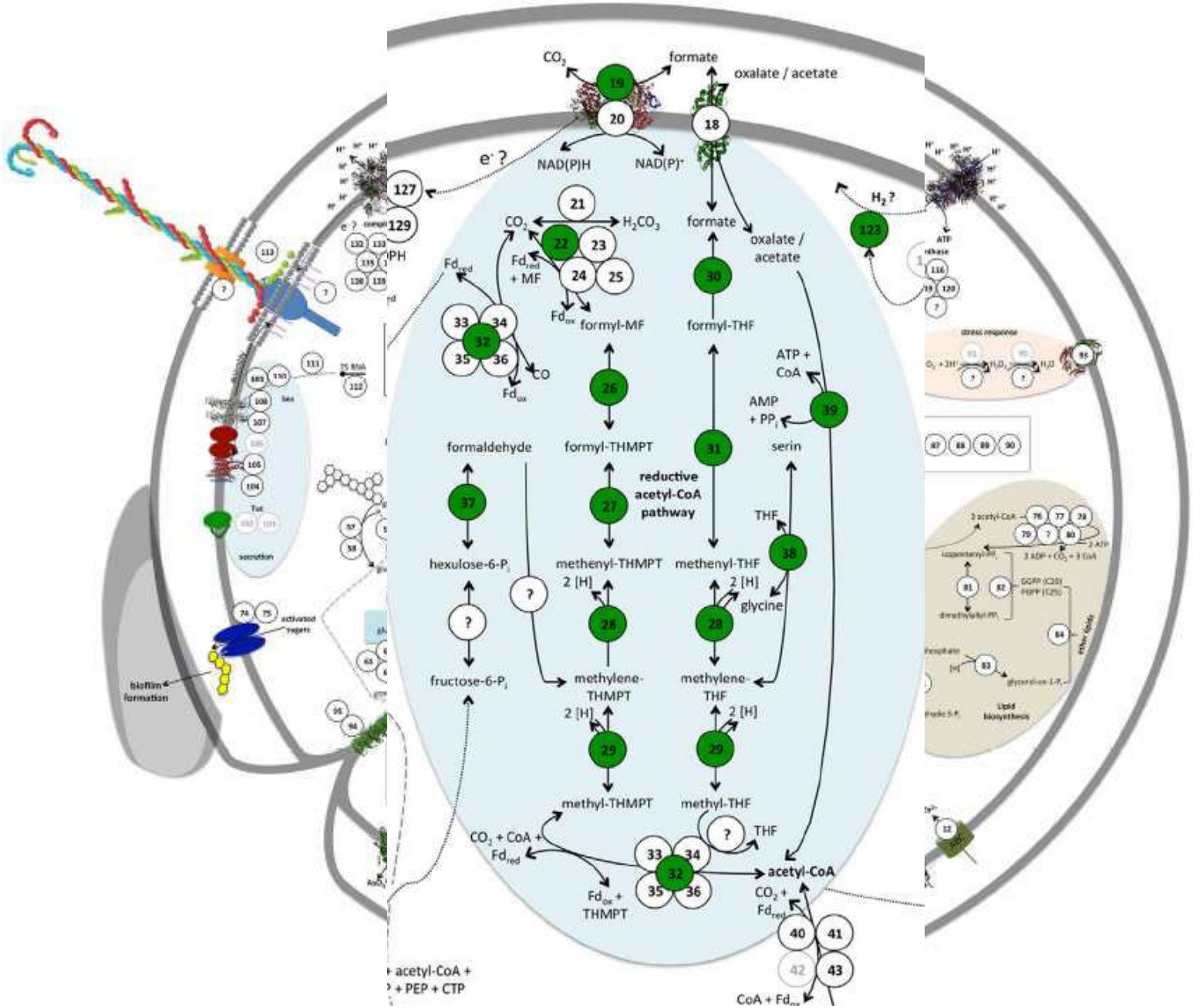

Metabolic pathway map of genes encoded in the SM1 euryarchaeal pangenome. Membrane proteins are indicated by symbols or protein structures of subunits (taken from Pfam database). Predicted proteins are indicated by numbers, which can be found in Supplementary Table 2. Grey numbers were found in SM1-MSI but not for SM1-CG. Specific enzymes were tested for presence of corresponding mRNA: Enzymes labeled in green were also detected in the mRNA pool of the biofilm, while enzymes with red color were absent in mRNA pool. Interrogation marks indicate potential metabolic pathway reactions that are likely present but are lacking evidence in the fragmented genomic bins.

Probst *et al.*, 2015

3-hydroxypropionate bicycle

- The **3-hydroxypropionate bicycle** (**3-hydroxypropionate/malyl-CoA cycle**) occurs in some green non-sulphur bacteria of the family Chloroflexaceae. This seems to be a singular invention, and the pathway has not been found elsewhere.
- The conversion of acetyl-CoA plus two bicarbonates to succinyl-CoA uses the same intermediates as in the hydroxypropionate–hydroxybutyrate cycle, but most of the enzymes are completely different.
- The regeneration of acetyl-CoA proceeds by the cleavage of malyl-CoA, yielding acetyl-CoA and glyoxylate. The assimilation of glyoxylate requires a second cycle (hence the name bicycle).

Berg et al., 2010

3-hydroxypropionate bicycle

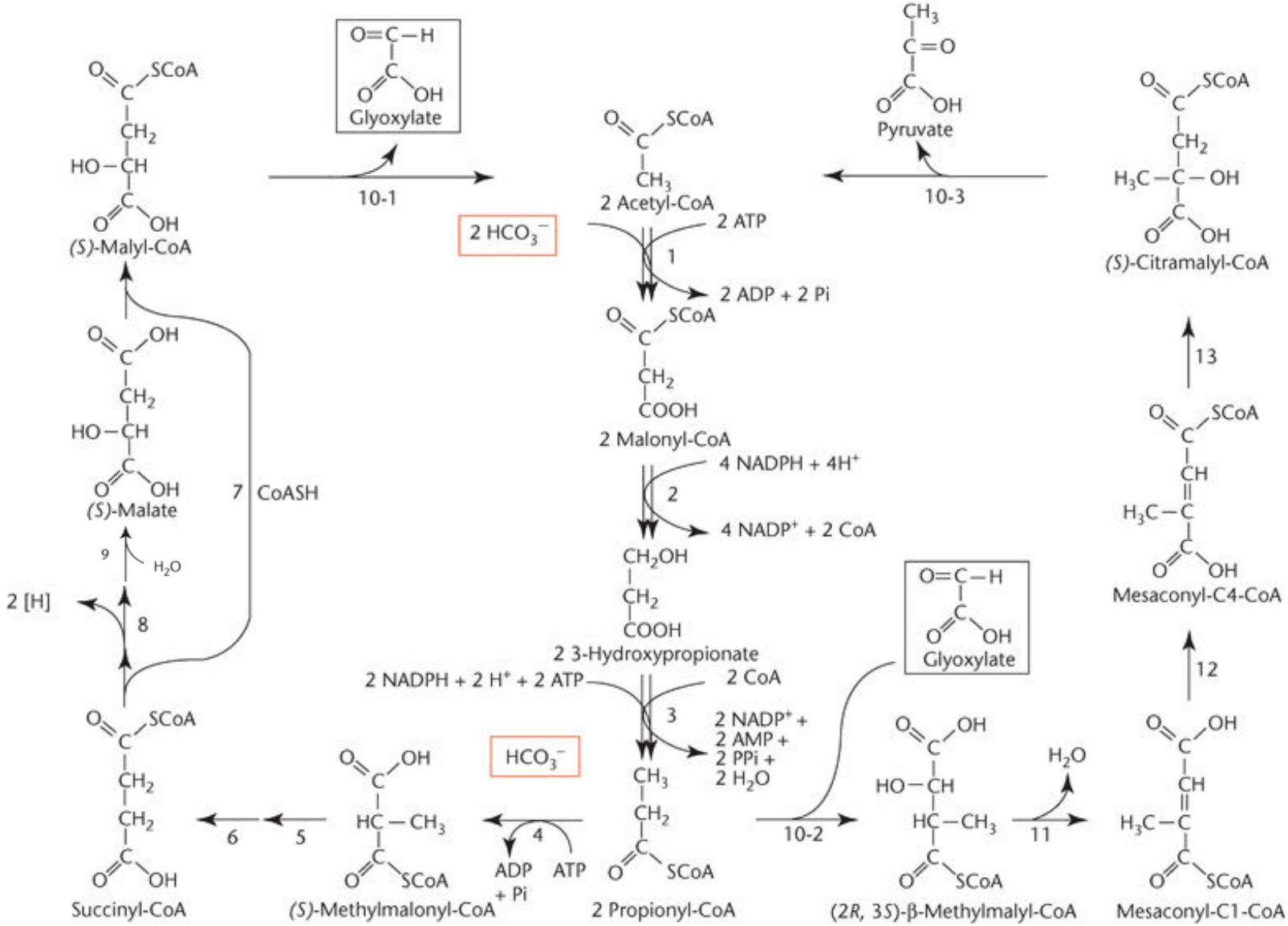

Diagram illustrating the reactions of the 3-hydroxypropionate bicycle (3-hydroxypropionate/malyl-CoA cycle). The corresponding enzymes are: 1: acetyl-CoA carboxylase, 2: malonyl-CoA reductase, 3: propionyl-CoA synthase, 4: propionyl-CoA carboxylase, 5: methylmalonyl-CoA epimerase, 6: methylmalonyl-CoA mutase, 7: succinyl-CoA:(S)-malate-CoA transferase, 8: succinate dehydrogenase, 9: fumarate hydratase, 10-1, 10-2, 10-3: (S)-malyl-CoA/β-methylmalyl-CoA/(S)-citramalyl-CoA (MMC) lyase, 11: mesaconyl-C1-CoA hydratase (β-methylmalyl-CoA dehydratase), 12: mesaconyl-CoA C1-C4 CoA transferase and 13: mesaconyl-C4-CoA hydratase. The directions of the arrows represent the direction of the pathway, and do not indicate that the enzyme reactions are irreversible.

Sato & Atomi , 2010

pathways of autotrophic CO_2 fixation in crenarchaeota

dicarboxylate–hydroxybutyrate cycle **hydroxypropionate–hydroxybutyrate cycle**

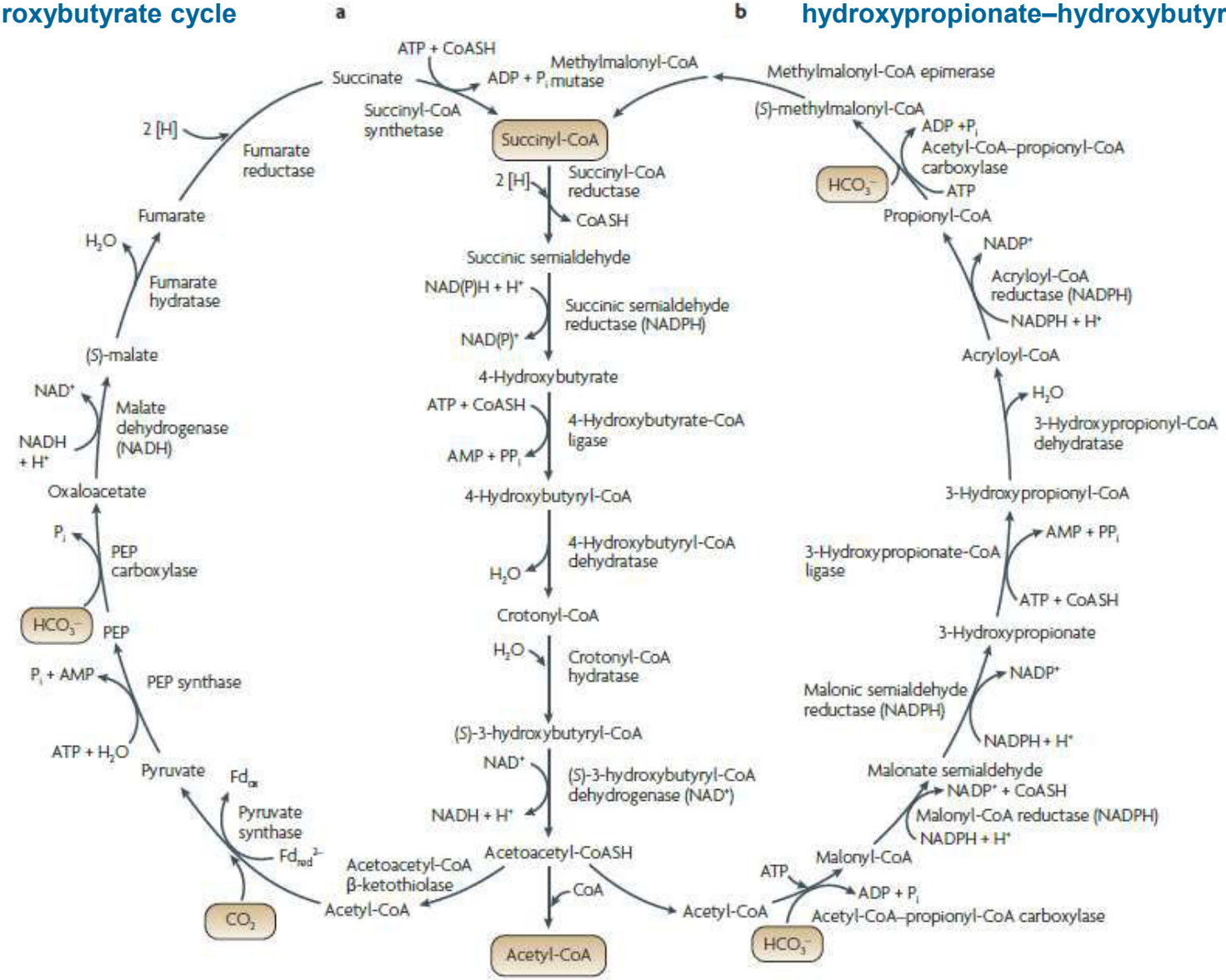

Pathways of autotrophic CO_2 fixation in crenarchaeota. The dicarboxylate–hydroxybutyrate cycle functions in **Desulfurococcales and Thermoproteales** (**a**) and the hydroxypropionate–hydroxybutyrate cycle functions in **Sulfolobales and Thaumarchaeota** (**b**). Note that succinyl-coenzyme A (succinyl-CoA) reductase in Thermoproteales and Sulfolobales uses NADPH and reduced methyl viologen (possibly as a substitute for reduced ferredoxin) in Desulfurococcales. In Sulfolobales, pyruvate might be derived from succinyl-CoA by C4 decarboxylation. CoASH, coenzyme A; Fdred 2–, reduced ferredoxin; Fdox, oxidized ferredoxin; PEP, phosphoenolpyruvate. **Berg et al., 2010**

3-hydroxypropionate/4-hydroxybutyrate cycle

- The 3-hydroxypropionate/4-hydroxybutyrate cycle (hydroxypropionate–hydroxybutyrate cycle) was discovered by Berg *et al*. in 2007.
- The hydroxypropionate–hydroxybutyrate cycle occurs in Sulfolobales and Thaumarchaeota. Although some of the intermediates and the carboxylation reactions are the same as in the 3-hydroxypropionate bicycle in Chloroflexaceae, the archaeal cycle probably has evolved independently.

Berg et al., 2007, 2010

3-hydroxypropionate/4-hydroxybutyrate cycle

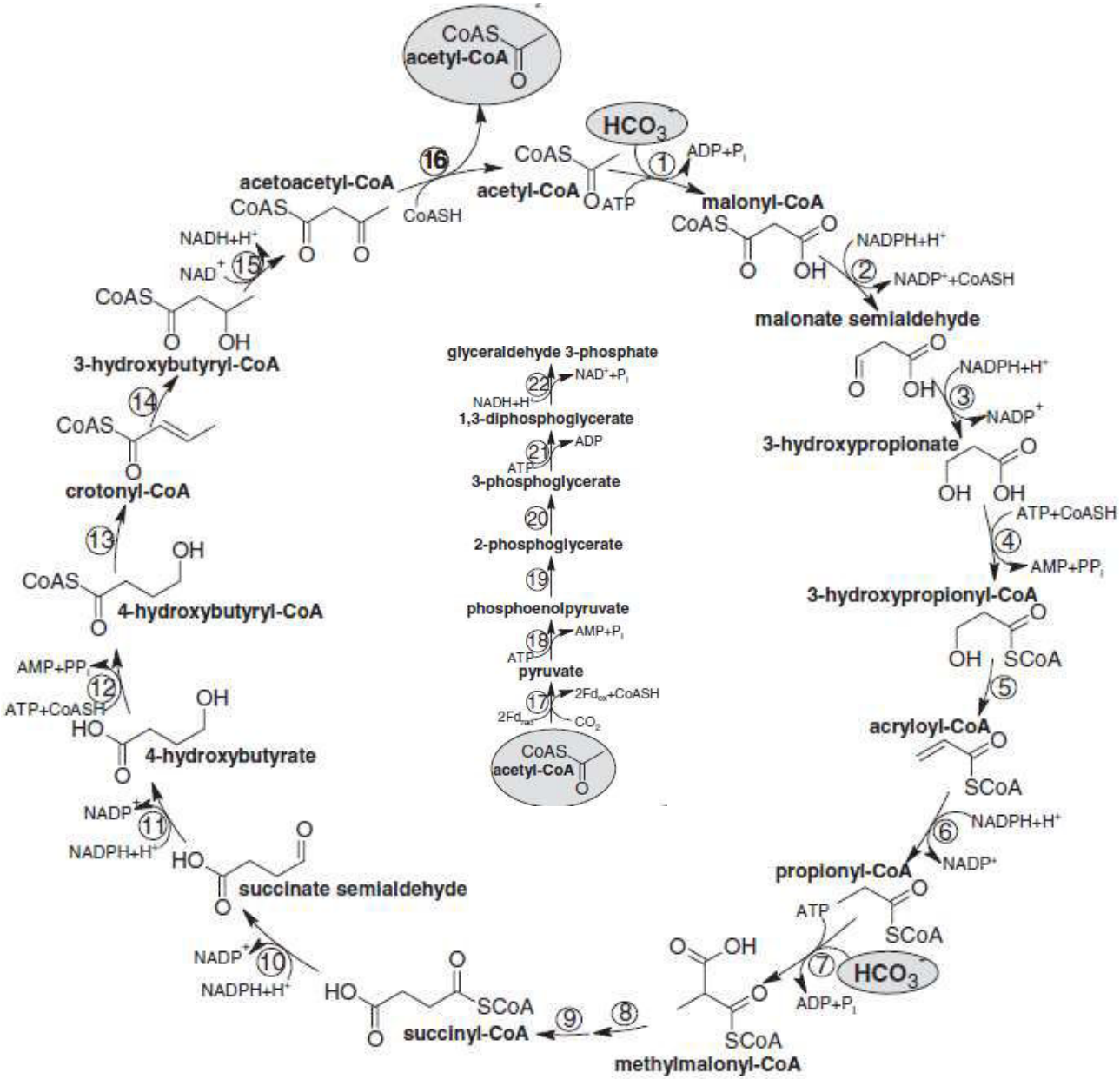

Proposed autotrophic 3-hydroxypropionate/4-hydroxybutyrate cycle in *M. sedula*. Reactions of the cycle are shown.

Enzymes:
1, acetyl-CoA carboxylase;
2, malonyl-CoA reductase (NADPH);
3, malonate semialdehyde reductase (NADPH);
4, 3-hydroxypropionyl-CoA synthetase (AMP-forming);
5, 3-hydroxypropionyl-CoA dehydratase;
6, acryloyl-CoA reductase (NADPH);
7, propionyl-CoA carboxylase;
8, methylmalonyl-CoA epimerase;
9, methylmalonyl-CoA mutase;
10, succinyl-CoA reductase (NADPH);
11, succinate semialdehyde reductase (NADPH);
12, 4-hydroxybutyryl-CoA synthetase (AMP-forming);
13, 4-hydroxybutyryl-CoA dehydratase;
14, crotonyl-CoA hydratase;
15, 3-hydroxybutyryl-CoA dehydrogenase (NAD+);
16, acetoacetyl-CoA β-ketothiolase.

The proposed pathway of glyceraldehyde 3-phosphate synthesis from acetyl-CoA and CO_2 is also shown.

Enzymes:
17, pyruvate synthase;
18, pyruvate, water dikinase [phosphoenolpyruvate (PEP) synthase];
19, enolase;
20, phosphoglycerate mutase;
21, 3-phosphoglycerate kinase;
22, glyceraldehyde 3-phosphate dehydrogenase.

Berg et al., 2007

3-hydroxypropionate/4-hydroxybutyrate cycle

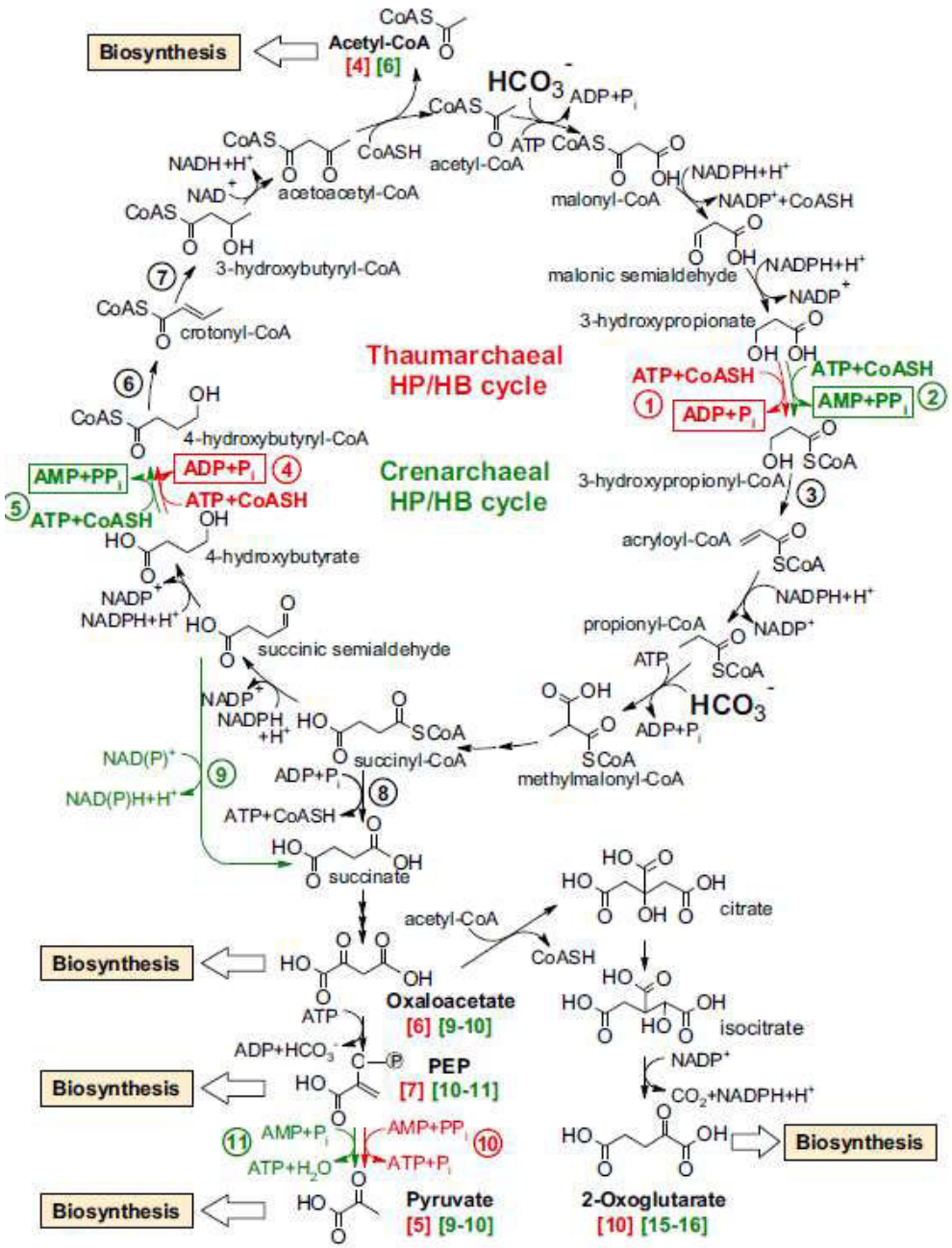

Reactions of the crenarchaeal and thaumarchaeal variants of the HP/ HB cycle.
The reactions determining energy efficiency of the crenarchaeal (*M. sedula*) cycle are shown in green, and those for the *N. maritimus* variant are shown in red. Reactions common to both are shown in black. Note that although the two pathways have similar reactions and intermediates, they are significantly different in energy efficiency and evolved independently in Crenarchaeota and Thaumarchaeota. The numbers in square brackets represent moles of high-energy anhydride bonds of ATP required to form 1 mol of the corresponding central precursor metabolites.

Enzymes as numbered in circles are:
1, 3-hydroxypropionyl-CoA synthetase (ADP-forming);
2, 3-hydroxypropionyl-CoA synthetase (AMP-forming);
3, 3-hydroxypropionyl-CoA dehydratase;
4, 4-hydroxybutyryl-CoA synthetase (ADP-forming);
5, 4-hydroxybutyryl-CoA synthetase (AMP-forming);
6, 4-hydroxybutyryl-CoA dehydratase;
7, crotonyl-CoA hydratase;
8, succinyl-CoA synthetase (ADP-forming);
9, succinic semialdehyde dehydrogenase;
10, pyruvate-phosphate dikinase; and
11, pyruvatewater dikinase.

Catalytic properties of recombinant enzymes

	3-Hydroxypropionyl-CoA synthetase		
Substrate	V_{max}, µmol·min^{-1}·mg^{-1} protein	K_m, mM	k_{cat}/K_m
3-Hydroxypropionate	0.59 ± 0.03	1.2 ± 0.2	0.64
4-Hydroxybutyrate	0.48 ± 0.04	5.6 ± 1.0	0.11
Acetate	–	–	–
Propionate	0.50 ± 0.10	17.0 ± 6.0	0.04
Butyrate	0.54 ± 0.01	12.4 ± 0.3	0.06
ATP	0.59 ± 0.03	0.6 ± 0.1	1.28
CoA	0.60 ± 0.10	0.16 ± 0.09	4.85

	4-Hydroxybutyryl-CoA synthetase		
Substrate	V_{max}, µmol·min^{-1}·mg^{-1} protein	K_m, mM	k_{cat}/K_m
3-Hydroxypropionate	–	–	–
4-Hydroxybutyrate	1.4 ± 0.01	0.37 ± 0.06	4.88
Acetate	0.22 ± 0.01	200 ± 5	0.001
Propionate	0.10 ± 0.01	88 ± 7	0.002
Butyrate	0.61 ± 0.05	5 ± 1	0.16
ATP	1.7 ± 0.2	0.22 ± 0.07	9.96
CoA	1.4 ± 0.1	0.16 ± 0.05	11.28

Könnecke et al,. 2015

universität wien

3-hydroxypropionate/4-hydroxybutyrate cycle

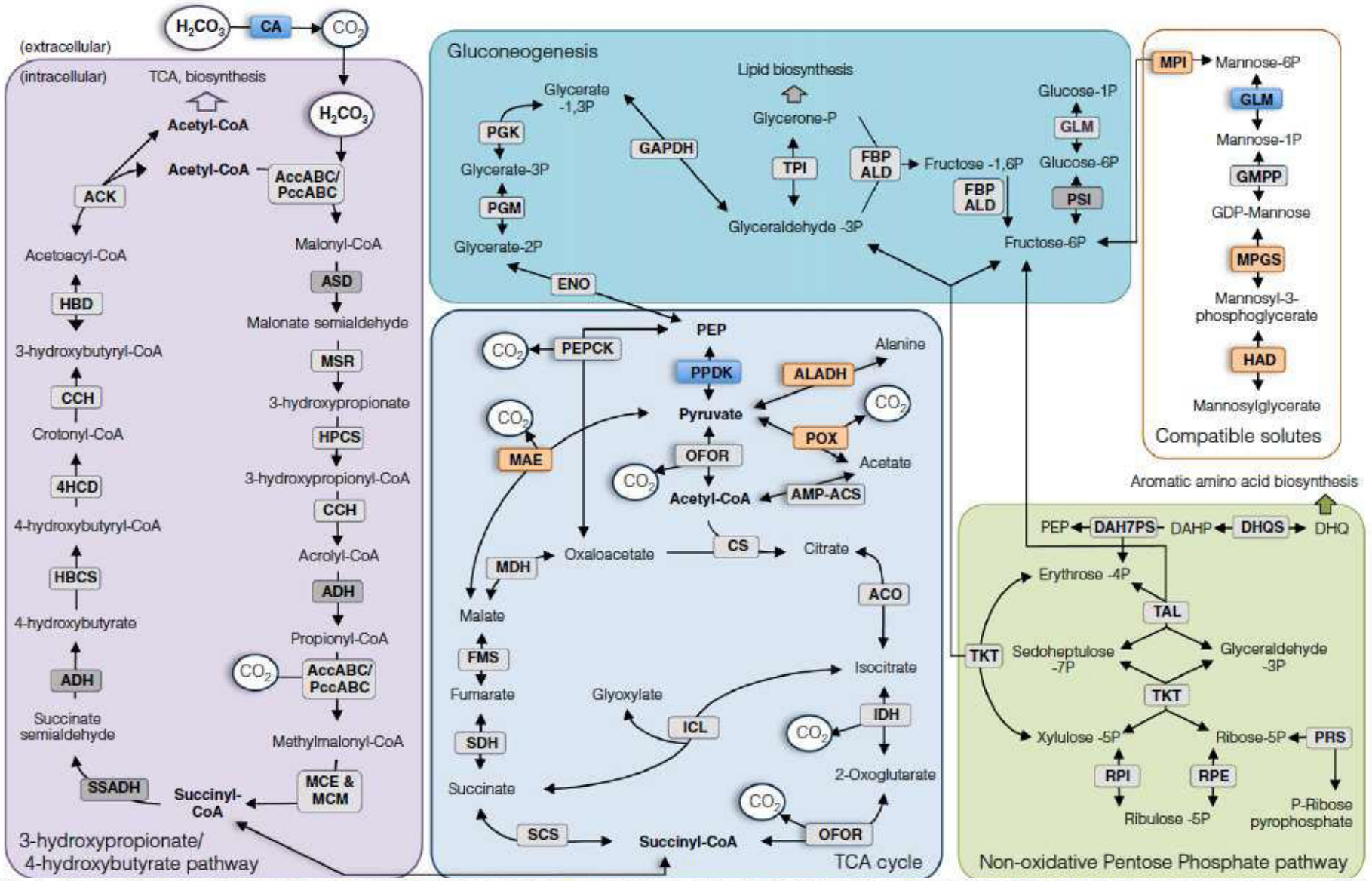

Fig. 2. Reconstruction of the predicted central carbon metabolism modules in AOA emphasizing the conservation of the core pathway enzymes and carriers and features of the Nitrososphaerales. Canonical enzymes belonging to the core COGs are depicted in light gray boxes, whereas candidate enzymes according to the work by Spang et al. (28) are in dark gray boxes. COGs conserved among Nitrososphaerales are depicted in orange boxes, and COGs present in some of the analyzed genomes are in blue (refer to the color key in Fig. 3). Proteins catalyzing all displayed reactions were detected in the proteome of *N. viennensis* by proteotypic peptides. Gene accession numbers and enzyme abbreviations are listed in Dataset S2.

3-hydroxypropionate/4-hydroxybutyrate cycle

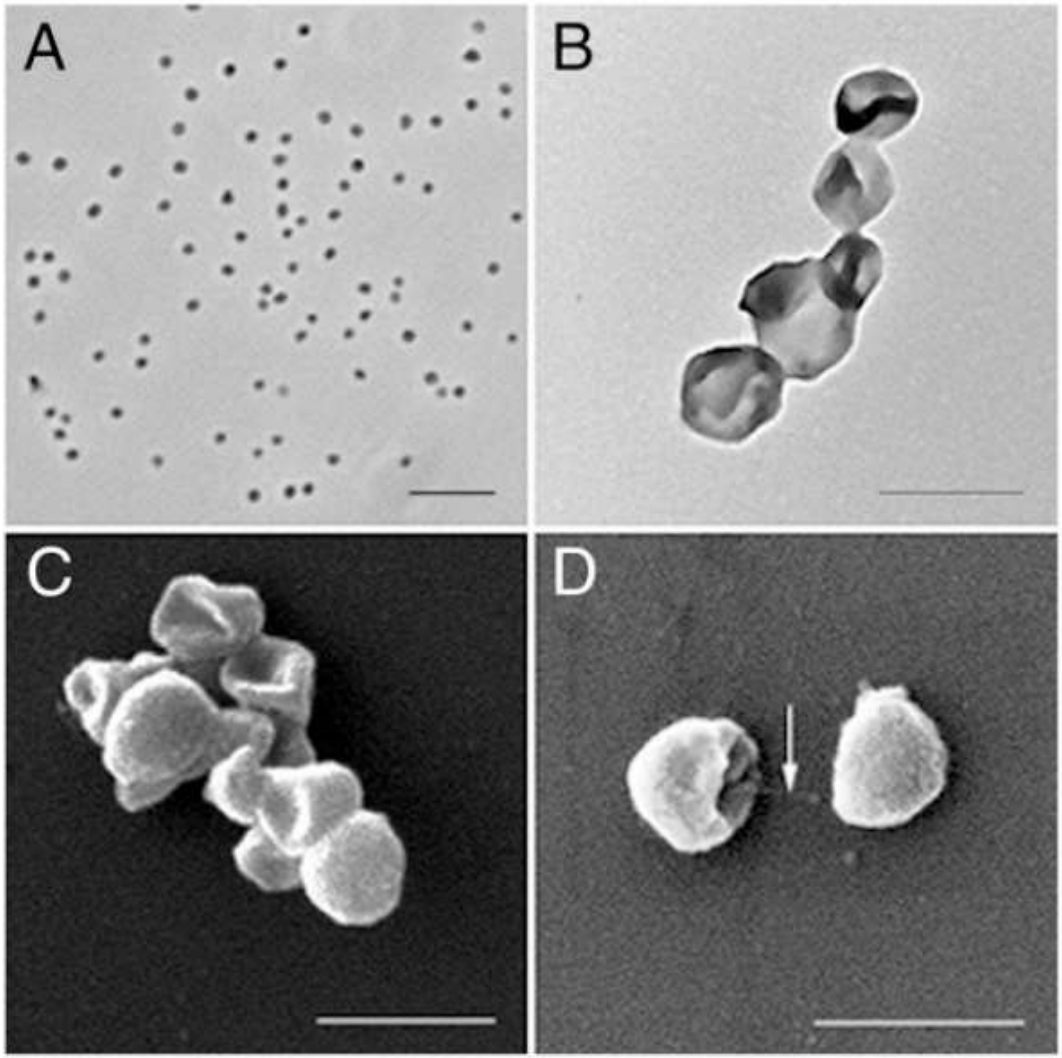

Fig. 5. Microscopy pictures of strain EN76 (*N. viennensis*) in pure culture. (*A*) Phase contrast-light micrograph. (Scale bar: 5 µm.) (*B*) Transmission EM image of negative stained cells. (Scale bar: 1 µm.) (*C* and *D*) Scanning EM images of cells. (Scale bar: 1 µm.) The arrow in *D* points to a cell appendage.

Fed-batch fermentation of *N. viennensis*

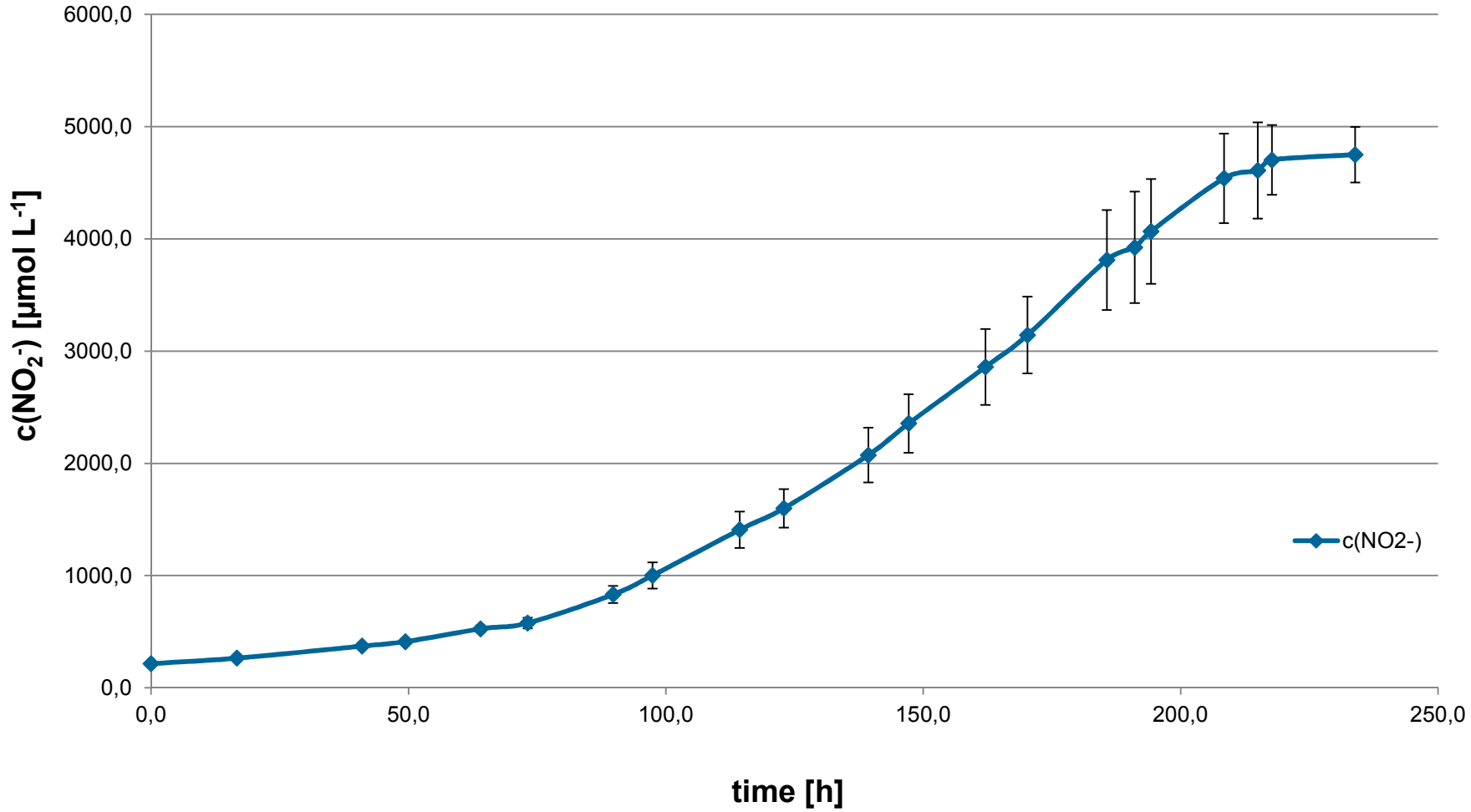

Results of quadruplicate batch fermentation of *N. viennensis* in a bioreactor system with continuous supply of 20% CO_2, 21% O_2, rest N_2.

dicarboxylate/4-hydroxybutyrate cycle

- The dicarboxylate/4-hydroxybutyrate cycle was discovered by Huber *et al*. in 2008.
- The dicarboxylate–hydroxybutyrate cycle occurs in the anaerobic crenarchaeal orders Thermoproteales and Desulfurococcales.

Huber et al., 2008

dicarboxylate/4-hydroxybutyrate cycle

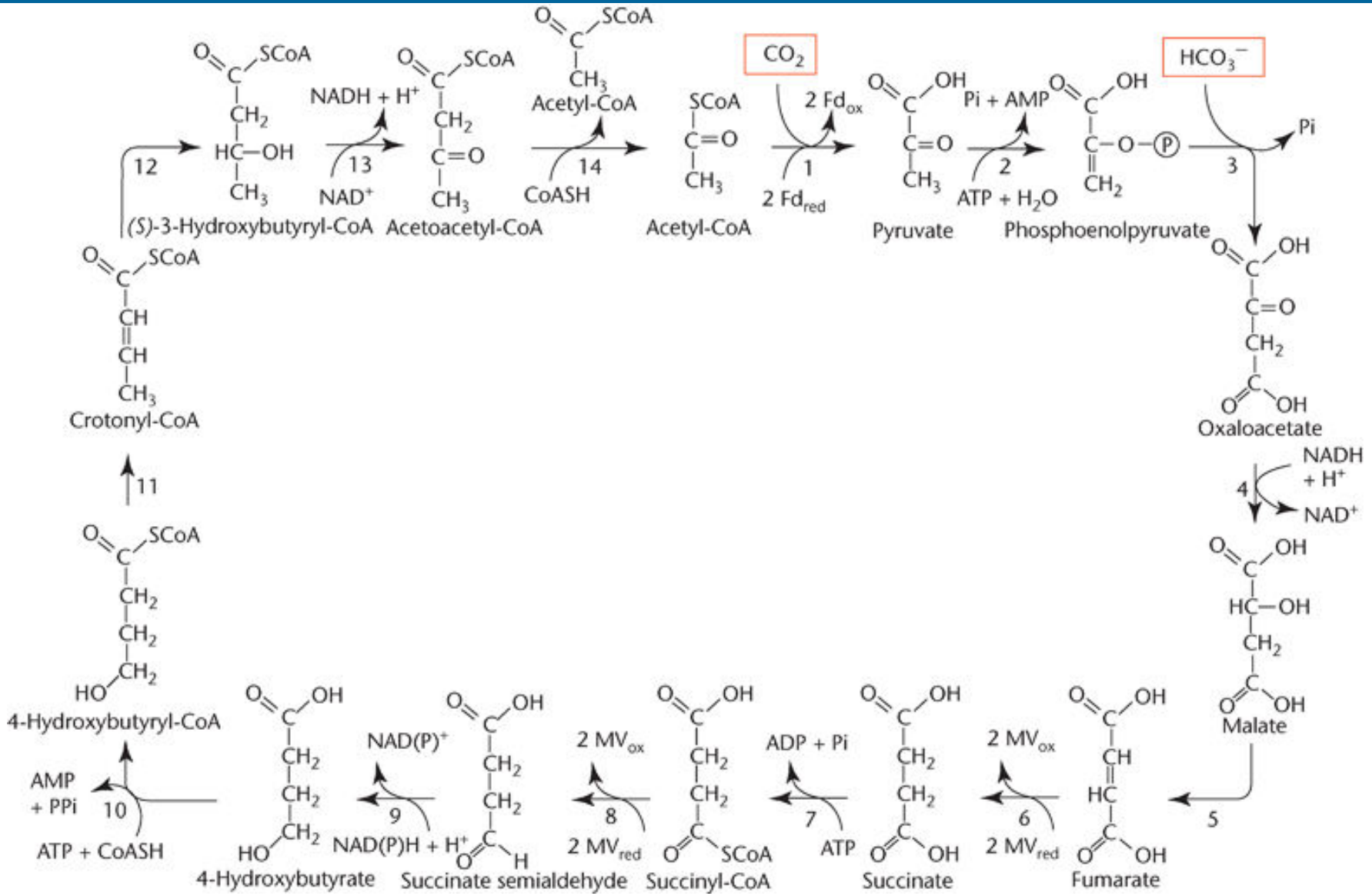

Diagram illustrating the reactions of the dicarboxylate/4-hydroxybutyrate cycle. The corresponding enzymes are: 1: pyruvate synthase, 2: pyruvate:water dikinase, 3: phosphoenolpyruvate carboxylase, 4: malate dehydrogenase, 5: fumarate hydratase, 6: fumarate reductase, 7: succinate thiokinase, 8: succinyl-CoA reductase, 9: succinate semialdehyde reductase, 10: 4-hydroxybutyryl-CoA synthetase, 11: 4-hydroxybutyryl-CoA dehydratase, 12: crotonyl-CoA hydratase, 13: 3-hydroxybutyryl-CoA dehydrogenase and 14: acetoacetyl-CoA β-ketothiolase. The directions of the arrows represent the direction of the pathway, and do not indicate that the enzyme reactions are irreversible

Sato & Atomi, 2010

Reductive hexulose-phosphate pathway

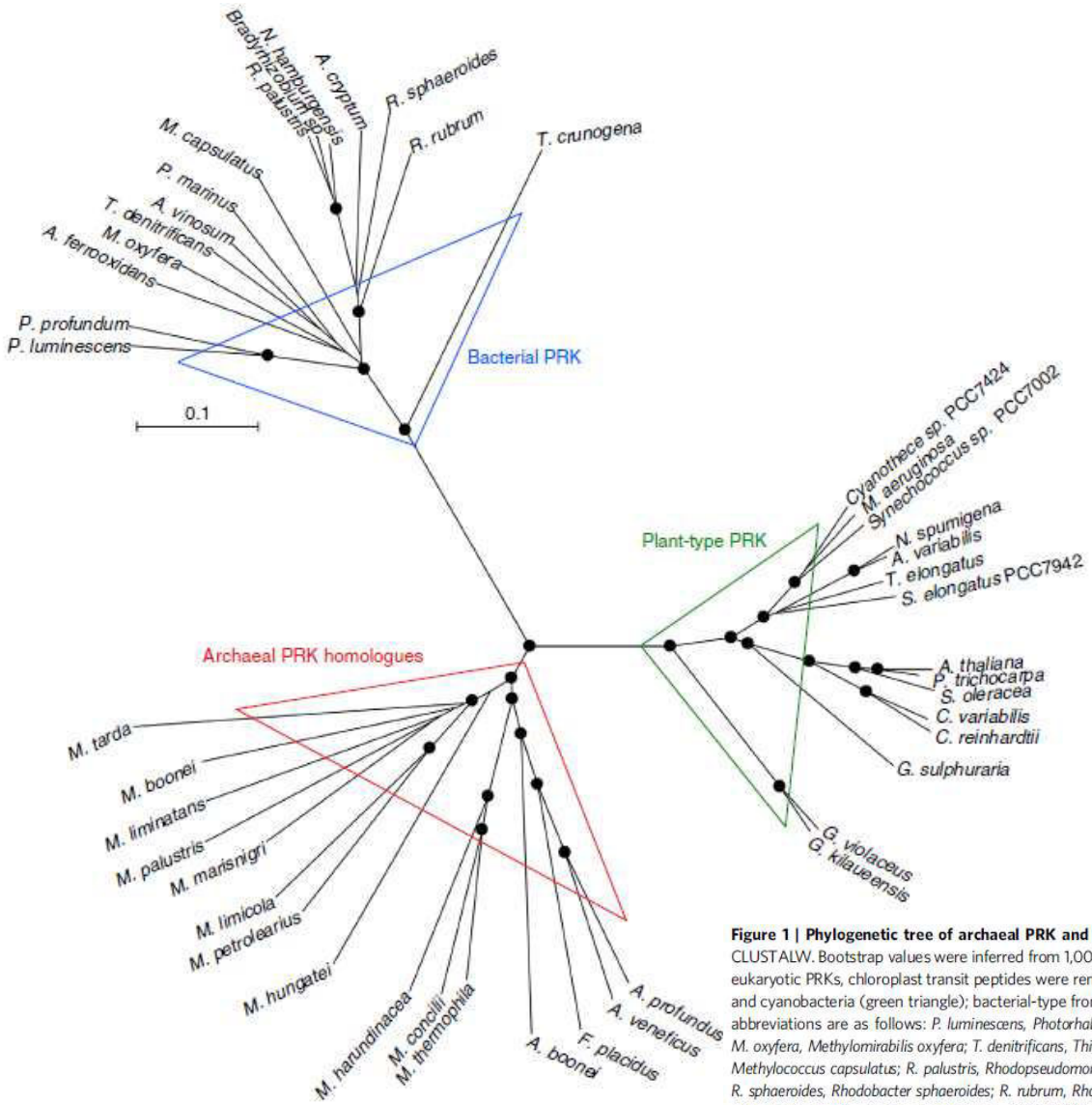

Figure 1 | Phylogenetic tree of archaeal PRK and photosynthetic PRK. The multiple sequence alignment and phylogenetic tree were produced using CLUSTALW. Bootstrap values were inferred from 1,000 replicates and significant bootstrapping values (>75%) are shown on the nodes as black filled circles. In eukaryotic PRKs, chloroplast transit peptides were removed according to ChloroP prediction[63]. PRKs are classified into three forms: plant-type from plants, algae and cyanobacteria (green triangle); bacterial-type from photosynthetic bacteria and chemoautotrophs (blue triangle); and archaeal-type (red triangles). Species abbreviations are as follows: *P. luminescens, Photorhabdus luminescens; P. profundum, Photobacterium profundum; A. ferrooxidans, Acidithiobacillus ferrooxidans; M. oxyfera, Methylomirabilis oxyfera; T. denitrificans, Thiobacillus denitrificans; A. vinosum, Allochromatium vinosum; P. marinus, Prochlorococcus marinus; M. capsulatus, Methylococcus capsulatus; R. palustris, Rhodopseudomonas palustris* BisA53; *N. hamburgensis, Nitrobacter hamburgensis; A. cryptum, Acidiphilium cryptum; R. sphaeroides, Rhodobacter sphaeroides; R. rubrum, Rhodospirillum rubrum; T. crunogena, Thiomicrospira crunogena; Cyanothece* sp. PCC 7424; *M. aeruginosa, Microcystis aeruginosa; Synechococcus* sp. PCC 7002; *A. variabilis, Anabaena variabilis; N. spumigena, Nodularia spumigena; T. elongatus, Thermosynechococcus elongatus; S. elongatus* PCC 7942, *Synechococcus elongatus* PCC 7942; *P. trichocarpa, Populus trichocarpa; A. thaliana, Arabidopsis thaliana; S. oleracea, Spinacia oleracea; C. variabilis, Chlorella variabilis; C. reinhardtii, Chlamydomonas reinhardtii; G. sulphuraria, Galdieria sulphuraria; G. violaceus, Gloeobacter violaceus; G. kilaueensis, Gloeobacter kilaueensis; M. marisnigri, Methanoculleus marisnigri; M. palustris, Methanosphaerula palustris; M. boonei, Methanoregula boonei; M. liminatans, Methanofollis liminatans; M. limicola, Methanoplanus limicola; M. petrolearius, Methanoplanus petrolearius; M. hungatei, Methanospirillum hungatei; M. tarda, Methanolinea tarda; M. concilii, Methanosaeta concilii; M. thermophile, Methanosaeta thermophila; M. harundinacea, Methanosaeta harundinacea; A. profundus, Archaeoglobus profundus; A. veneficus, Archaeoglobus veneficus; F. placidus, Ferroglobus placidus* and *A. boonei, Aciduliprofundum boonei.*

Kono *et al.*, 2016

Reductive hexulose-phosphate pathway

Table 1 | Enzymatic parameters of PRKs from archaea and photosynthetic organisms.

Species	V_{max}(μmol min^{-1}mg protein^{-1})	K_m(Ru5P) (mM)	K_m(ATP) (μM)
Methanospirillum hungatei (Archaeon)	29.28 ± 1.70	0.28 ± 0.05	20.70 ± 1.70
Methanoculleus marisnigri (Archaeon)	36.77 ± 3.09*	N.A.	N.A.
Methanosaeta thermophila (Archaeon)	19.10 ± 0.59	0.23 ± 0.05	5.66 ± 0.21
Methanosaeta concilii (Archaeon)	43.84 ± 2.84	0.31 ± 0.08	17.91 ± 2.02
Archaeoglobus profundus (Archaeon)	1.68 ± 0.06*	N.A.	N.A.
Spinacia oleracea (Plant)	410†	0.22†	62†
Synechococcus elongatus PCC 7942 (Cyanobacterium)	230‡	0.27‡	90‡
Rhodobacter sphaeroides (Bacterium)	338§	0.10§	550§
Halothiobacillus neapolitanus (Bacterium)	50‖	0.24‖	710‖

Data for archaeal PRKs in this study are means ± s.d. of three replicates. N.A., not analysed.
*Specific activity.
†Porter *et al.*[65]
‡Kobayashi *et al.*[49]
§ATP concentration at half-maximal rate, as calculated from fitting ATP saturation data to the Hill equation, Runquist and Miziorko[25].
‖MacElroy *et al.*[66]

Kono *et al.*, 2016

universität wien

Reductive hexulose-phosphate pathway

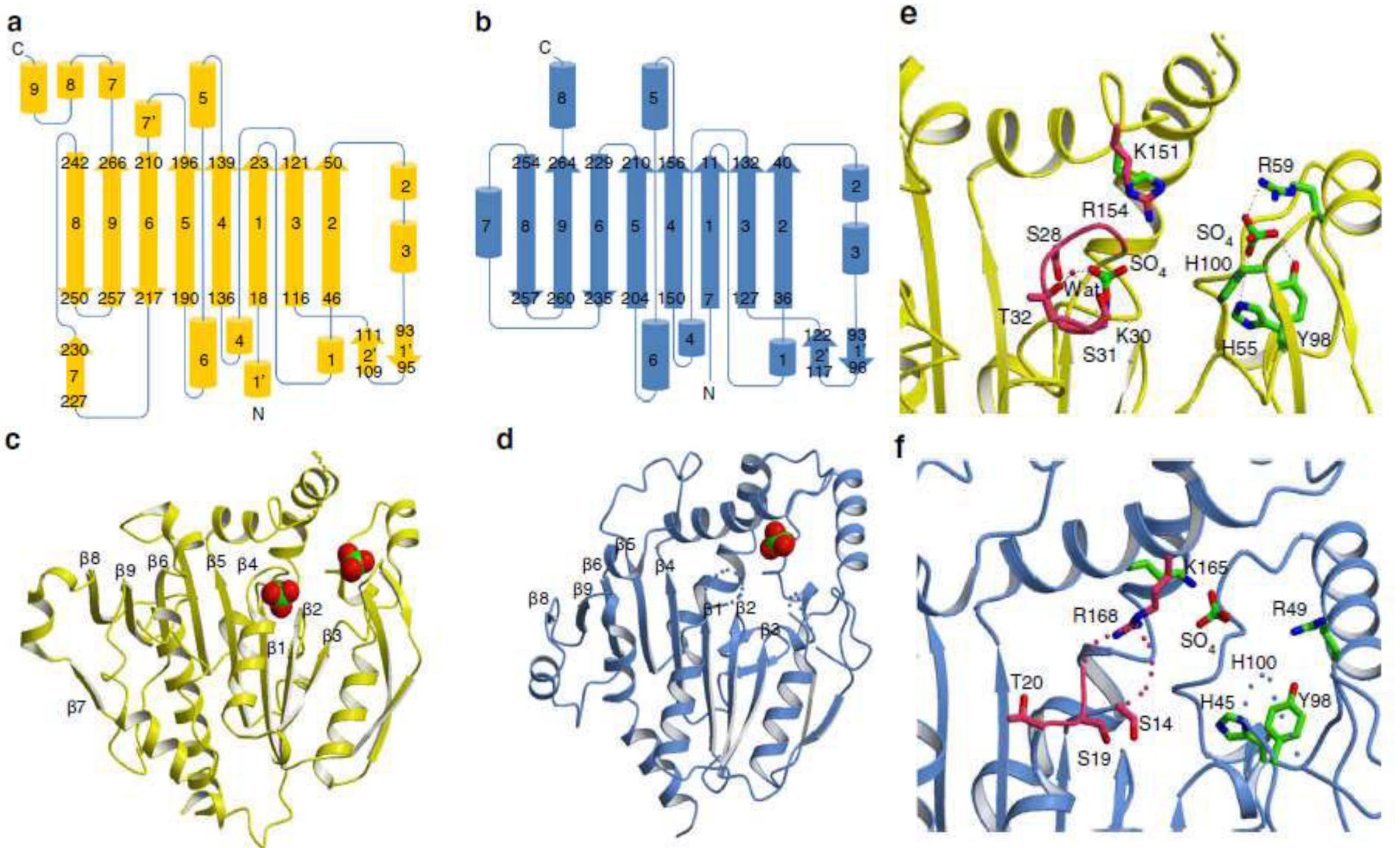

Structural comparison of archaeal and photosynthetic PRKs. (a,b) Topology diagrams of the folding patterns in protomers of (a) ***M. hungatei*** **PRK** (MhPRK) and (b) ***R. sphaeroides*** **PRK** (RsPRK) are shown in yellow and blue, respectively. a-helices are denoted by cylinders, b-sheets by arrows and connecting loops by lines. Positions in the sequence that start and end each major secondary structural element are shown. (c,d) Ribbon diagrams of (c) MhPRK (Protein Data Bank (PDB) ID 5B3F) monomer and (d) RsPRK (PDB ID 1A7J) monomer. Sulphate ions are bound to the active site of MhPRK and RsPRK. Disordered regions of missing electron density are shown as dots for residues for 156–163 in MhPRK, residues 15–17 corresponding to a part of the P-loop, and residues 100–105 in RsPRK. (e,f) Active-site structures of (e) MhPRK and (f) RsPRK. Side chains of residues involved in ATP- and Ru5P-binding are shown as pink and green sticks, respectively, with oxygen atoms in red and nitrogen atoms in blue. Sulphate ions are shown in MhPRK and RsPRK, with sulphur atoms in green, and oxygen and nitrogen atoms in the same colours as those in residue side chains. Small red balls represent water molecules. Disordered regions are shown as dots, and P-loop containing residues involved in ATP binding are shown in pink. Dotted lines show interactions of active site sulphate ions.

Kono *et al.*, 2016

Reductive hexulose-phosphate pathway

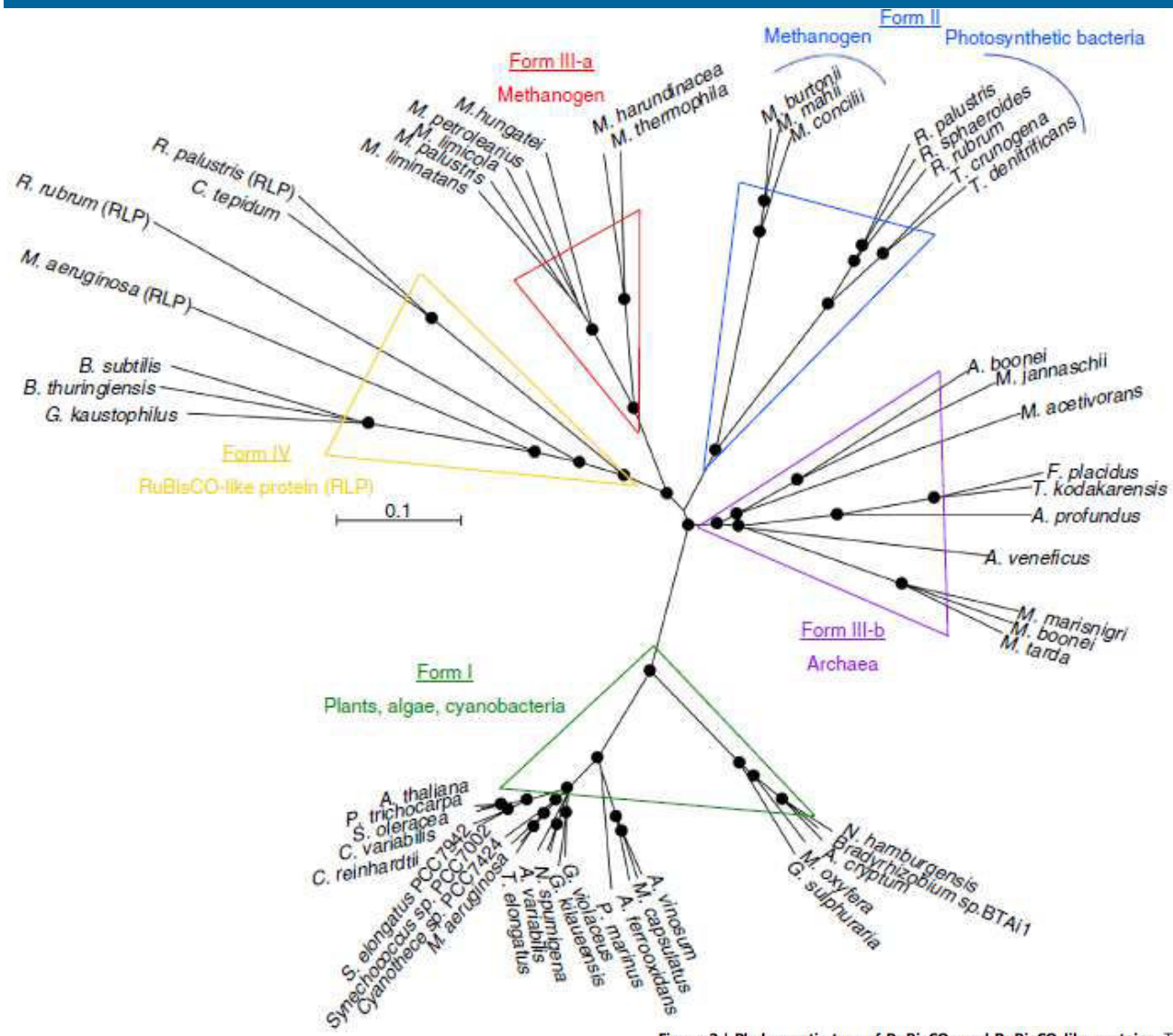

Figure 3 | Phylogenetic tree of RuBisCOs and RuBisCO-like proteins. The phylogenetic tree was produced using CLUSTALW. Bootstrap values were inferred from 1,000 replicates and significant bootstrapping values (>75%) are shown on the nodes as black filled circles. RuBisCO clades are indicated as follows: green for form I, blue for form II, red for form III-a and purple for form III-b (methanogenic archaea). We propose the latter two novel small clades because form III is prominently divided. The form IV clade of RuBisCO-like proteins (RLPs), which function as enolases/isomerases in methionine recycling in some bacteria, is shown in yellow[64]. Species abbreviations are as follows: *C. tepidum, Chlorobium tepidum; B. subtilis, Bacillus subtilis; G. kaustophilus, Geobacillus kaustophilus; B. thuringiensis, Bacillus thuringiensis; M. burtonii, Methanococcoides burtonii; M. mahii, Methanohalophilus mahii; M. jannaschii, Methanocaldococcus jannaschii; M. acetivorans, Methanosarcina acetivorans; T. kodakarensis, Thermococcus kodakarensis; R. palustris, Rhodopseudomonas palustris* and *N. spumigena, Nodularia spumigena.*

Kono *et al.*, 2016

Reductive hexulose-phosphate pathway

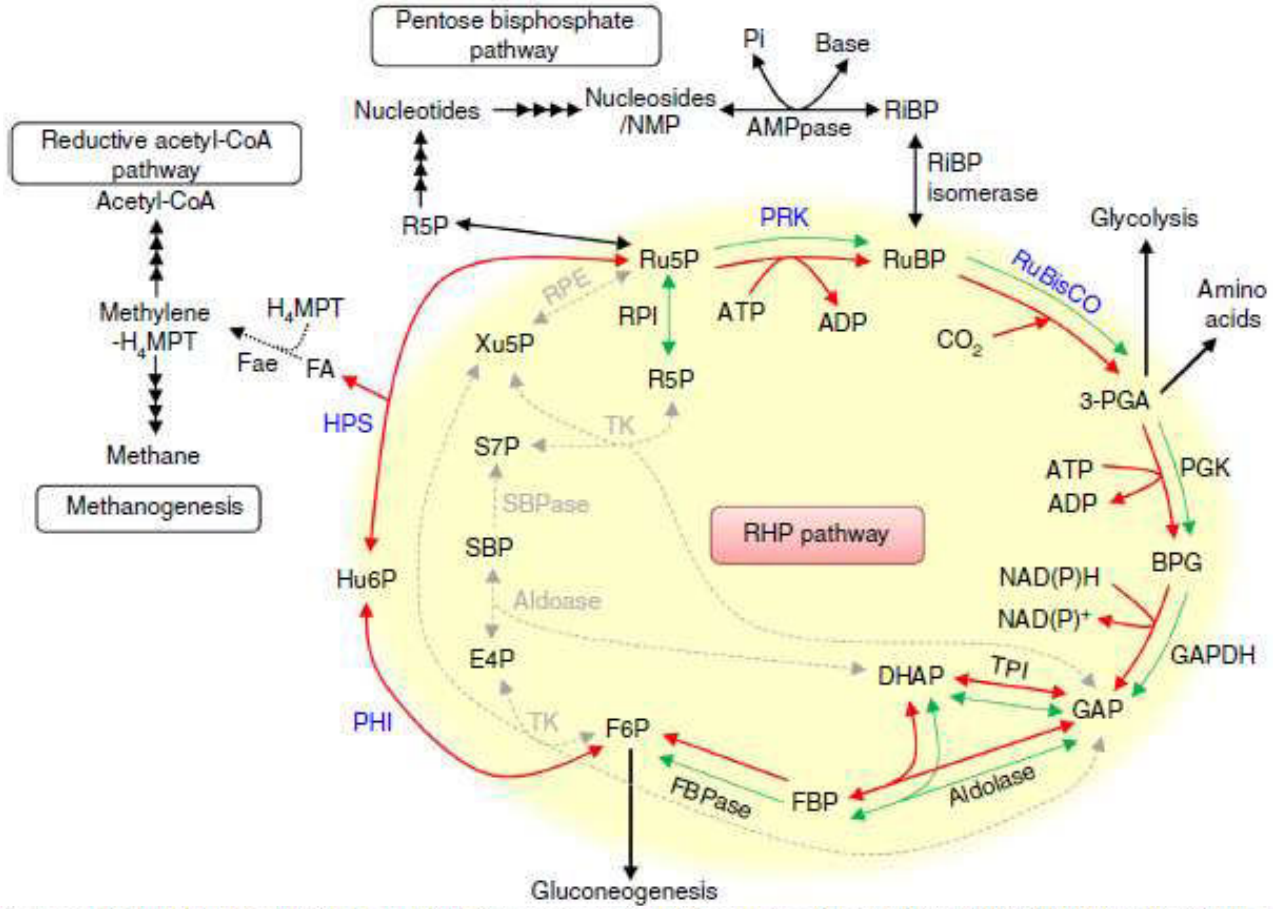

Figure 4 | Proposed RHP pathway and related metabolic processes in Archaea. The RHP pathway (highlighted in yellow) has metabolic links to methanogenesis, reductive acetyl-CoA pathway, pentose bisphosphate pathway, glycolysis, gluconeogenesis, and amino acid metabolism. Methanogenesis and reductive acetyl-CoA pathways share a metabolic intermediate, methylene-H_4MPT that might be synthesized by Fae with released formaldehyde from the RHP pathway (dotted black line). The successive black arrows show multiple reaction steps. The RHP pathway (red lines and arrows) is superimposed on the Calvin–Benson cycle (green lines and arrows), and reaction steps from Ru5P to F6P are common in both cycles. Missing Calvin–Benson-cycle steps in *M. hungatei* are indicated by grey dashed lines and arrows. Ru5P, ribulose-5-phosphate; RuBP, ribulose-1,5-bisphosphate; 3-PGA, 3-phosphoglycerate; BPG, 1,3-diphosphoglycerate; GAP, glyceraldehyde-3-phosphate; DHAP, dihydroxyacetone phosphate; FBP, fructose-1,6-bisphosphate; F6P, fructose-6-phosphate; Hu6P, D-arabino-3-hexulose-6-phosphate; FA, formaldehyde; E4P, erythrose-4-phosphate; Xu5P, xylulose-5-phosphate; SBP, sedoheptulose-1,7-bisphosphate; S7P, sedoheptulose-7-phosphate; R5P, ribose-5-phosphate; NMP, nucleoside 5′-monophosphate; RiBP, ribose-1,5-bisphosphate; H_4MPT, tetrahydromethanopterin; MF, methanofuran; PGK, 3-phosphoglycerate kinase; GAPDH, glyceraldehyde-3-phosphate dehydrogenase; FBPase, fructose-1,6-bisphosphatase; TK, transketolase; SBPase, sedoheptulose-1,7-bisphosphatase; RPE, ribulose-5-phosphate 3-epimerase; RPI, ribose-5-phosphate isomerase; AMPpase, AMP phosphorylase; RiBP isomerase, ribose-1,5-bisphosphate isomerase.

Kono *et al.*, 2016

universität wien

CO_2 fixation pathways

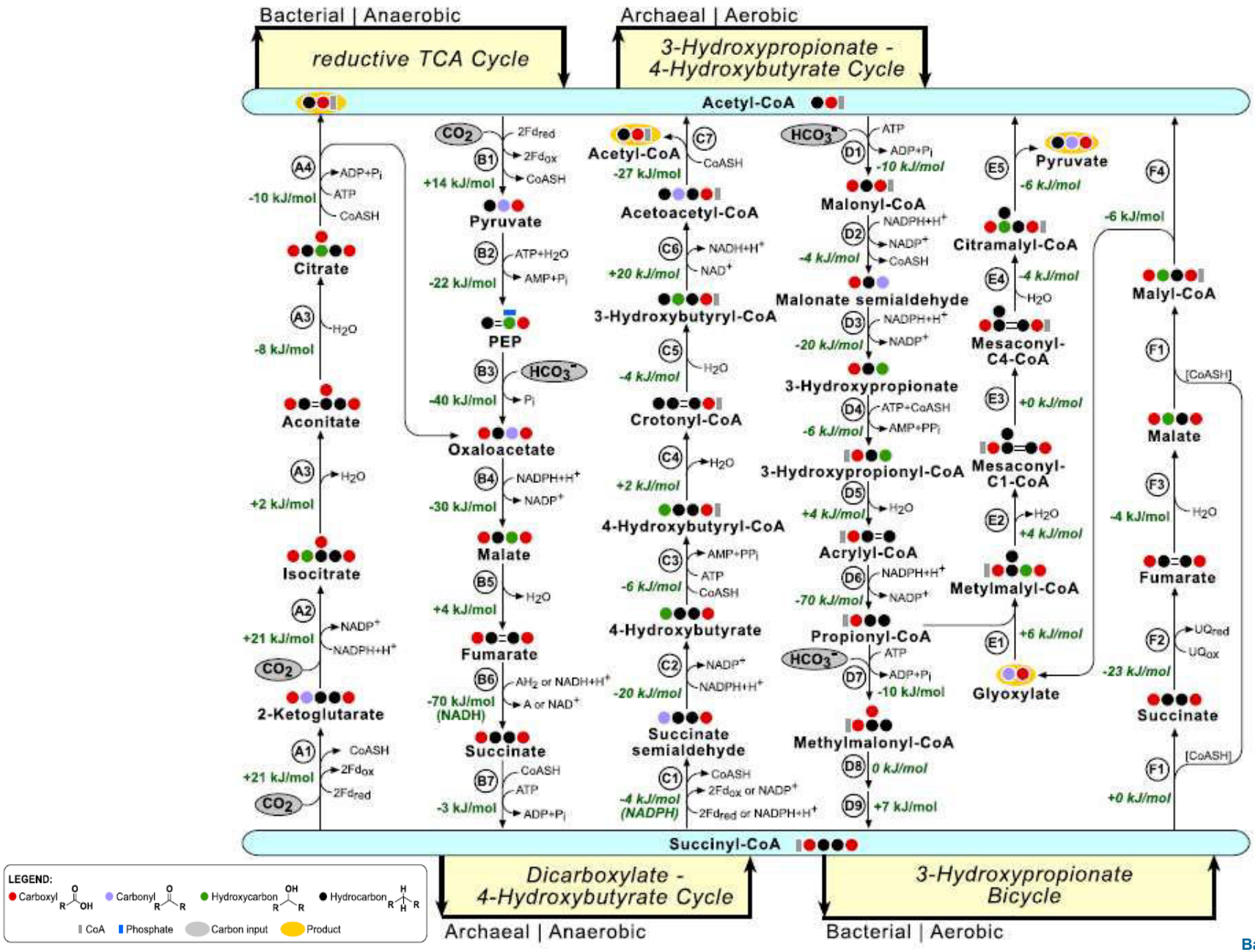

Bar-Even et al., 2012

Benefits of the different autotrophic pathways

Oxygen, metals and supply of C_1 compounds

Autotrophic **Euryarchaeota** are strictly confined to anoxic conditions, generally specialized in metabolizing C_1 compounds and/or acetate, and their energy metabolism has low ATP yields. Therefore, they need much of the C_1-transforming machinery for their energy metabolism. The reductive acetyl-coenzyme A (acetyl-CoA) pathway ideally copes with such constraints. Also, essential metals are more available under anoxic conditions owing to the higher solubility of the reduced forms of most metals.

In **Crenarchaeota**, the oxygen-sensitive dicarboxylate–hydroxybutyrate cycle is restricted to the anaerobic Thermoproteales and Desulfurococcales, whereas the oxygen-insensitive hydroxypropionate– hydroxybutyrate cycle is restricted to the mostly aerobic Sulfolobales and Thaumarchaeota. The two lifestyles presuppose different electron donors with different redox potentials and different oxygen sensitivity of cofactors and enzymes.

In a nutshell, energy cost-effective but oxygen-sensitive mechanisms cannot exist in aerobes because the enzymes would be inactivated by oxygen; and not all anaerobes have C_1 substrates at their disposal.

Berg et al., 2010

Benefits of the different autotrophic pathways

Energy demands

The different pathways require different amounts of ATP to make the cellular precursor metabolites. The costs for synthesizing all auxiliary, CO_2 fixation-related enzymes also differ, which might determine the energy costs involved. The synthesis of the catalysts itself can require a huge amount of energy as well as nitrogen and sulphur sources, especially if the pathways involve many auxiliary enzymes. Carboxylases with low catalytic efficiency must be synthesized in large amounts, as is the case for ribulose 1,5-bisphosphate carboxylase–oxygenase (RUBISCO). So, energy limitation exerts a strong selective pressure in favour of energy-saving mechanisms, and the energy costs are largely spent for the synthesis of autotrophy-related enzymes.

Berg et al., 2010

Table 4. Comparison of the energy efficiency of aerobic autotrophic CO_2 fixation cycles

1 mole precursor or 1 g biomass	Calvin–Benson cycle*	3-Hydroxypropionate bicycle	Crenarchaeal HP/HB cycle	Thaumarchaeal HP/HB cycle
Acetyl-CoA	7	7	6	4
Pyruvate	7	7	9–10†	5
Phosphoenolpyruvate	8	9	10–11†	7
Oxaloacetate	8	9	9–10†	6
2-Oxoglutarate	15	16	15–16†	10
Biomass (1 g)	0.12*	0.13	0.13–0.15†	0.09

The numbers represent moles of high-energy anhydride bonds of ATP required to form 1 mole of central precursor metabolite or of the main precursors for the synthesis of 1 g of dry biomass. For the details of calculations, see *SI Appendix, SI Text*. The estimated amount of the central metabolic precursors acetyl-CoA, pyruvate, phosphoenolpyruvate, oxaloacetate, and 2-oxoglutarate necessary for the synthesis of 1 g of dry cells was taken from ref. 42.
*Note that the costs of the oxygenase side reaction of the key enzyme of the Calvin–Benson cycle (ribulose 1,5-bisphosphate carboxylase) are not taken into account in this table. C_3 plants lose about 20% of fixed carbon in photorespiration (15, 37).
†The costs of the synthesis of pyruvate, phosphoenolpyruvate, oxaloacetate, and 2-oxoglutarate in *M. sedula* vary depending on the pathway of succinyl-CoA conversion to succinate (27).

Könnicke et al., 2015

Properties of the CO_2 fixation pathways

Pathway*	ATP equivalents for synthesis of one pyruvate	Reductants for synthesis of one pyruvate (10 [H])	CO_2-fixing enzymes	Active CO_2 species	Intermediates that can be used for biosynthesis	Carbon isotope fractionation‡	Key enzymes
Reductive pentose phosphate cycle (Calvin–Benson–Bassham cycle)	Seven	Five NADH or NADPH	RubisCO	CO_2	3-Phosphoglycerate, triose phosphates and sugar phosphates	−20 to −30 ‰[113,114]	RubisCO and phosphoribulokinase
Reductive citric acid cycle (Arnon–Buchanan cycle)	Two§	Two NADH or NADPH, one unknown donor‖ and two ferredoxin¶	2-Oxoglutarate synthase	CO_2	Acetyl-CoA, pyruvate, PEP, oxaloacetate, succinyl-CoA and 2-oxoglutarate	−2 to −12 ‰[115,116]	2-Oxoglutarate synthase and ATP-citrate lyase
			Isocitrate dehydrogenase	CO_2§			
			Pyruvate synthase	CO_2			
			PEP carboxylase	HCO_3^-			
Reductive acetyl-CoA pathway (Wood–Ljungdahl pathway)	Approx. one	Three ferredoxin¶ and two $F_{420}H_2$ (in methanogens)	Acetyl-CoA synthase–CO dehydrogenase	CO_2	Acetyl-CoA and pyruvate	< −30 ‰[83,115,117]	Acetyl-CoA synthase–CO dehydrogenase and enzymes reducing CO_2 to methyltetrahydropterin
			Formylmethanofuran dehydrogenase (in methanogens)	CO_2			
			Pyruvate synthase	HCO_2^-			
3-Hydroxypropionate bicycle	Seven	Six NADH or NADPH, but one FAD is reduced	Acetyl-CoA and propionyl-CoA carboxylase	HCO_3^-	Acetyl-CoA, pyruvate and succinyl-CoA	−12.5 to −13.7 ‰[118–120]	Malonyl-CoA reductase, propionyl-CoA synthase and malyl-CoA lyase
3-Hydroxypropionate–4-hydroxybutyrate cycle	Nine	Six NADH or NADPH, but one FAD is reduced	Acetyl-CoA and propionyl-CoA carboxylase	HCO_3^-	Acetyl-CoA and succinyl-CoA	−0.2 to −3.8[121]	Acetyl-CoA–propionyl-CoA carboxylase, enzymes reducing malonyl-CoA to propionyl-CoA, methylmalonyl-CoA mutase and 4-hydroxybutyryl-CoA dehydratase
Dicarboxylate–4-hydroxybutyrate cycle	Five	Two or three ferredoxin¶, one or two NADH or NADPH, and one unknown donor	Pyruvate synthase	CO_2	Acetyl-CoA, pyruvate, PEP, oxaloacetate and succinyl-CoA	−0.2 to −3.8[121]	4-Hydroxybutyryl-CoA dehydratase
			PEP carboxylase	HCO_3^-			

Berg et al., 2010; Bar-Even et al., 2012

Benefits of the different autotrophic pathways

Metabolic fluxes

In bacteria and archaea, the need for sugar phosphates in the biosynthesis of cell walls is lower than in plants, which also synthesize huge amounts of cellulose and lignin that is derived from erythrose 4-phosphate and phosphoenolpyruvate (PEP). The main metabolic fluxes are diverted from acetyl-CoA, pyruvate, oxaloacetate and 2-oxoglutarate, and their synthesis from 3-phosphoglycerate is partly connected with a loss of CO_2. Therefore, in bacteria autotrophic pathways directly yielding acetyl-CoA are more economical. Still, most facultative aerobic bacteria use the Calvin cycle, the regulation of which is almost detached from the central carbon metabolism and therefore may be particularly robust.

Berg et al., 2010

Benefits of the different autotrophic pathways

CO_2 species

As the bicarbonate (HCO_3^-) concentration in slightly alkaline water is much higher than the concentration of dissolved CO_2, autotrophs might profit from using bicarbonate instead of CO_2. The usage of bicarbonate is a special feature of PEP carboxylase and biotin-dependent carboxylases (that is, acetyl-CoA–propionyl-CoA carboxylase).

This property of PEP carboxylase is used in plants in the crassulacean acid and C_4 metabolism to increase the efficiency of photosynthesis. The same might be true for acetyl-CoA–propionyl-CoA carboxylase, and the higher bicarbonate concentration could potentially make up for a lower bicarbonate affinity.

Berg et al., 2010

Benefits of the different autotrophic pathways

Co-assimilation of organic compounds

Many autotrophic bacteria and archaea living in aquatic habitats probably encounter carbon oligotrophic conditions and grow as mixotrophs. Co-assimilation of traces of organic compounds might pay off. A complete or even a rudimentary hydroxypropionate–hydroxybutyrate cycle, for instance, allows the co-assimilation of numerous compounds. These include fermentation products and 3-hydroxypropionate, an intermediate in the metabolism of the ubiquitous osmoprotectant dimethylsulphoniopropionate. It is possible that various widespread marine aerobic phototrophic bacteria have genes encoding a rudimentary 3-hydroxypropionate cycle for that purpose. Similarly, the dicarboxylate– hydroxybutyrate cycle allows the co-assimilation of dicarboxylic acids and substrates that are metabolized through acetyl-CoA.

Berg et al., 2010

Microbial formate utilization

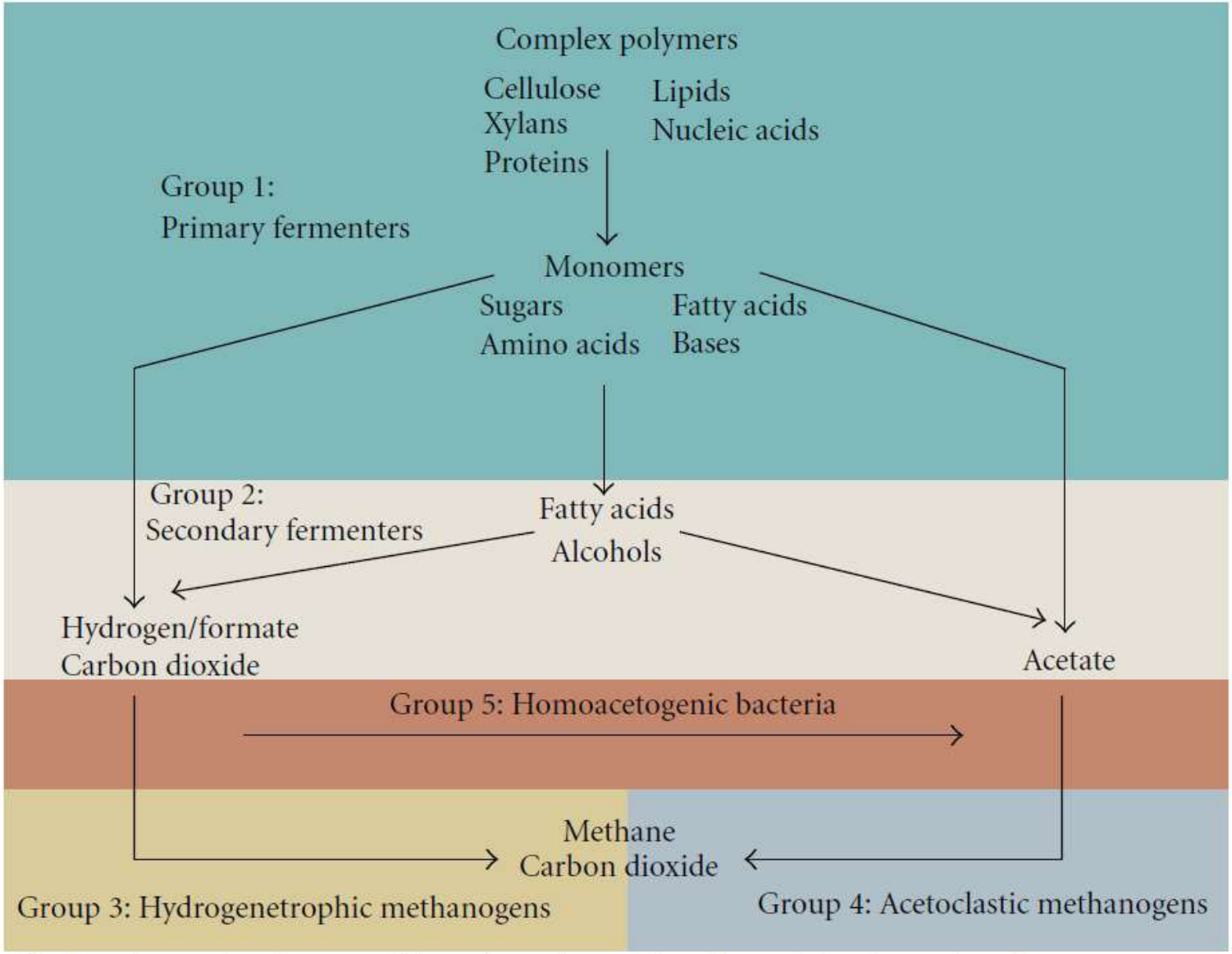

FIGURE 2: Carbon flux in methanogenic environments. Primary fermenting organisms (Group 1) degrade complex polymers to monomers, fatty acids, alcohols, hydrogen, carbon dioxide, acetate, and formate. Secondary fermenting organisms (Group 2) degrade fatty acids and alcohols to hydrogen, carbon dioxide, acetate, and formate. Hydrogenotrophic methanogens (Group 3) and acetoclastic methanogens (Group 4) convert carbon dioxide and formate or acetate to methane, respectively. For a more detailed discussion see accompanying text.

Crable et al. , 2011

Microbial formate utilization

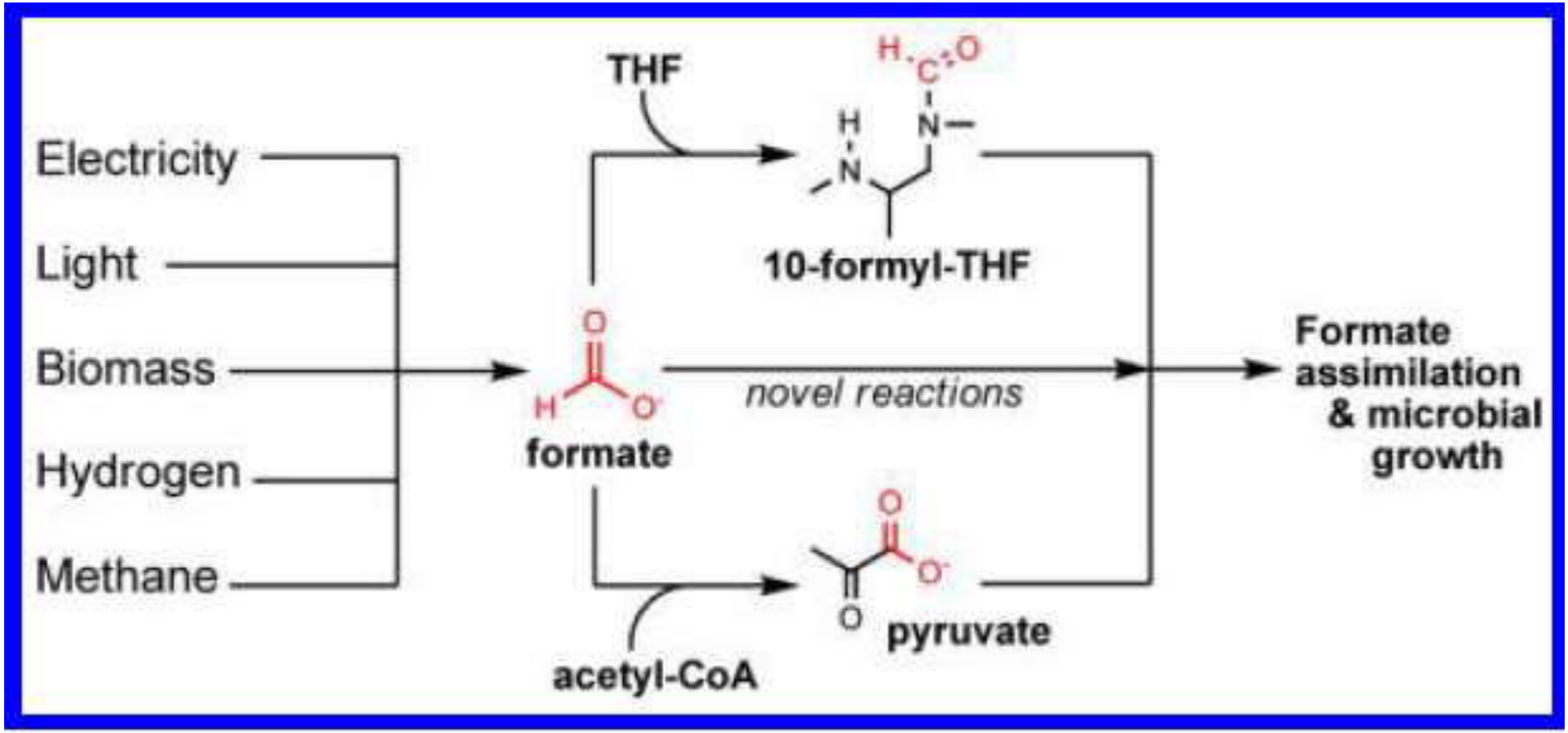

Bar-Even, 2016

Microbial formate utilization

$$HCOO^- + H^+ \rightarrow CO_2 + H_2 \quad \Delta G^{\circ\prime} = -3.4 \text{ kJ per mol}$$

Reaction conditions: pH 7,0; 1M concentration, gases at 1 atm

$$HCOO^- + H_2O \rightarrow HCO_3^- + H_2 \quad \Delta G^{\circ\prime} = +1.3 \text{ kJ per mol}$$

$$HCOO^- + OH^- \rightarrow H_2 + CO_3^{2-}$$

Schink et al., 2017

Microbial formate utilization

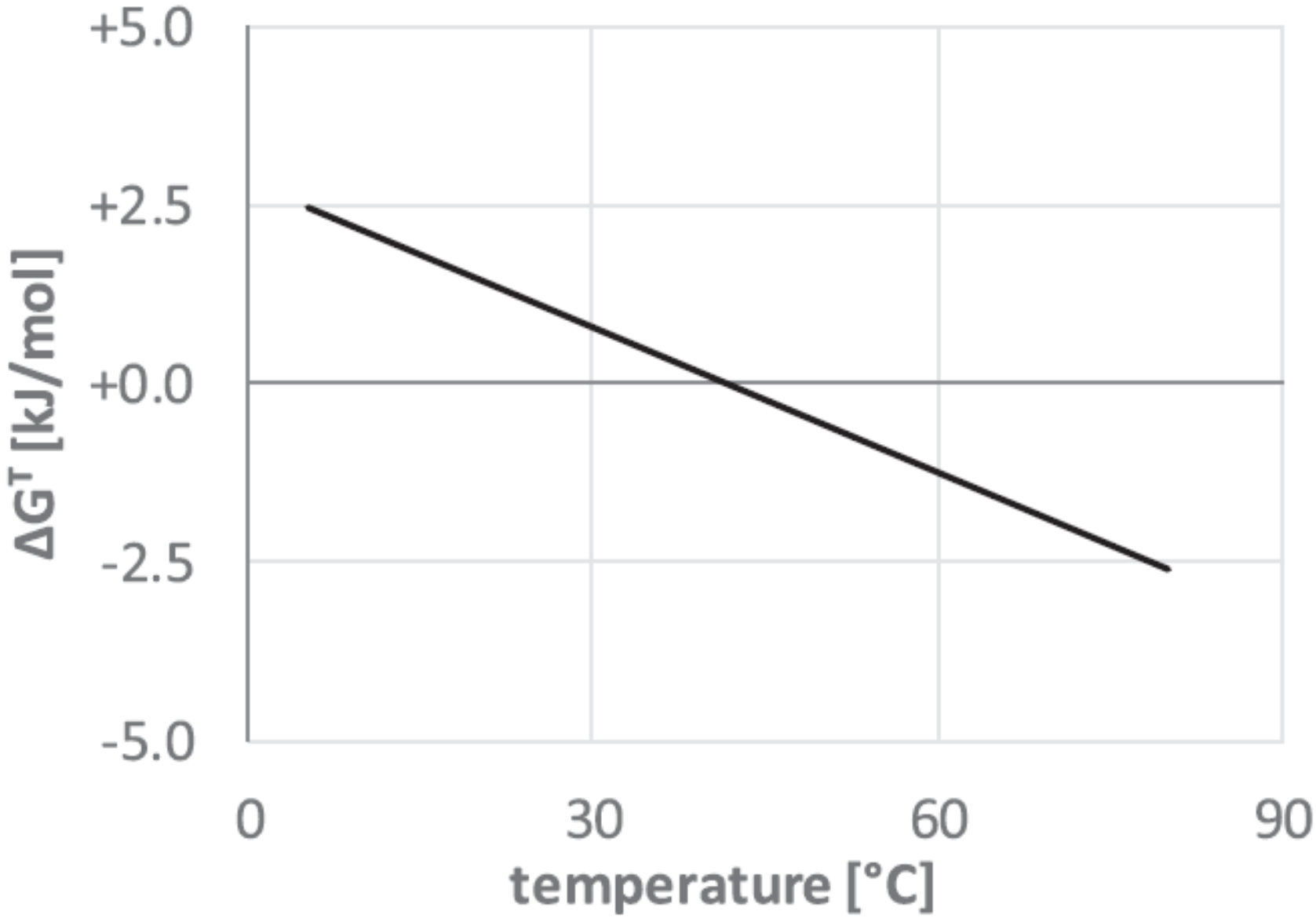

Fig. 2. Impact of temperature on Gibbs' free energy of formate-to-hydrogen conversion with HCO_3^- as reaction partner at pH 7.0.

Schink et al., 2017

Microbial formate utilization

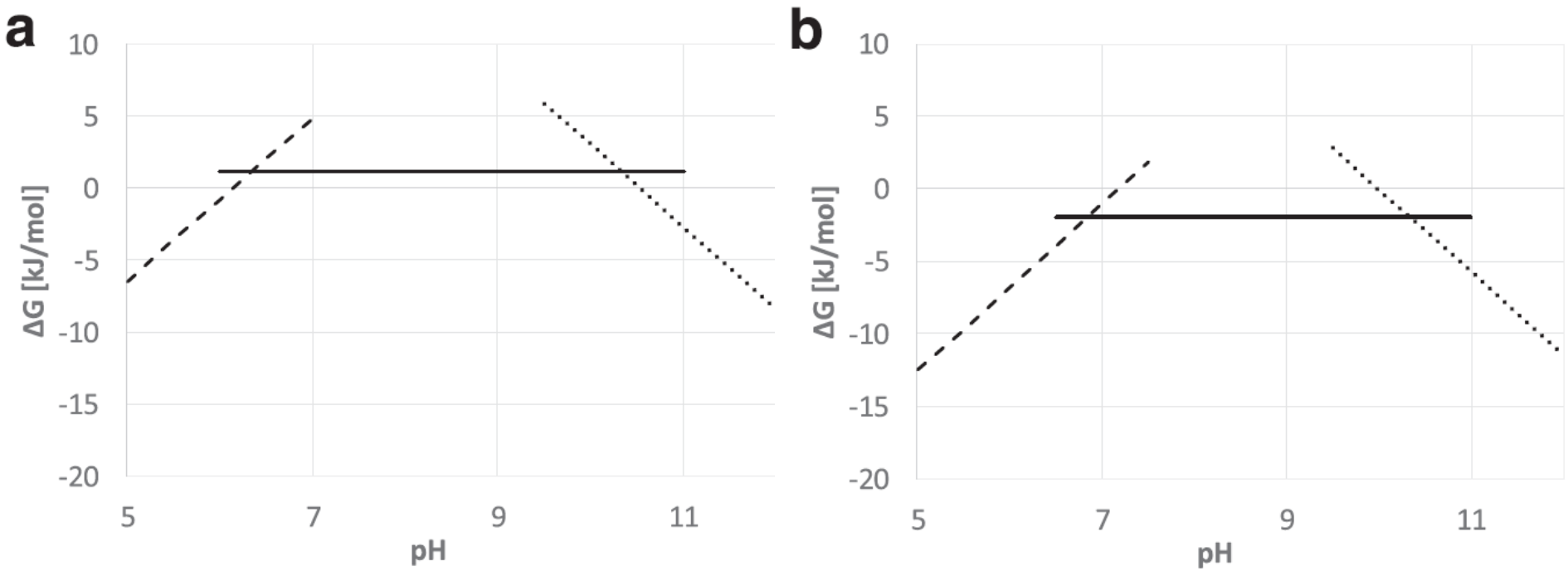

Fig. 1. Impact of pH on Gibbs' free energy of formate-to-hydrogen conversion; with CO_2 (dashed line) HCO_3^- (solid line) and CO_3^{2-} (dotted line) as reaction partner at 25°C, according to equations 1–3 for the respective pH ranges; a) standard conditions, except for pH; b) 'realistic' conditions in a sewage sludge digestor, with reactant activity $1 \cdot 10^4$ for hydrogen, $1 \cdot 10^5$ for formate, 0.2 for CO_2 and $2 \cdot 10^2$ for HCO_3^- and CO_3^{2-}.

Schink et al., 2017

Microbial formate utilization

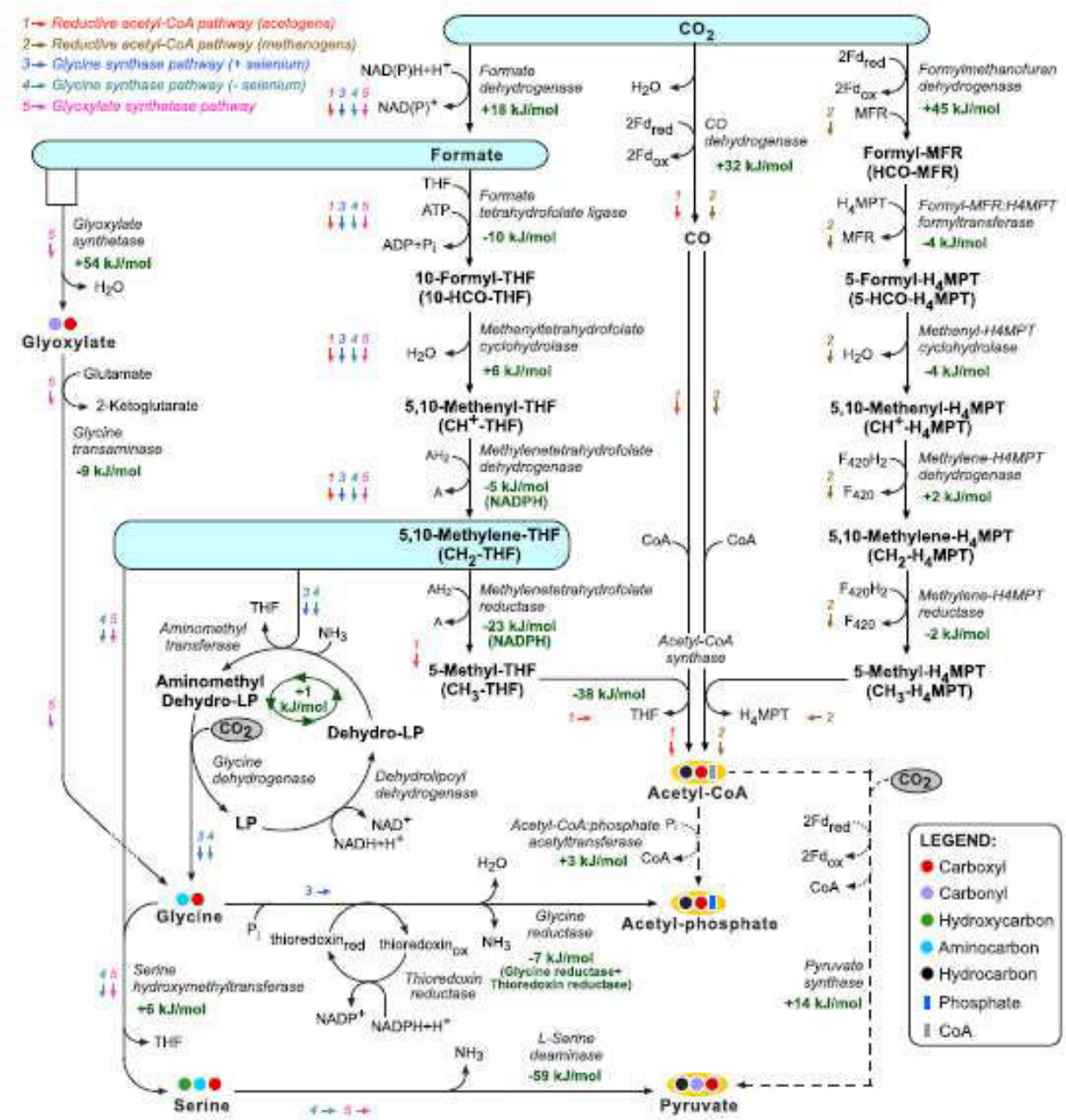

Bar-Even et al., 2012

Microbial formate utilization

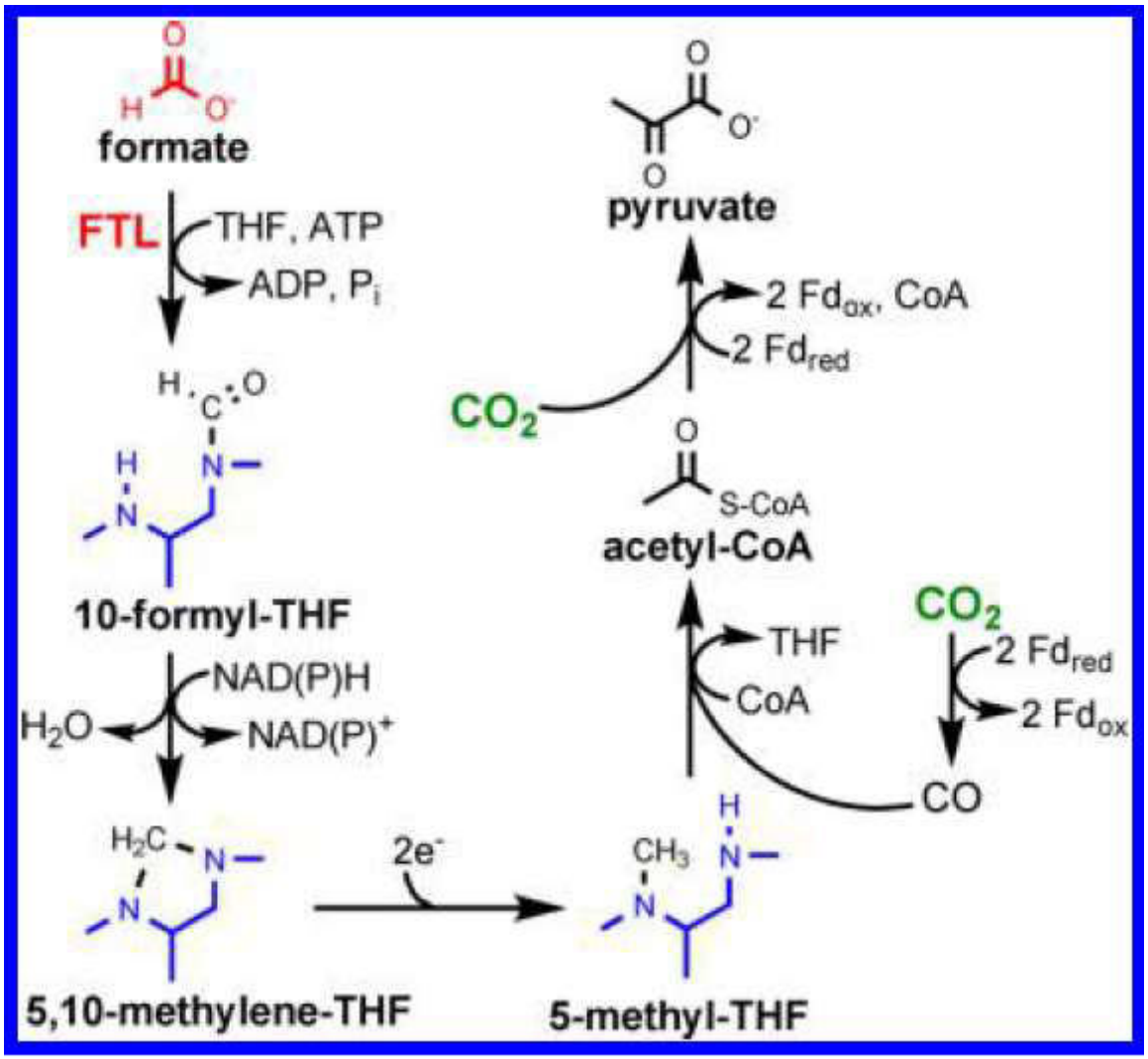

Reductive acetyl-CoA pathway

Figure 2. Reductive acetyl-CoA (Wood–Ljungdahl) pathway, a naturally occurring metabolic route for the assimilation of formate. Formate (colored red) is fixed by the enzyme formate-tetrahydrofolate ligase (FTL). A substructure of tetrahydrofolate (THF) is colored blue. Inorganic carbon, carbon dioxide in this case, is fixed during pathway activity (green).

Bar-Even, 2016

Microbial formate utilization

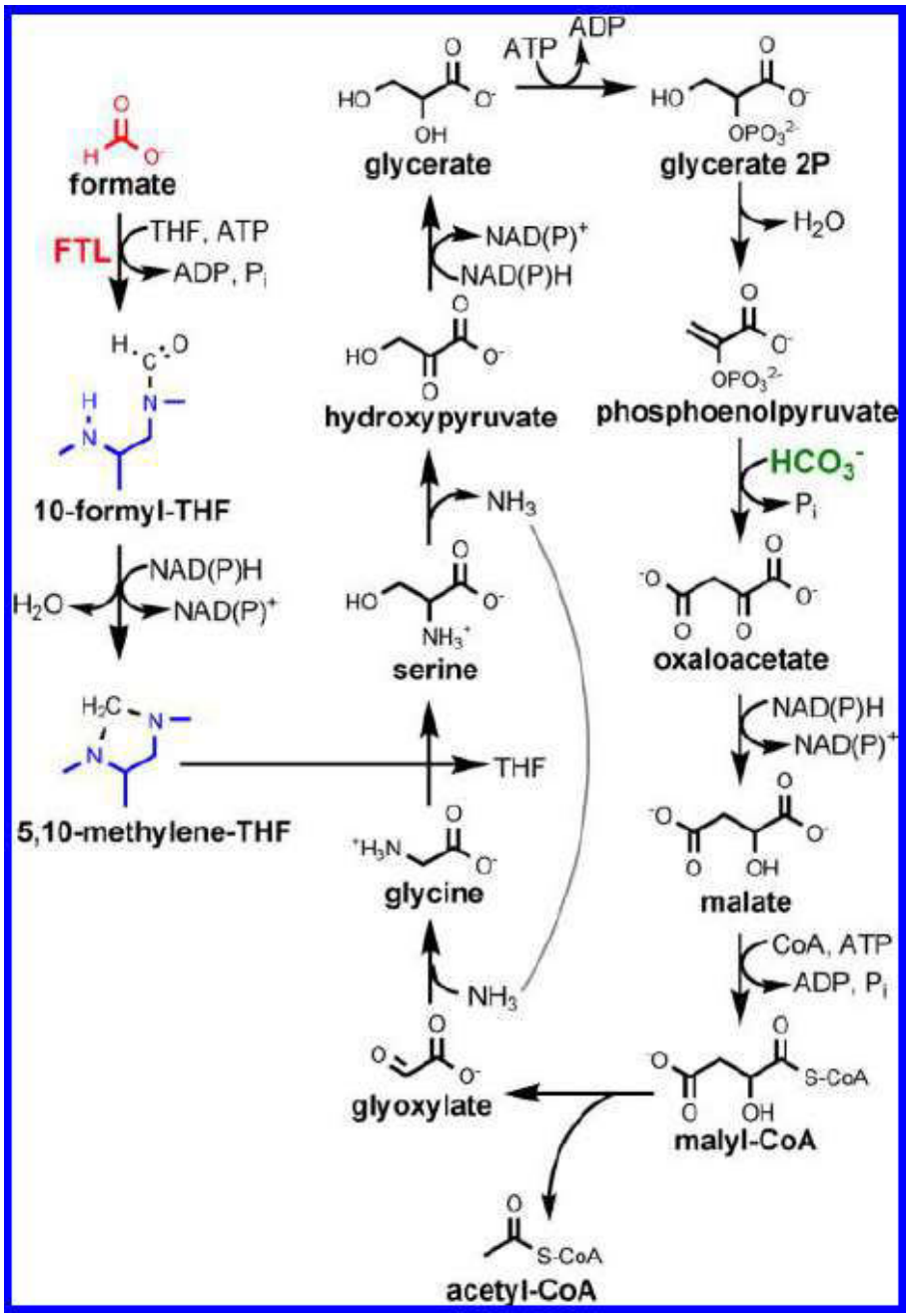

Serine cycle

Figure 1. Serine cycle, a naturally occurring metabolic route for the assimilation of formate. Formate (colored red) is fixed by the enzyme formate-tetrahydrofolate ligase (FTL). A substructure of tetrahydrofolate (THF) is colored blue. Inorganic carbon, bicarbonate in this case, is fixed during pathway activity (green). Acetyl-CoA is the cycle's product. The thin gray line corresponds to a transaminase reaction between serine and glyoxylate.

Bar-Even, 2016

Microbial formate utilization

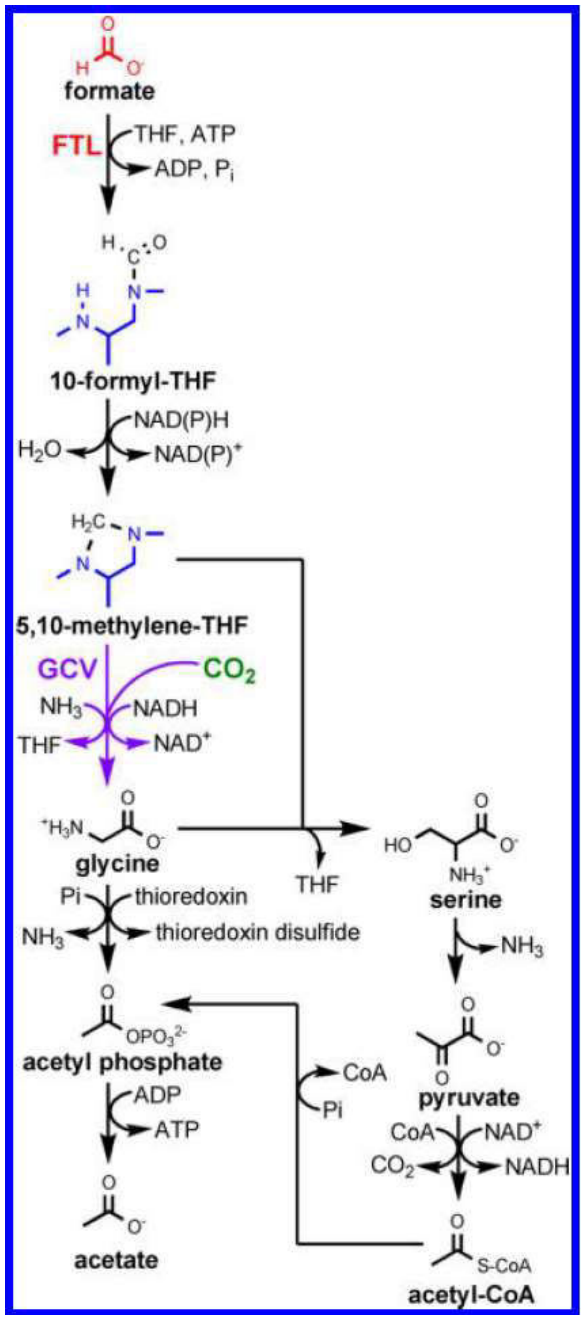

Reductive glycine pathway

Figure 3. Reductive glycine pathway, a naturally occurring metabolic route for the assimilation of formate. The glycine cleavage system is colored purple. The pathway has two variants. The left side shows the selenium-dependent glycine reductase route, while the right side shows the selenium-independent serine-pyruvate route. Formate (colored red) is fixed by the enzyme formate-tetrahydrofolate ligase (FTL). A substructure of tetrahydrofolate (THF) is colored blue. Inorganic carbon, carbon dioxide in this case, is fixed during pathway activity (green). Acetate is assumed as the product of both pathway variants.

Bar-Even, 2016

H_2 production from formate

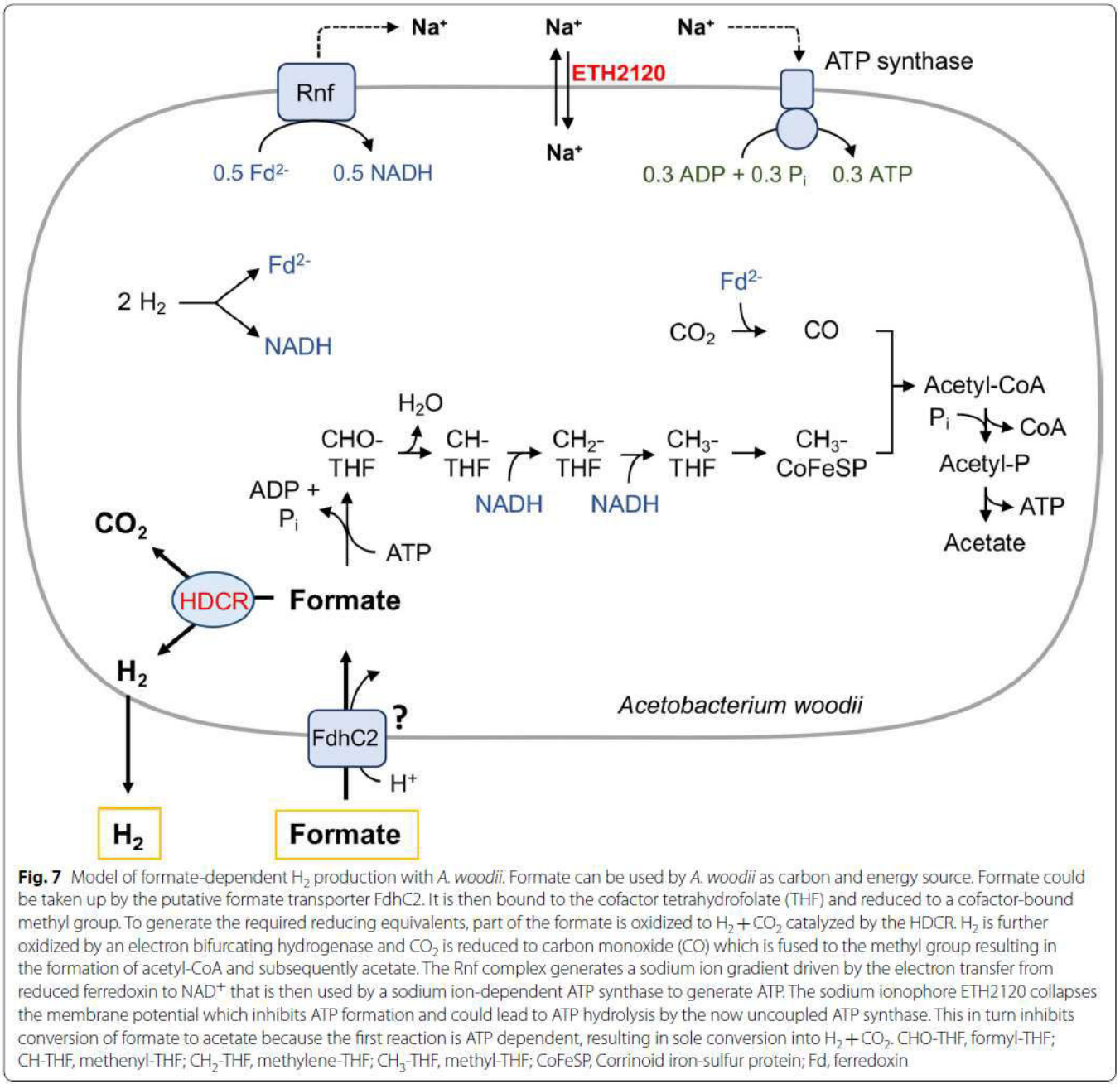

Fig. 7 Model of formate-dependent H_2 production with *A. woodii*. Formate can be used by *A. woodii* as carbon and energy source. Formate could be taken up by the putative formate transporter FdhC2. It is then bound to the cofactor tetrahydrofolate (THF) and reduced to a cofactor-bound methyl group. To generate the required reducing equivalents, part of the formate is oxidized to $H_2 + CO_2$ catalyzed by the HDCR. H_2 is further oxidized by an electron bifurcating hydrogenase and CO_2 is reduced to carbon monoxide (CO) which is fused to the methyl group resulting in the formation of acetyl-CoA and subsequently acetate. The Rnf complex generates a sodium ion gradient driven by the electron transfer from reduced ferredoxin to NAD^+ that is then used by a sodium ion-dependent ATP synthase to generate ATP. The sodium ionophore ETH2120 collapses the membrane potential which inhibits ATP formation and could lead to ATP hydrolysis by the now uncoupled ATP synthase. This in turn inhibits conversion of formate to acetate because the first reaction is ATP dependent, resulting in sole conversion into $H_2 + CO_2$. CHO-THF, formyl-THF; CH-THF, methenyl-THF; CH_2-THF, methylene-THF; CH_3-THF, methyl-THF; CoFeSP, Corrinoid iron-sulfur protein; Fd, ferredoxin

Kottenhahn et al., 2018

Microbial formate utilization

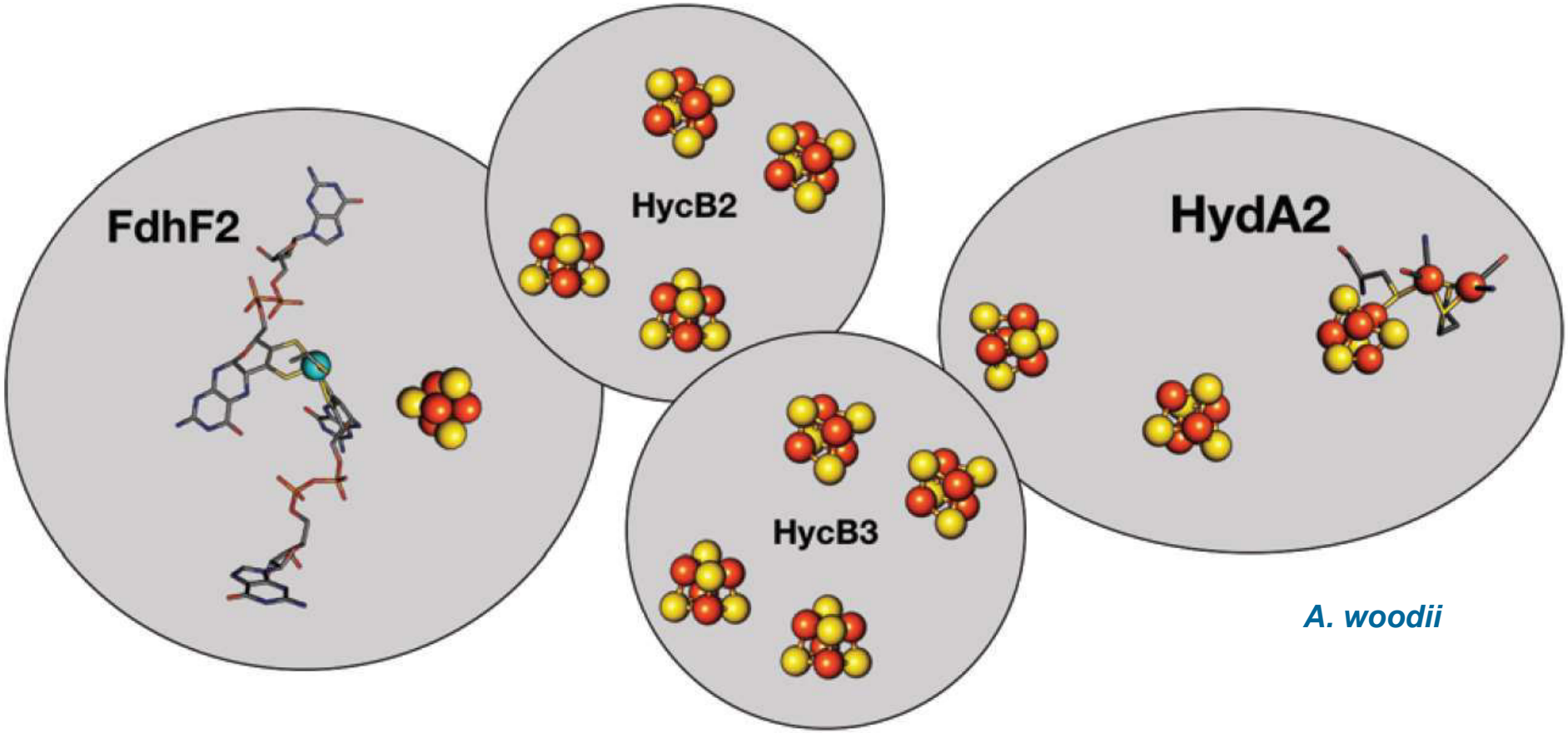

Fig. 1 Schematic representation of HDCR.[2] The formate dehydrogenase unit FdhF2 belongs to the bisPGD superfamily,[4] and the HydA2 subunit is a typical FeFe-hydrogenase, with two FeS clusters besides the active site. Depicted cluster numbers and stoichiometries are predicted on the basis of amino acid sequence.

Ceccaldi et al., 2017

H_2 production from formate

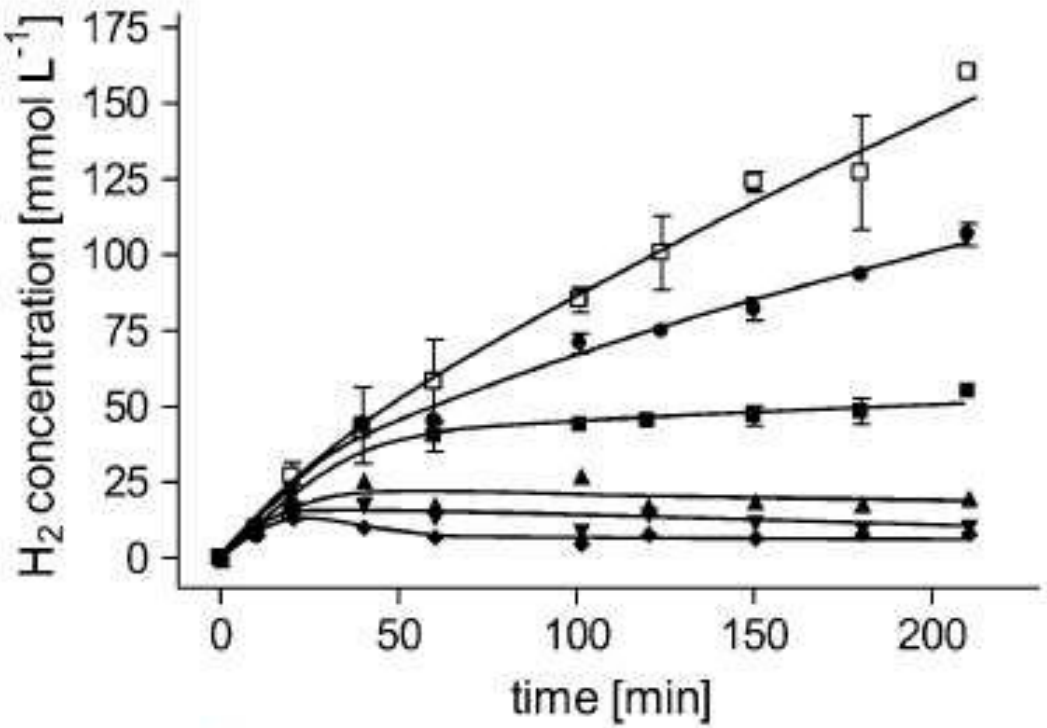

Fig. 4 Influence of the formate concentration on H_2 production. Cells were grown with 20 mM fructose, harvested in the exponential growth phase, and suspended in buffer (50 mM imidazole, 20 mM KCl, 20 mM $MgSO_4$, 30 µM ETH2120, 20 mM NaCl, 4 mM DTE, pH 7) to a final protein concentration of 1 mg mL^{-1} (corresponding to a CDW of 2.3 g L^{-1}). Experiments were started by the addition of 25 mM (diamonds), 50 mM (triangles down), 100 mM (triangles up), 200 mM (closed squares), 400 mM (circles), 600 mM formate (open squares)

Kottenhahn et al., 2018

H_2 production from formate

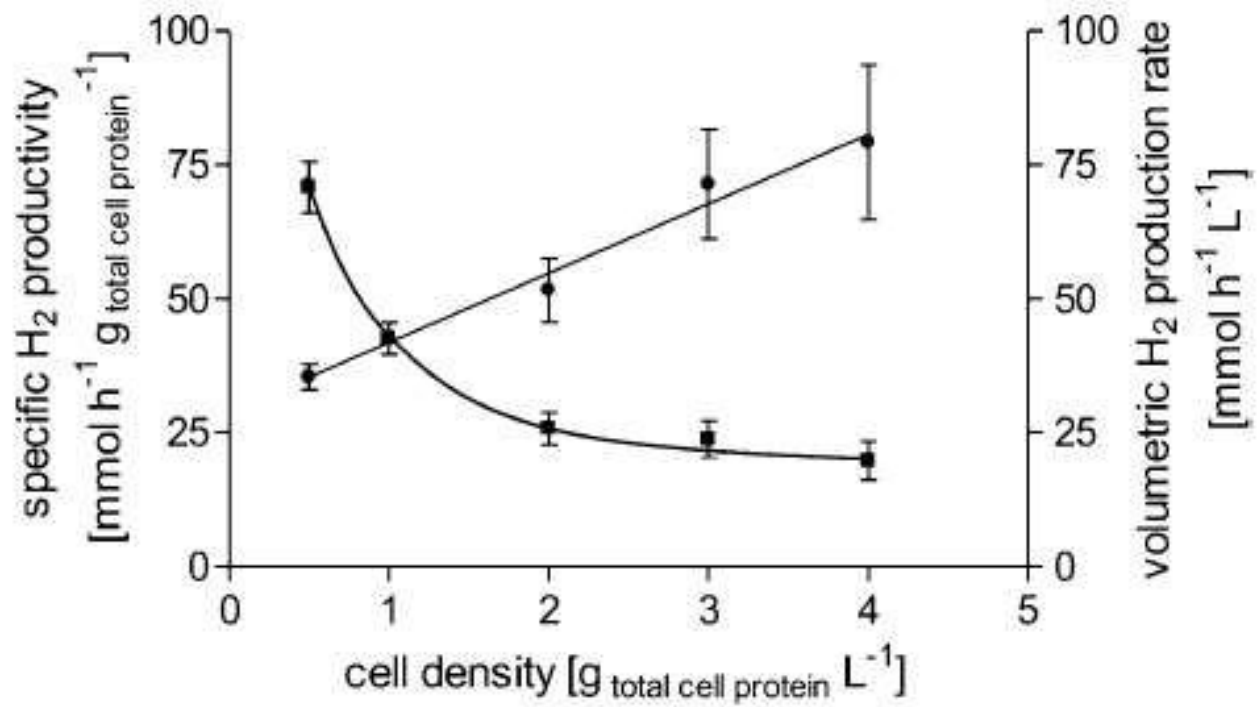

Fig. 3 Influence of the cell density on volumetric and specific H_2 production rates. Cells were grown with 20 mM fructose, harvested in the exponential growth phase, and suspended in buffer (50 mM imidazole, 20 mM KCl, 20 mM $MgSO_4$, 30 µM ETH2120, 20 mM NaCl, 4 mM DTE, pH 7) to a final protein concentration of 0.5–4 mg mL^{-1} (corresponding to a CDW of 1.2–9.7 g L^{-1}). Experiments were started by the addition of 100 mM sodium formate. Initial specific H_2 production rates (squares) or initial volumetric H_2 production rates (circles) are plotted against the cell density used

Kottenhahn et al., 2018

Microbial formate utilization

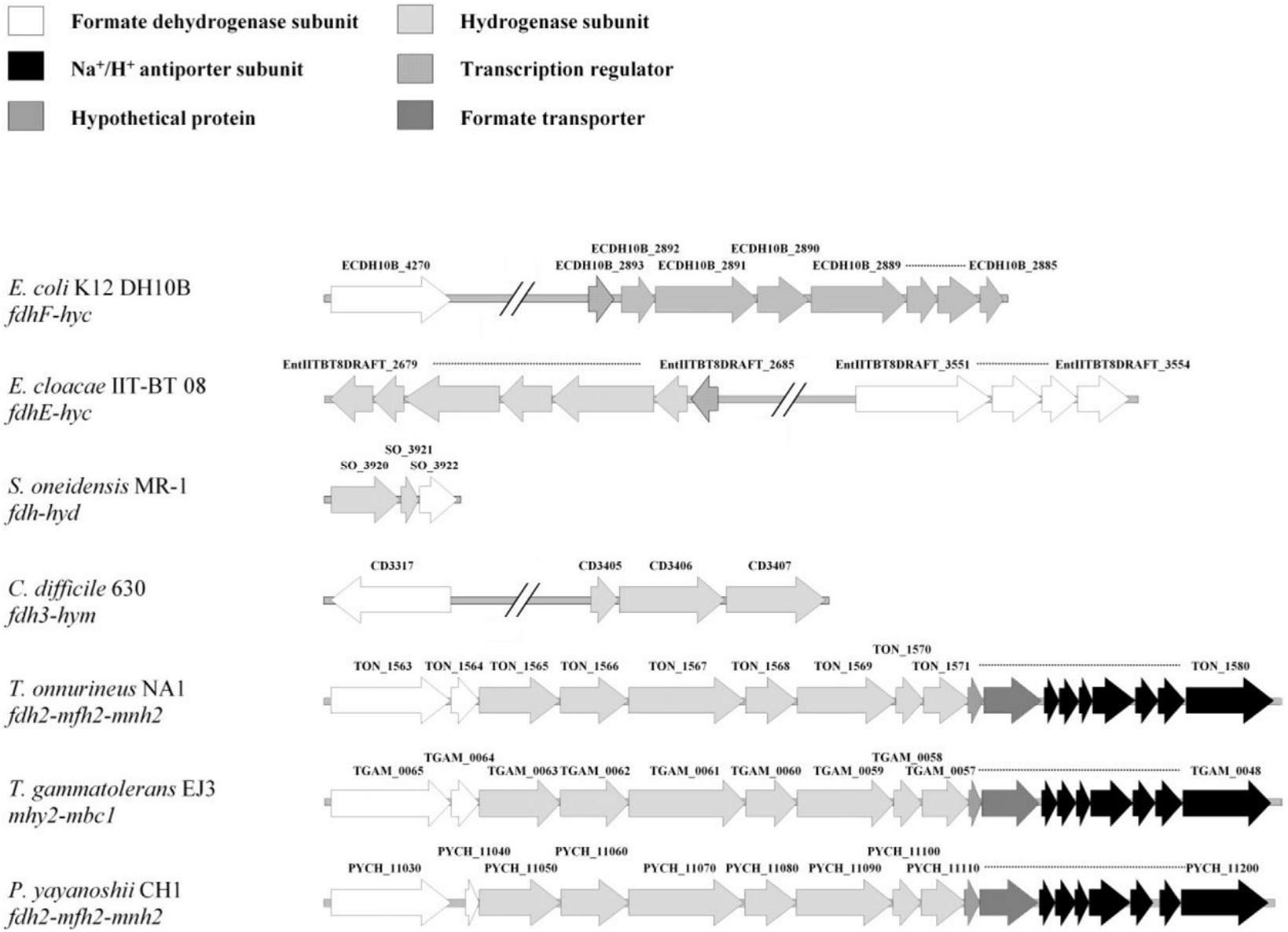

Fig. 1. Genetic organization of the genes encoding the FHL complex subunits in *Escherichia coli* K12 DH10B, *Enterobacter* sp. IIT-BT 08 (MTCC 5373, DSM 24603) (Khanna et al., 2013), *Shewanella oneidensis* MR-1 (Heidelberg et al., 2002), *Clostridium difficile* 630 (Köpke et al., 2013), *Thermococcus onnurineus* NA1 (Lee et al., 2008), *Thermococcus gammatolerans* (Zivanovic et al., 2009), and *Pyrococcus yayanoshii* CH1 (Jun et al., 2011). The locus tags of the genes are shown at the center of the genes.

Rittmann et al. , 2015

Microbial formate utilization

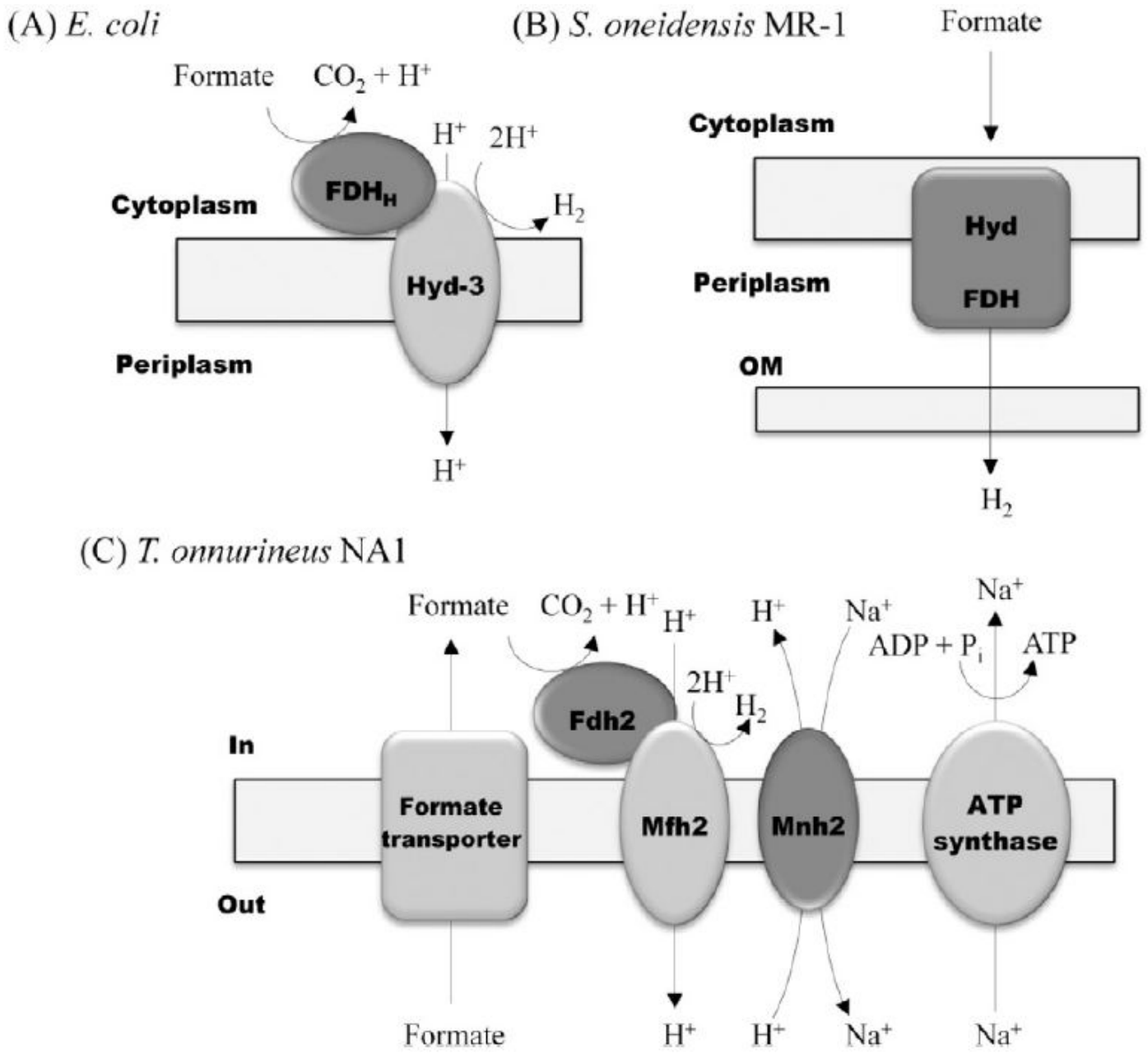

Rittmann et al. , 2015

universität wien

H_2 production from formate

Strain	Isolation site	H_2 production	growth
T. gammatolerans	Hydrothermal chimney samples from the Guaymas basin	+	+
T. alcaliphilus	Shallow marine hydrothermal system from Vulcano	–	–
T. celer	Solfataric marine water holes from Vulcano	–	–
T. chitonophagus	Hydrothermal vent off the Mexican west coast	–	–
T. profundus	Deep-sea thermal vent from the middle Okinawa trench	–	–
T. peptonophilus	Izu-Bonin arc	–	–
T. stetteri	Marine volcanic crater fields from Kraternya cove	–	–
T. sibiricus	Oil wells in western Siberia	–	–
T. onnurineus NA1	Deep-sea hydrothermal vent in the PACMANUS field	+	+
T. barophilus Ch5	Deep-sea hydrothermal field on the Mid-Atlantic Ridge	+	+
Thermococcus sp. DS-1	Hydrothermal field on the East Pacific Rise	+	+
Thermococcus sp. DT-4	Deep-sea hot vents from the southern Pacific basin	+	+
T. litoralis Sh1B	Shallow water hot vent off the Kuril Islands	–	–
T. stetteri K1A	Shallow water hot vent off the Kuril Islands	–	–
Thermococcus sp. AM4	Deep-sea hot vent on the East Pacific Rise	–	–
Thermococcus sp. Ch1	Hydrothermal structures on the Mid-Atlantic Ridge	–	–

Kim *et al.*, 2010

universität wien

H_2 production from formate

Strain	Strategy	HER [mmol L^{-1} h^{-1}]	Reference
Cupriavidus necator ATCC 17699	Immobilization of cells	5.8	Klibanov et al., 1982
Salmonella enterica	Closed batch mode	0.3	Pakes and Jollyman, 1901
Escherichia coli SH5	Fed-batch mode with immobilized cells	73.3	Seol et al., 2011
Escherichia coli SR13	*hycA* disruption and *fhlA* overexpression	11625	Yoshida et al., 2005
Clostridium butyricum IFO 3847t1	Addition of co-substrate mannitol	0.21	Heyndrickx et al., 1989
Desulfovibrio vulgaris Hildenborough	Optimization of reaction conditions	0.67	Martins and Pereira, 2013
Thermococcus onnurineus NA1	Use of high cell density	2820	Lim et al., 2012
Acetobacterium woodii DSM 1030	Resting cell system	80	Kottenhahn et al., 2018

HER: hydrogen evolution rate

Rittmann *et al*. (2012) Microbial Cell Factories
Rittmann *et al*. (2015) Biotechnology Advances
Ergal *et al*. (2018) Biotechnology Advances

Microbial formate utilization

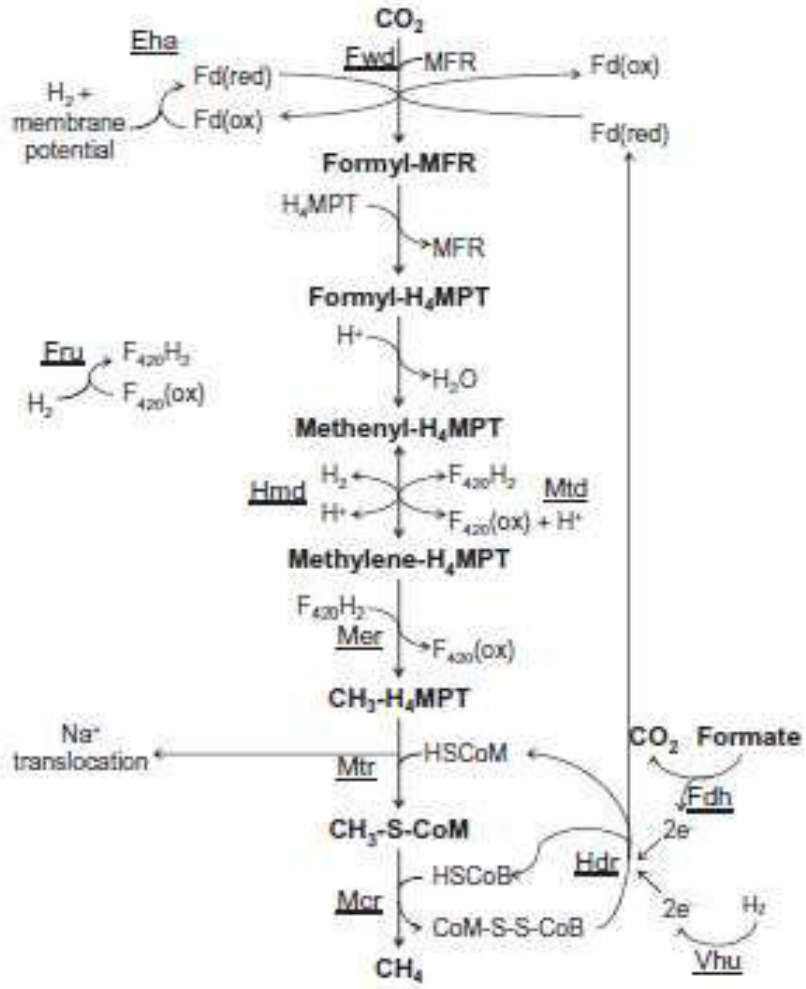

Fig. 1. The methanogenic pathway with hypothesized roles for the heterodisulfide reductase complex. Electron flow from formate or hydrogen to Hdr may drive the reduction of the CoM-S-S-CoB heterodisulfide, as well as the reduction of ferredoxin via flavin-mediated electron bifurcation as outlined by Thauer et al. (1). Eha, energy-conserving hydrogenase; Fdh, formate dehydrogenase; Fru, F_{420}-reducing hydrogenase; Fwd, formyl-MFR dehydrogenase; Hdr, heterodisulfide reductase; Hmd, H_2-dependent methylene-H_4MPT dehydrogenase; Mcr, methyl-CoM reductase; Mer, methylene-H_4MPT reductase; Mtd, F_{420}-dependent methylene-H_4MPT dehydrogenase; Mtr, methyl-H_4MPT-CoM methyltransferase; Vhu, F_{420}-nonreducing hydrogenase.

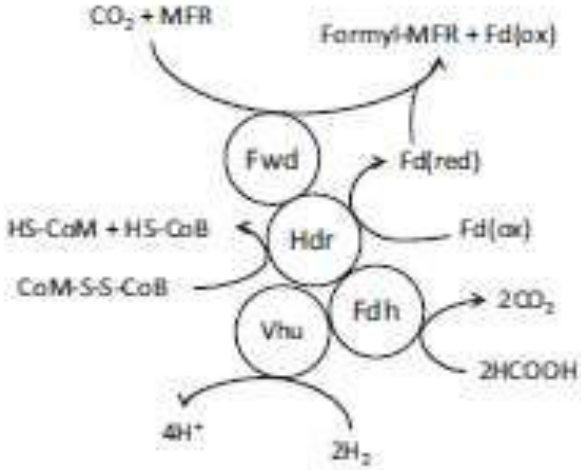

Fig. 3. Model of complex of proteins that interact with Hdr. When H_2 is used as the electron donor for methanogenesis, electrons are transferred to Hdr via Vhu. Flavin-mediated electron bifurcation at HdrA then results in reduction of the CoM-S-S-CoB heterodisulfide and a ferredoxin that is used by Fwd for the first step in methanogenesis. When hydrogen is limiting or is replaced by formate, Fdh is highly expressed (10) and incorporates into the complex. When formate is used as the electron donor for methanogenesis, electrons are transferred to Hdr from formate via Fdh. Fd(red), reduced ferredoxin; Fd(ox), oxidized ferredoxin.

Costa et al., 2010

Microbial formate utilization

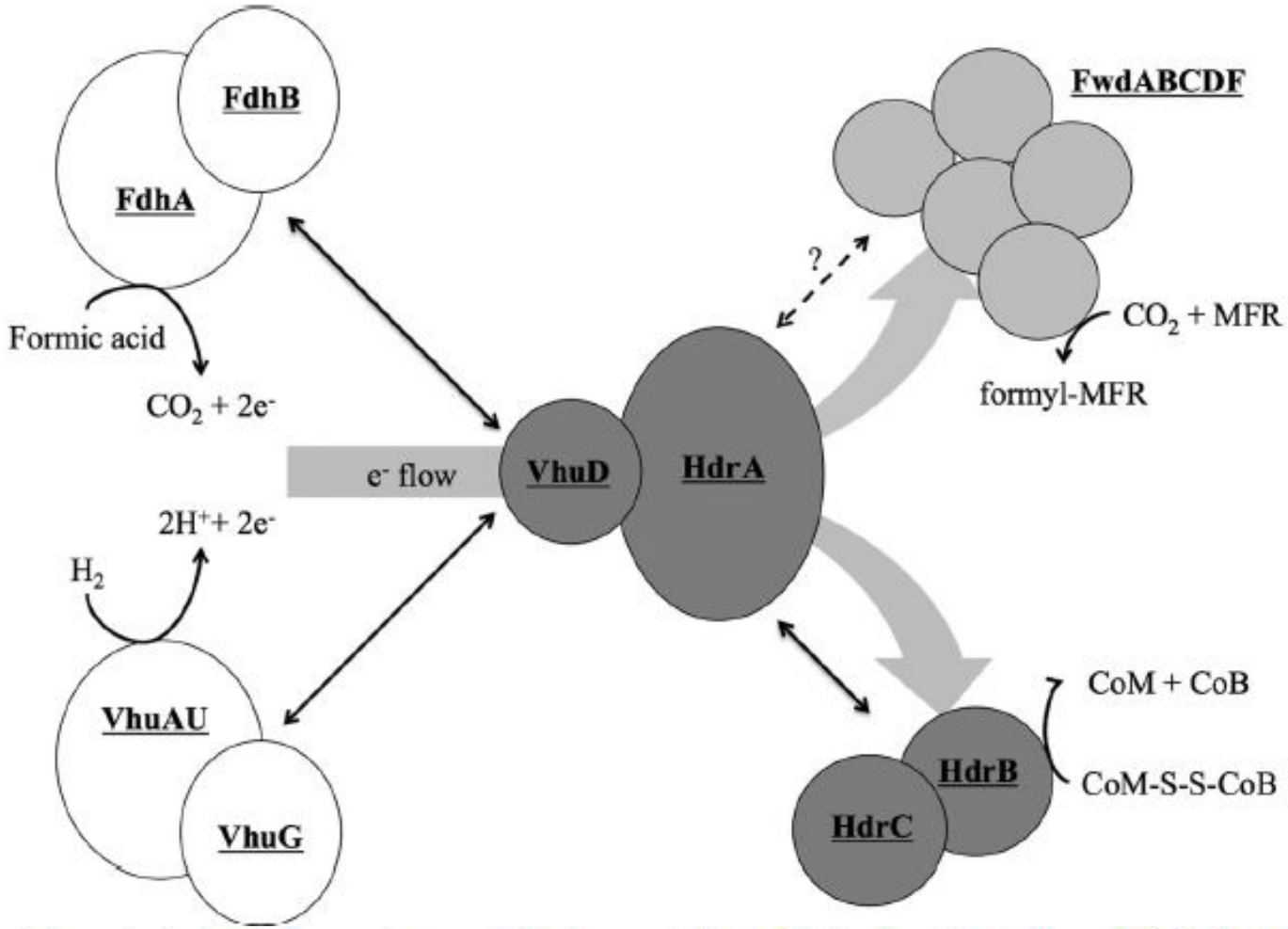

FIG 5 Protein interactions in the Hdr supercomplex. Formate dehydrogenase (FdhAB) and hydrogenase (VhuAGU) compete for binding to VhuD. VhuA and VhuU are drawn together, since they form the catalytic site of H_2 oxidation (30, 31). Electrons flow to HdrA, where their path is bifurcated to both FwdABCDF and HdrBC. Black double arrows indicate known interactions between subcomplexes. The dashed line between HdrA and Fwd signifies a hypothesized site of interaction between these subcomplexes. Reactions catalyzed by the individual enzymes are shown. The model only shows one of each enzyme, despite the fact that two of each are in the *M. maripaludis* genome (8). This reflects that, for the most part, the alternative forms are not expressed under the growth conditions used. HdrA, Vhu, and Fwd (as well as Fru) contain selenocysteine. *M. maripaludis* also encodes cysteine-containing versions, but these are repressed by selenium (19, 32). Additionally, Fwd contains tungsten, and its paralog, the molybdenum-containing formylmethanofuran dehydrogenase Fmd, requires high molybdenum for expression (33). In the case of Fdh, the genes for the alternative form of the enzyme are only expressed when cells are grown with limiting concentrations of formate in the absence of H_2 (20). Analysis of the *M. maripaludis* proteome verifies that only one form of these enzymes is highly expressed under our culture conditions (28, 34).

Costa et al., 2013(c)

Microbial formate utilization

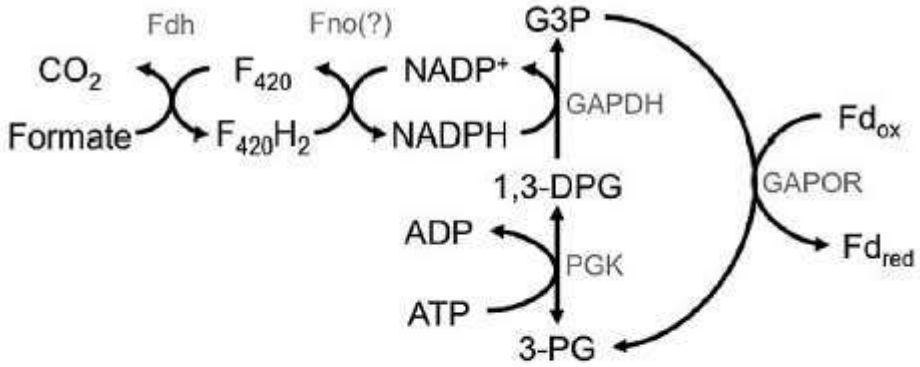

FIG 6 Glyceraldehyde-3-phosphate:ferredoxin oxidoreductase cycle for ATP-dependent ferredoxin reduction. The GAPOR cycle of *M. maripaludis* as originally described by Park et al. (29) is shown with potential input from $F_{420}H_2$. Fdh, formate dehydrogenase; Fno, $F_{420}H_2$:NADP$^+$ oxidoreductase; GAPDH, glyceraldehyde-3-phosphate dehydrogenase; GAPOR, glyceraldehyde-3-phosphate: ferredoxin oxidoreductase; PGK, phosphoglycerate kinase. G3P, glyceraldehyde-3-phosphate; 1,3-DPG, 1,3-diphosphoglycerate; 3-PG, 3-phosphoglycerate.

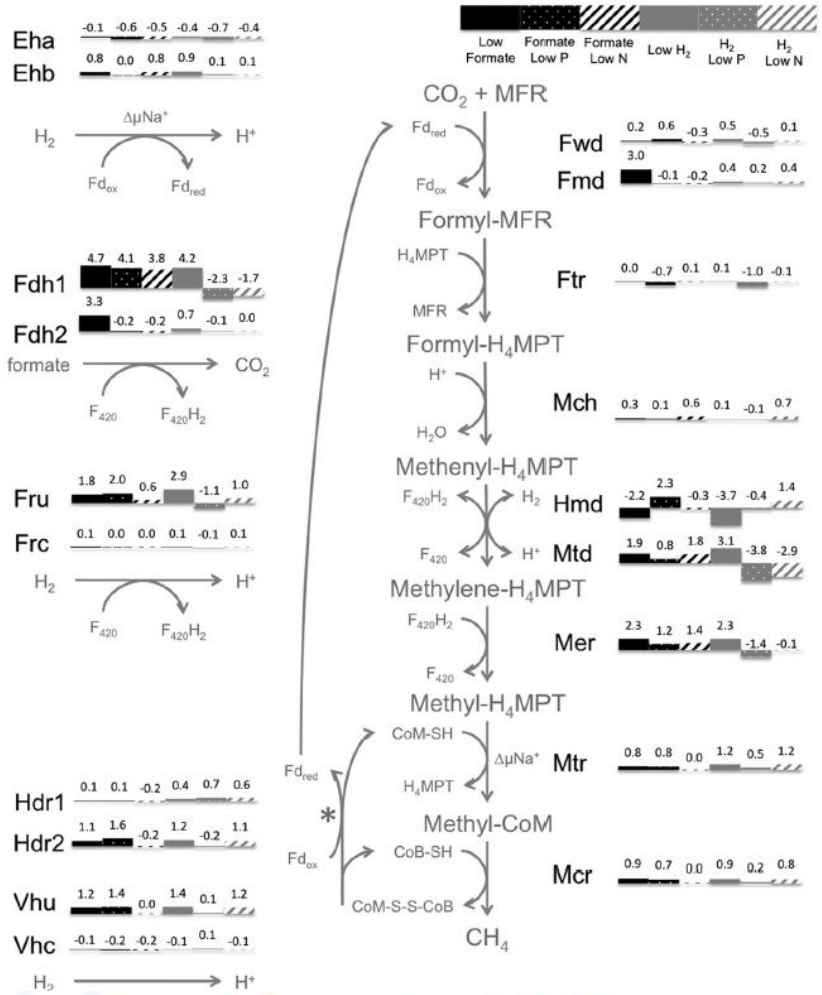

FIG 4 Expression of methanogenesis genes in response to nutrient limitations. Bars and numbers show $\log_2$ expression ratios relative to an arbitrary standard (23). Values are for genes encoding active-site enzymes (except *fdh*; see below). $\Delta\mu Na^+$, change in Na^+ across membrane; H_4MPT, tetrahydromethanopterin; MFR, methanofuran; CoM-SH, coenzyme M; CoB-SH, coenzyme B; CoM-S-S-CoB, heterodisulfide of CoM and CoB; $F_{420}/F_{420}H_2$, coenzyme F_{420}; Fd_{ox}/Fd_{red}, ferredoxin; Eha/Ehb, energy-converting hydrogenase A or B; Fdh, formate dehydrogenase; Ftr, formyltransferase; Fmd/Fwd, formylmethanofuran dehydrogenase; Fru/Frc, F_{420}-reducing hydrogenase; Hdr, heterodisulfide reductase; Hmd, H_2-dependent methylene-H_4MPT dehydrogenase; Mch, methenyl-H_4MPT cyclohydrolase; Mcr, methyl-CoM reductase; Mer, methylene-H_4MPT reductase; Mtd, F_{420}-dependent methylene-H_4MPT dehydrogenase; Mtr, methyl-H_4MPT:CoM methyltransferase; Vhu/Vhc, Hdr-associated hydrogenase. *, either H_2 or formate acts as the electron donor for the reaction. (Note: *fdhB* transcript abundance [MMP0139 and MMP1297] was used to assess *fdh* expression. There is a known artifact where portions of *fdhA2* [MMP0138] sometimes appear highly expressed under H_2 limitation in microarrays, most likely due to probe cross-hybridization with *fdhA1* [MMP1298] transcripts which share high [~73%] nucleotide identity [23]. However, both gene expression and protein abundance analyses have demonstrated that *fdhA2* is not differentially expressed between H_2 limitation and excess [8, 9]. Due to this documented ambiguity in determining *fdhA2* gene expression using microarray data, *fdhA* was ignored in our analysis in favor of *fdhB*.)

Costa et al., 2013(a,b)

Microbial formate utilization

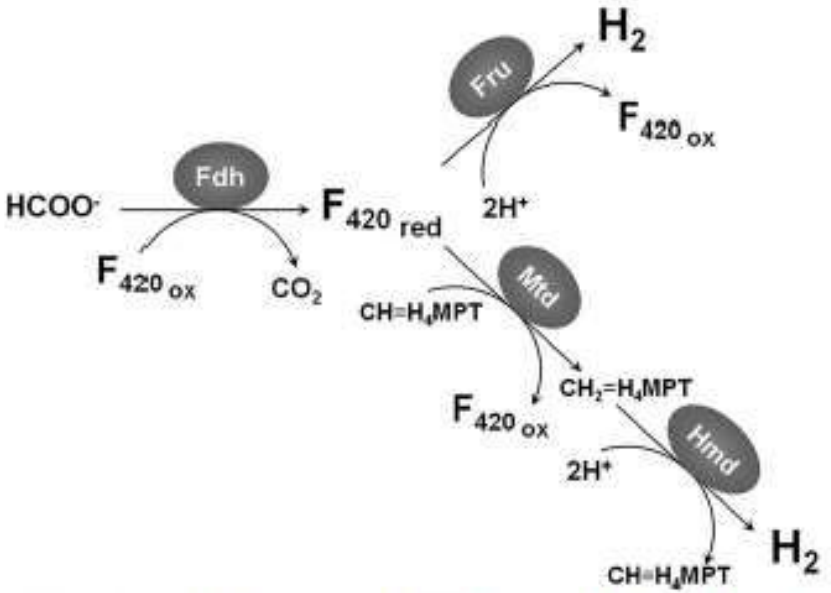

FIG. 1. Potential pathways of H_2 production in the hydrogenotrophic methanogens. The first pathway includes Fdh and Fru. In this pathway, Fdh reduces F_{420}. In selenium-grown cells, $F_{420}H_2$ is oxidized by the [Ni-Fe] hydrogenase Fru. In the second pathway, $F_{420}H_2$ is oxidized by Mtd to reduce methenyl-H_4MPT to methylene-H_4MPT, which is then reoxidized by Hmd, a Ni-free hydrogenase, to produce H_2. Abbreviations: Fdh, formate dehydrogenase; Fru, F_{420}-reducing hydrogenase; $F_{420\ ox}$, oxidized coenzyme F_{420}; $F_{420\ red}$, reduced coenzyme F_{420}; Mtd, F_{420}-dependent methylene-H_4MPT dehydrogenase; Hmd, H_2-forming methylene-H_4MPT dehydrogenase.

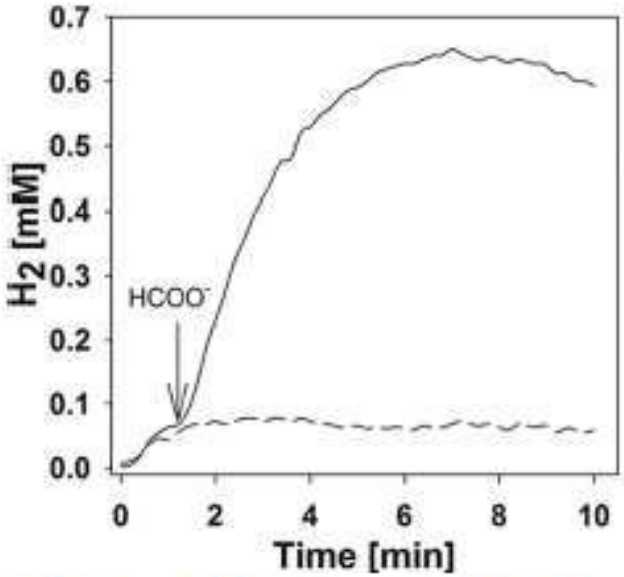

FIG. 2. Initial rates of H_2 production from formate (solid line) by resting cells of *M. maripaludis*. Cells were grown with formate, washed in buffer, and resuspended in the reaction cuvette. Assays were initiated by adding 20 mM sodium formate (arrow). Results from incubation of the cell suspension in the absence of formate is shown by the broken line.

Lupa et al., 2008

Microbial formate utilization

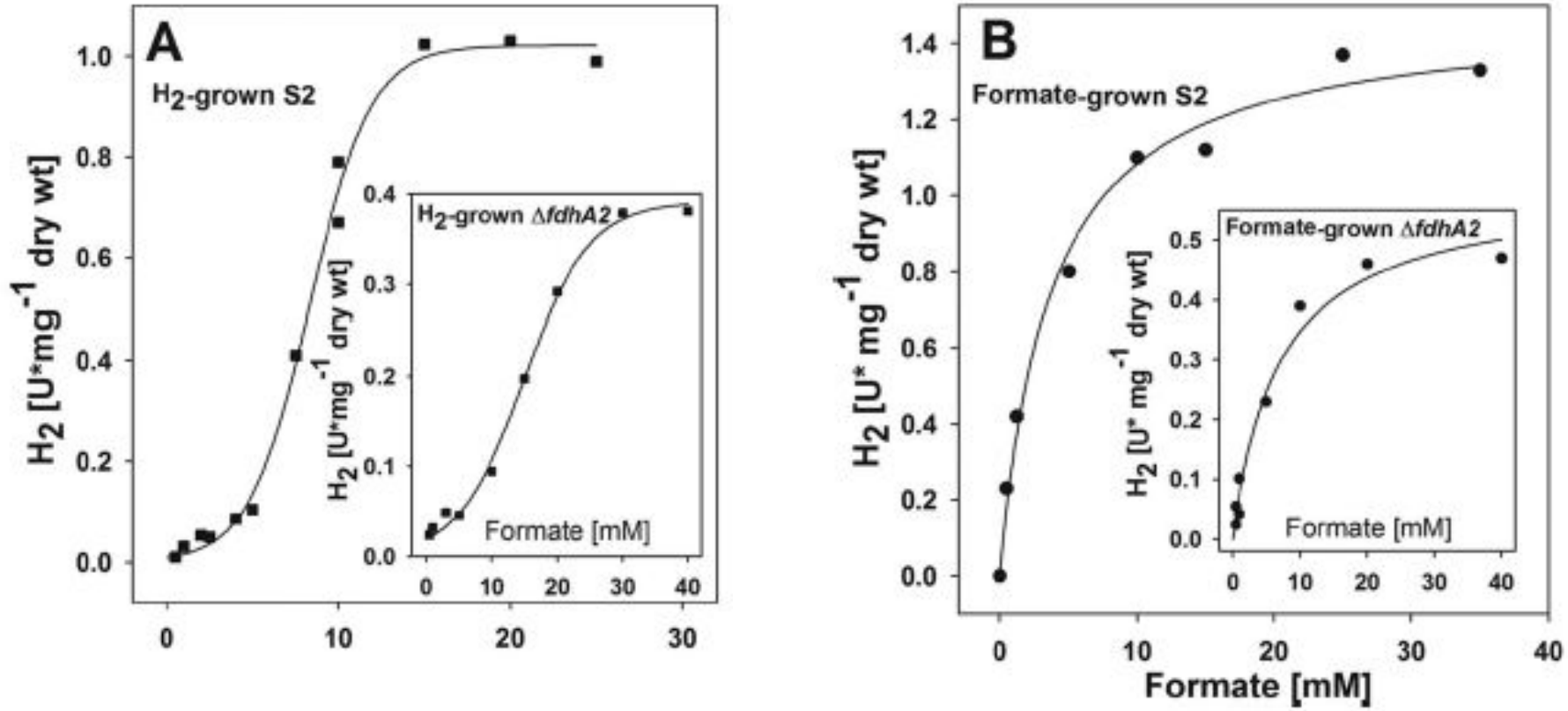

FIG. 5. Kinetics of formate-dependent H_2 production by resting cells of the wild-type strain S2 previously grown either with H_2 (A) or formate (B). The kinetics of the Δ*fdhA2* mutant are shown in the insets. The S2 and Δ*fdhA2* mutant strains were grown to absorbances of about 0.8 and 0.6, respectively.

Lupa et al. , 2008

Microbial formate utilization

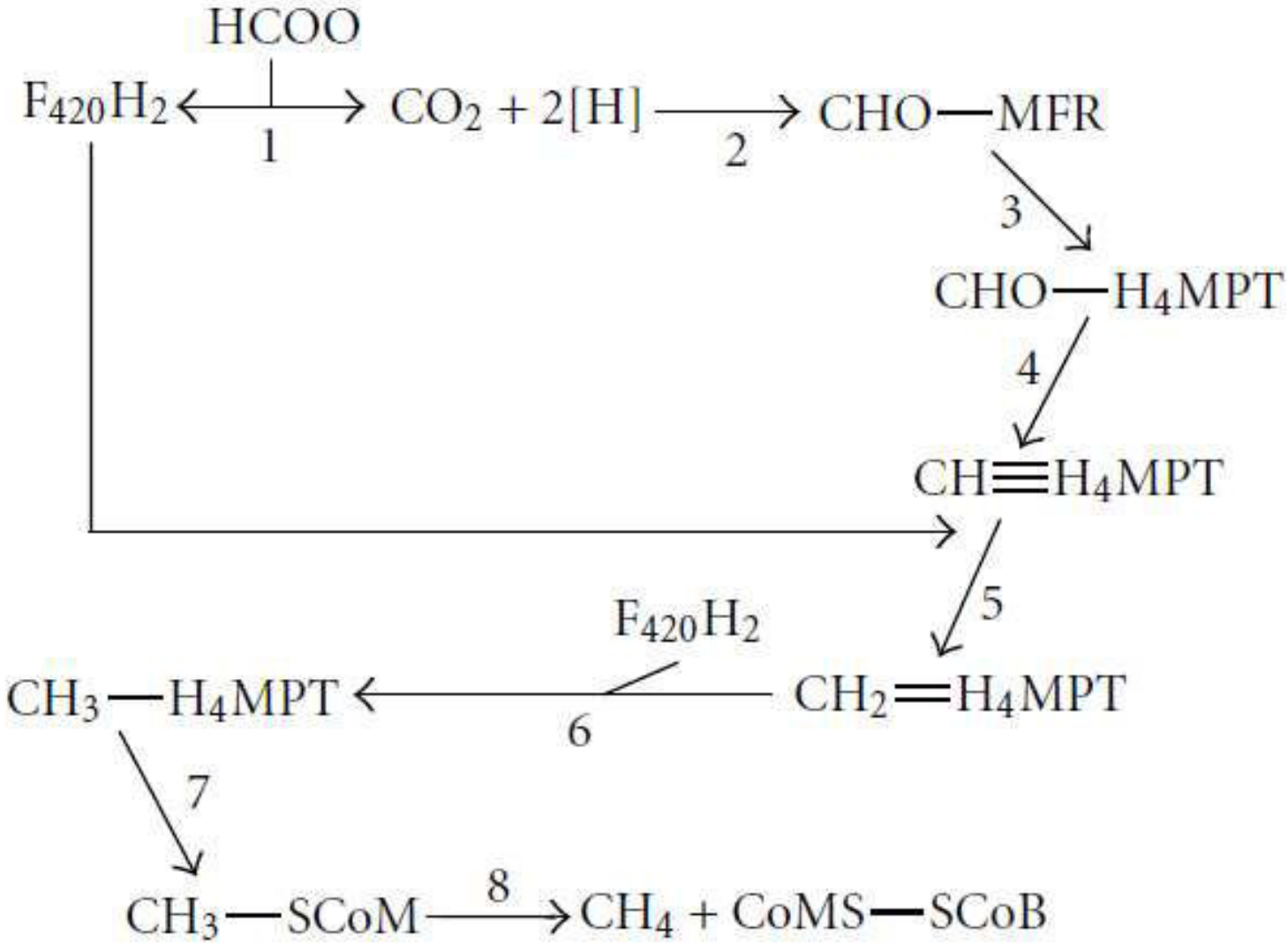

FIGURE 1: Pathway of hydrogenotrophic methanogenesis from formate. Abbreviations used: $HCOO^-$: formate; $F_{420}H_2$: reduced factor 420; MFR: methanofuran; H_4MPT: tetrahydromethanopterin; CoMS: CoEnzyme S; SCoB: CoEnzyme B. For details regarding enzymes and reactions please see accompanying text.

Crable et al. , 2011

C-cycle

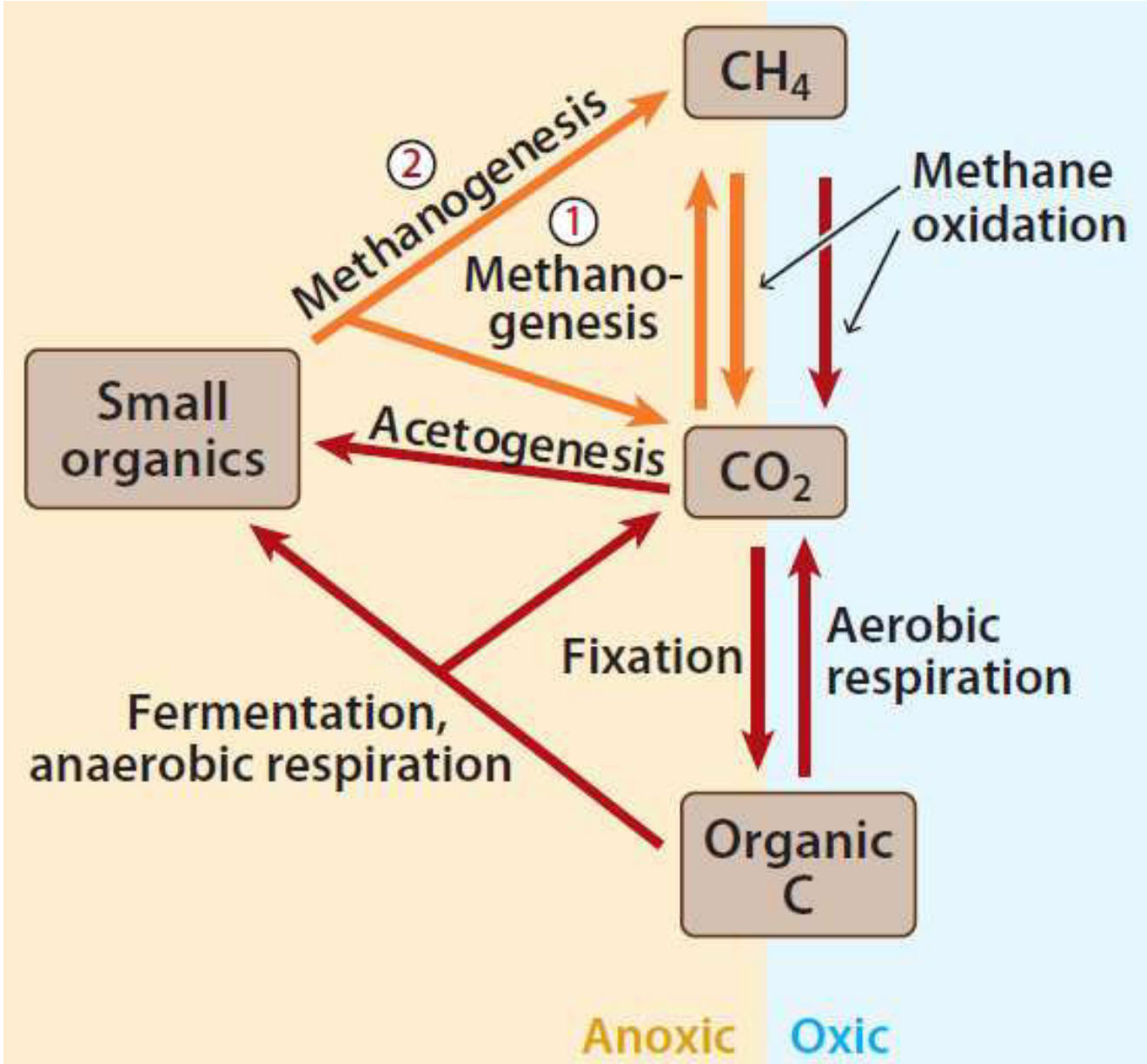

Red arrows: metabolic stepts related to archaea and bacteria; Organge arrows: exclusive metabolic routes only related to arcahea

Offre et al., 2014

Microbial methane oxidation

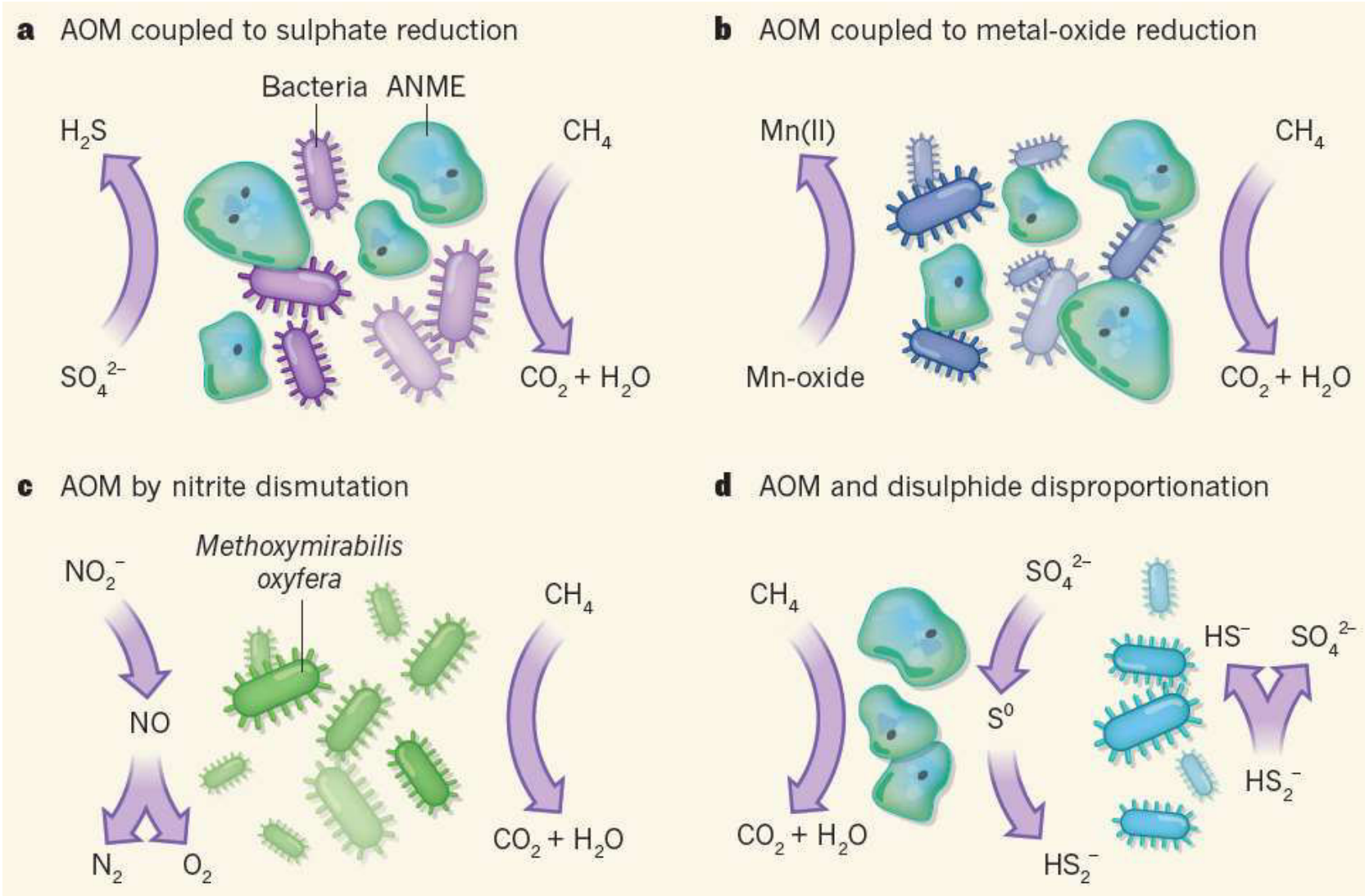

Modes of microbial anaerobic methane oxidation. There are four known ways in which microorganisms achieve anaerobic oxidation of methane (AOM). Two of these (**a**, **b**) are thought to rely on obligate associations between two or more microbial partners, one of which performs oxidation and the other reduction; in the other two cases (**c**, **d**), a single microorganism performs both reactions. **a**, **Anaerobic methanotrophic archaea (ANMEs)** oxidize methane (CH4) and convert it to carbon dioxide and water, in cooperation with sulphate-reducing bacteria, which convert sulphate (SO42−) to hydrogen sulphide (H2S). The mechanism of energy exchange between the ANMEs and the sulphate-reducing bacteria is unknown. **b**, The **oxidation of methane to CO2 by ANMEs is coupled to the reduction of metal oxides**, whereby metals such as manganese (Mn) or iron (Fe) are reduced to the +2 oxidation state. **c**, The bacterium ***Methoxymirabilis oxyfera*** converts nitrite (NO2−) to nitric oxide (NO) and then dismutates (splits) NO into nitrogen and oxygen as diatomic gases. The bacterium then uses the resulting O2 to support methane oxidation. **d**, Milucka *et al*. show that some **ANMEs oxidize methane** (as in **a**) but also reduce sulphate to zero-valent sulphur (S0), which they produce in the form of disulphide (HS2−). The disulphide can be used by associated bacteria, Deltaproteobacteria, to yield sulphide (HS−) and sulphate, but this is an association of convenience, rather than necessity.

Joye, 2012

Microbial methane oxidation

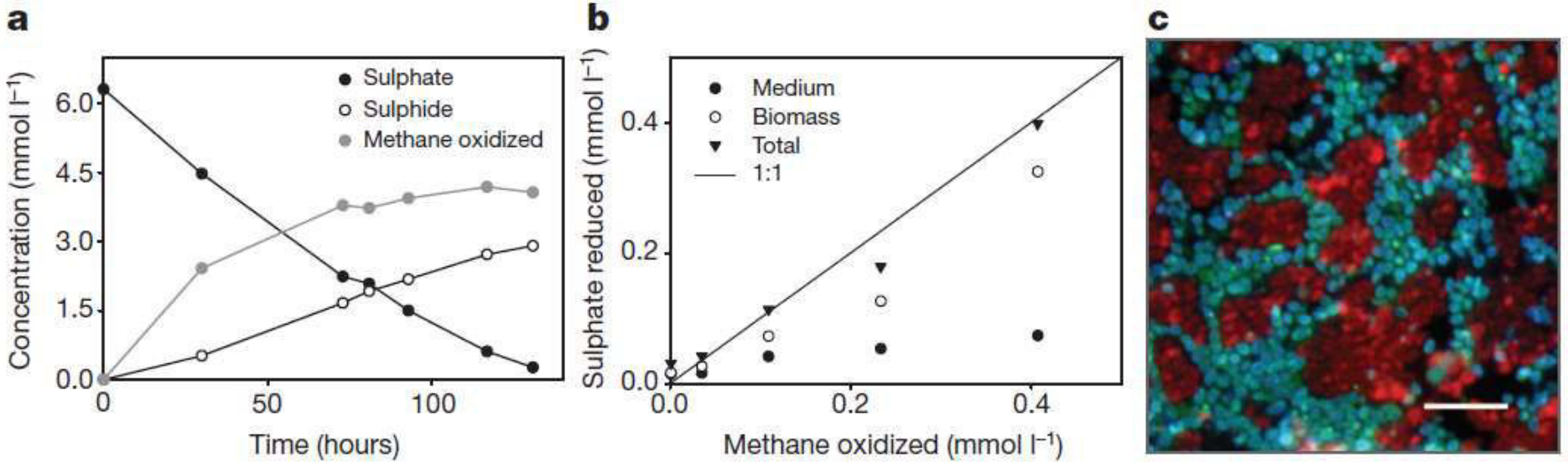

Figure 1 | Microbial activity and composition of the Isis enrichment culture. **a**, Anaerobic oxidation of methane determined from $^{13}CO_2$ production, decrease in sulphate concentration and increase in sulphide concentration versus time (hours) in incubations with added $^{13}CH_4$ ($n = 3$). **b**, Total sulphate-derived reduced sulphur species (a sum of reduced sulphur in medium and reduced sulphur in biomass) as determined from ^{35}S accumulation versus methane oxidation as determined from $^{14}CO_2$ production in incubations with added [^{35}S]sulphate and $^{14}CH_4$ during the first 11 h of a batch incubation ($n = 1$; this experiment was repeated twice). **c**, AOM aggregate labelled with anti-Sat (ATP sulphurylase, green), anti-Dsr (dissimilatory sulphite reductase, blue) and anti-Mcr (methyl-CoM reductase, red) antibodies. Mcr is localized in the larger, irregularly shaped ANME-2 (red), whereas Sat and Dsr co-localize in the rod-shaped DSS bacteria (turquoise). Scale bar, 5 μm.

$$CH_{4(aq)} + SO_4^{2-} \rightarrow HS^- + HCO_3^- + H_2O \quad \Delta G = -34\ \text{kJ mol}^{-1}\ CH_4$$

Milucka et al., 2008

Microbial methane oxidation

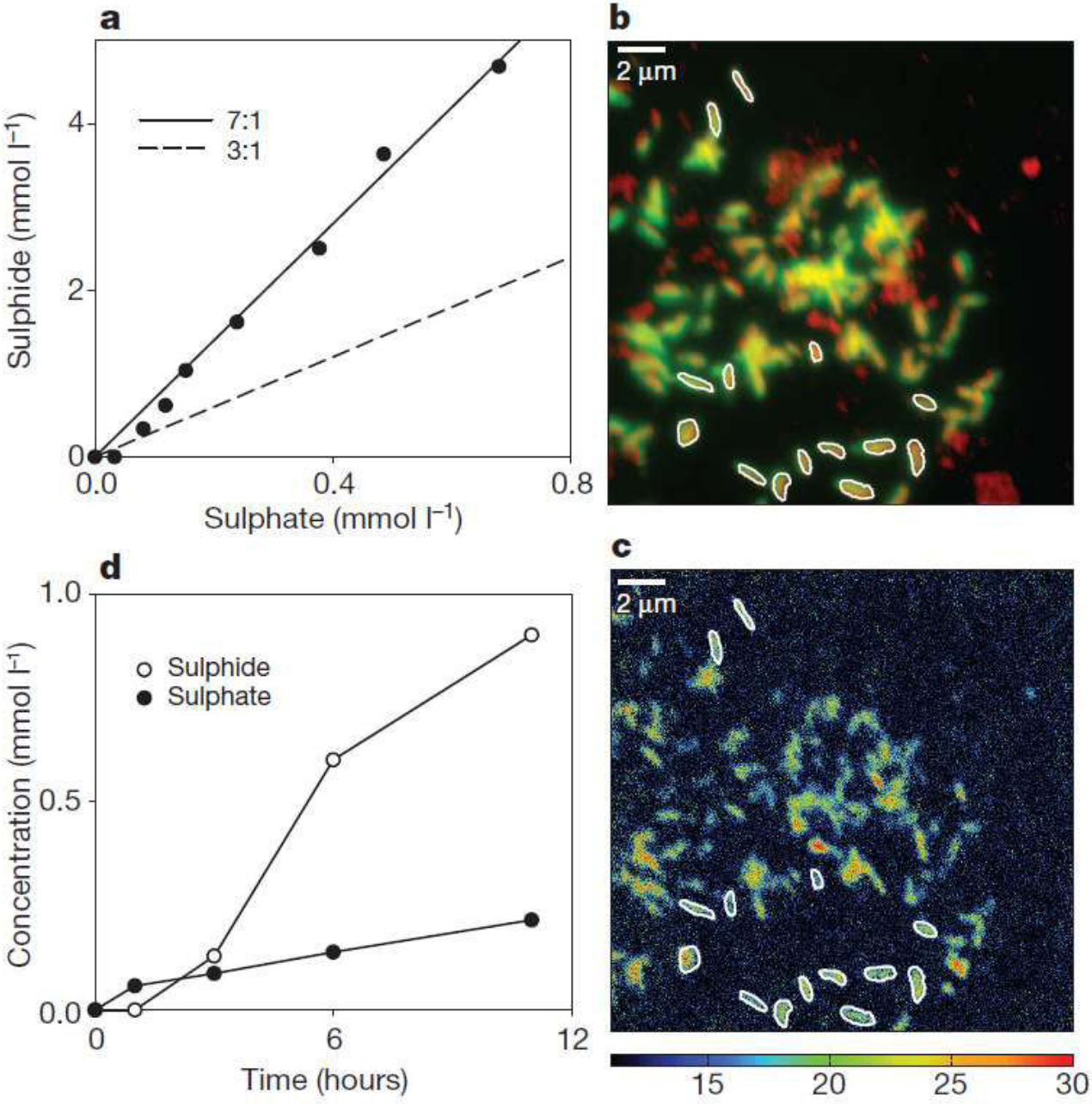

Disulphide disproportionation by Isis enrichment culture.

a, Linear correlation between sulphate and sulphide production in the Isis enrichment culture incubated with $13CO_2$ and colloidal sulphur in the absence of methane over the course of 70 days (n=51) follows the 7:1 ratio inferred for disulphide disproportionation.

b, Overlay of nanoSIMS12C14Nimage (red) and fluorescence image of microorganisms from the enrichment culture stained with the DSS-658 probe (green).

c, The 13C/12C image shows that the DSS cells (several of which are shown by white outlines) are enriched in 13C. Coloured scale below panel c shows ratio of the respective ions.

d, Production of sulphide and sulphate (based on 35S accumulation in sulphate after the addition of 35Ssulphide) under AOM conditions (n=51; this experiment was repeated twice).

$$4HS_2^- + 4H_2O \rightarrow SO_4^{2-} + 7HS^- + 5H^+$$

$$\Delta G = -12.7\ \text{kJ mol}^{-1}\ HS_2^-$$

Milucka et al., 2008

Microbial methane oxidation

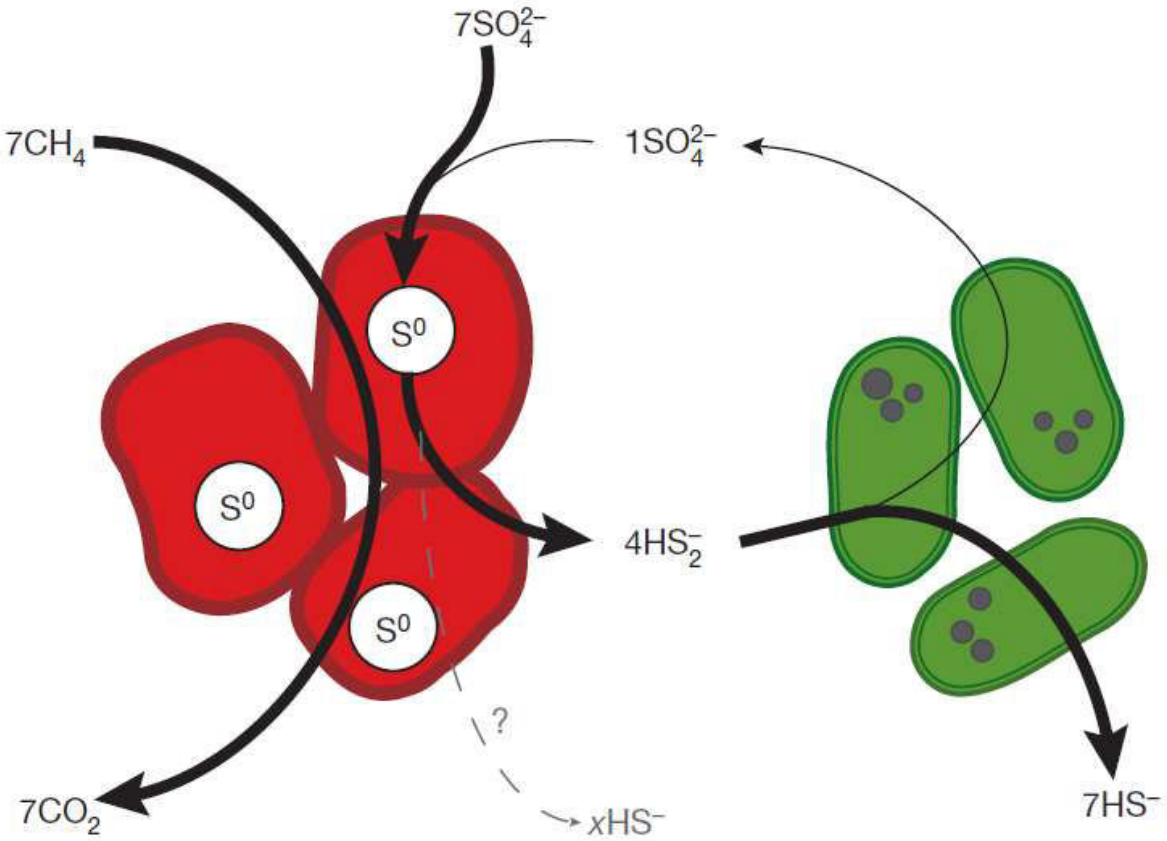

Revised model of anaerobic oxidation of methane coupled to sulphate reduction.

ANME-2 oxidize methane with a concomitant reduction of sulphate to zero-valent sulphur (S0, elemental sulphur) that is partially deposited or bound intracellularly. Produced S0 is exported or diffuses outside the cell where it reacts with sulphide to form polysulphides (disulphide, among others).

Disulphide is taken up by the associated **Deltaproteobacteria** and is disproportionated to sulphate and sulphide. Sulphate produced during disproportionation might be re-used by the **ANME** and the **ANME** may also reduce some of the sulphate all the way to sulphide (grey dotted line). Dark circles in the bacteria represent intracellular precipitates rich in iron and phosphorus.

$$4HS_2^- + 4H_2O \rightarrow SO_4^{2-} + 7HS^- + 5H^+ \quad \Delta G = -12.7\ \text{kJ mol}^{-1}\ HS_2^-$$

$$7CH_{4(aq)} + 8SO_4^{2-} + 5H^+ \rightarrow 4HS_2^- + 7HCO_3^- + 11H_2O$$
$$\Delta G = -26.5\ \text{kJ mol}^{-1}\ CH_4$$

Milucka et al., 2008

Microbial methane oxidation

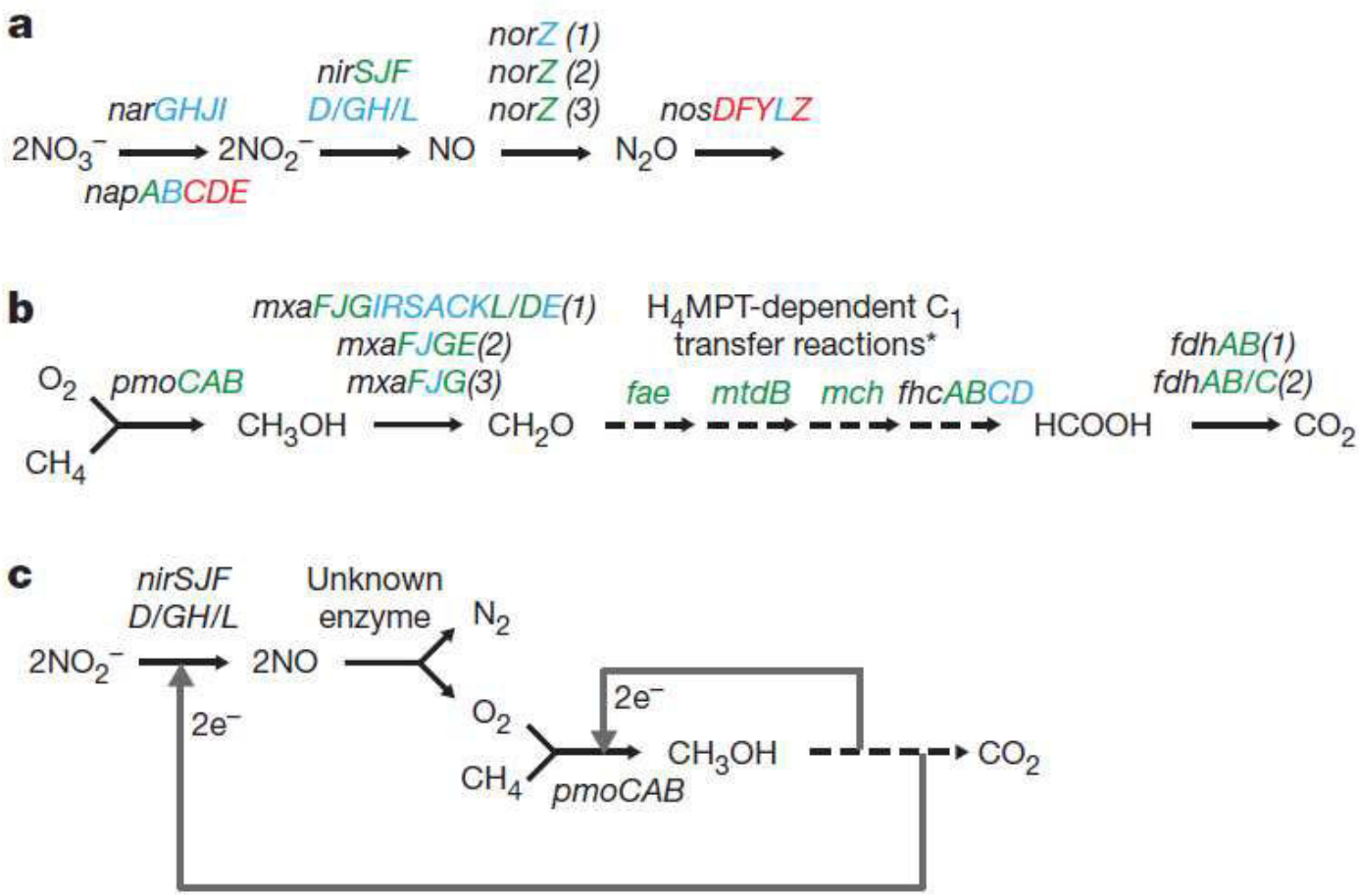

Significant pathways of *Methylomirabilis oxyfera*.
Canonical pathways of denitrification (a), aerobic methane oxidation (b) and proposed pathway of methane oxidation with nitrite (c).

narGHJI, nitrate reductase; napABCDE, periplasmic nitrate reductase; nirSJFD/GH/L, nitrite reductase; norZ, nitric oxide reductase; nosDFYLZ, nitrous oxide reductase; pmoCAB, particulate methane monooxygenase; mxaFJGIRSACKL/DE, methanol dehydrogenase; fae, formaldehyde-activating enzyme; mtdB, methylenetetrahydromethanopterin (H4MPT) dehydrogenase; mch, methenyl-H4MPT cyclohydrolase; fhcABCD, formyltransferase/hydrolase; fdhABC, formate dehydrogenase.

Genes in **red are absent from the genome**, those in **blue are present in the genome** and those **genes in green are present in both the proteome and the genome**.
Asterisk, H4MPT-dependent reactions involve the intermediates methylene H4MPT, methenyl-H4MPT and formyl-H4MPT.

$$3CH_4 + 8NO_2^- + 8H^+ = 3CO_2 + 4N_2 + 10H_2O$$

$$(\Delta G^{\circ\prime} = -928\,\mathrm{kJ\,mol^{-1}}\ CH_4)$$

Ettwig et al. , 2010

Microbial methane oxidation

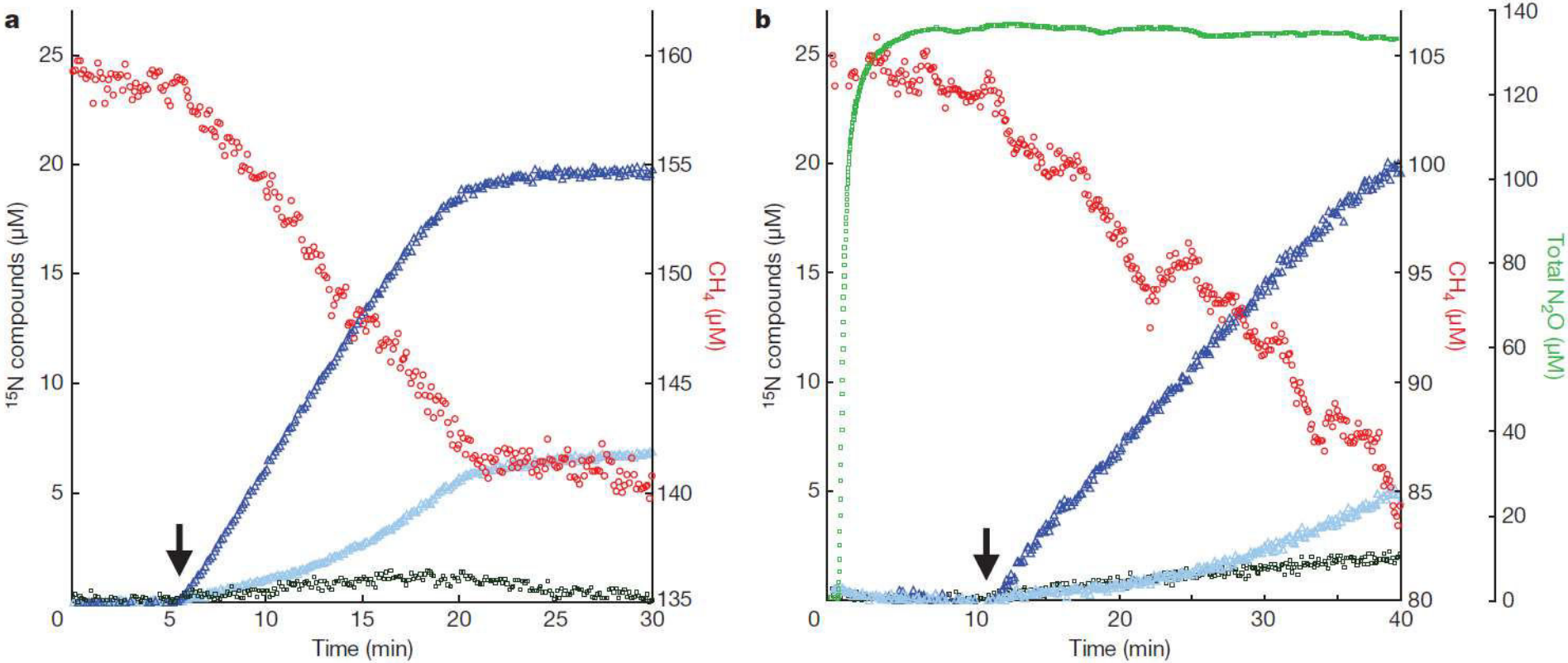

Figure 3 | Coupling of methane oxidation and nitrite reduction in enrichment cultures of '*Methylomirabilis oxyfera*'. Methane is oxidized only after addition of ^{15}N-labelled nitrite (50 μM, arrow), which is converted to ^{15}N-labelled dinitrogen gas in the presence of about 2,000 μM ^{14}N-nitrate (**a**) or 2,000 μM ^{14}N-nitrate and 135 μM ^{14}N-N_2O (**b**). Experiments were performed with 380 ml of anoxic, stirred enrichment culture 'Ooij' (protein content 147 ± 11 mg). Red circles, CH_4; dark blue triangles, $^{15,15}N_2$; light blue triangles, $^{15,14}N_2$; green squares, total N_2O; dark green squares, $^{14,15}N_2O$ and $^{15,15}N_2O$.

Ettwig et al. , 2010

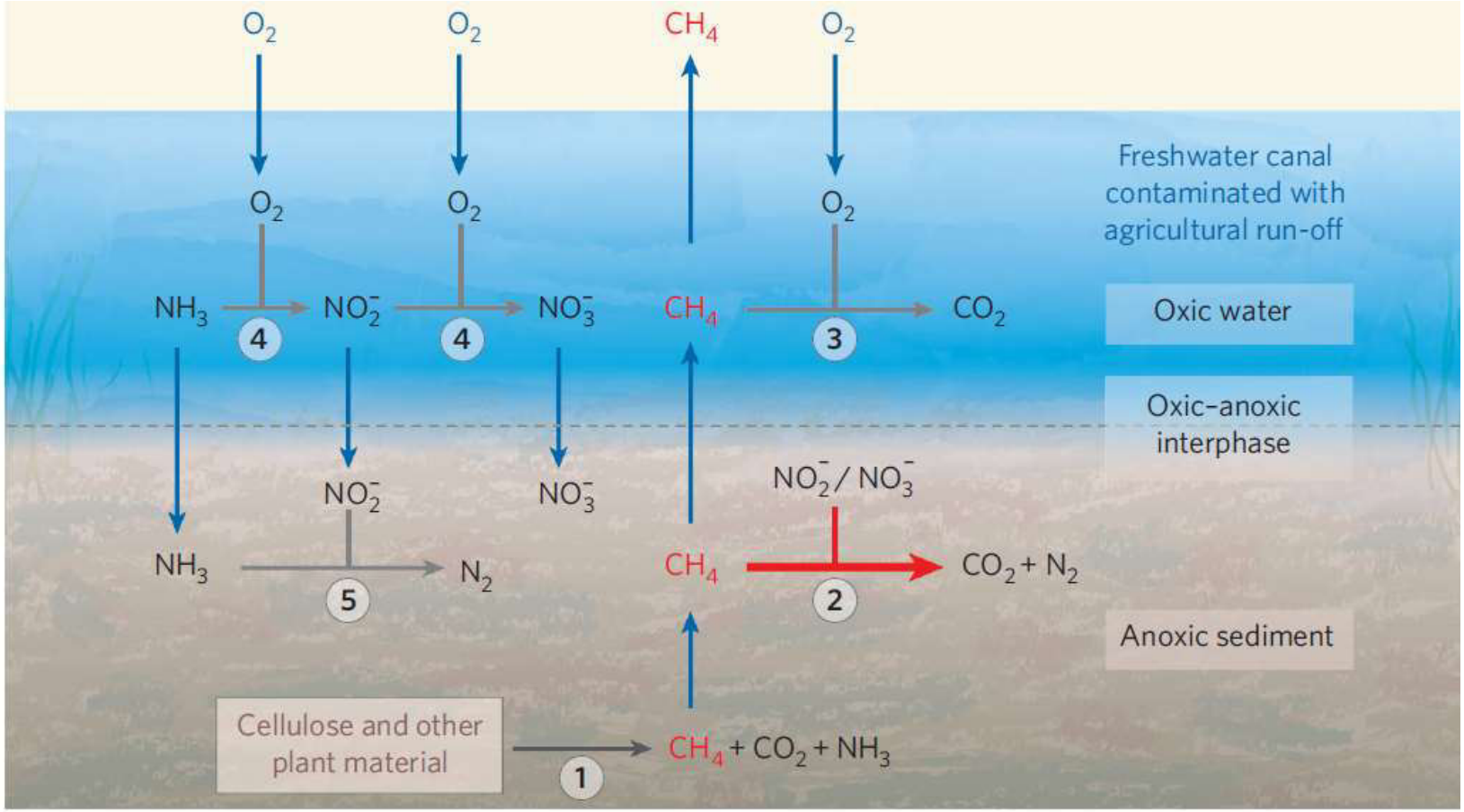

Figure 2 | Nitrate-dependent anaerobic oxidation of methane[1] and related processes. Methane oxidation is coupled to denitrification (NO_3^- and NO_2^- reduction to N_2) in fresh water that receives agricultural run-off and so contains high concentrations of ammonia (NH_3), nitrate (NO_3^-) and nitrite (NO_2^-). The sediment is anoxic and is saturated with methane. The blue arrows indicate transport by diffusion. The different processes (grey and red arrows) are mediated by different microorganisms. **1**, Anaerobic bacteria, protozoa and methane-producing archaea. **2**, Archaea related to methane-producing archaea and bacteria belonging to a new phylum (reaction 1 in Fig. 1)[1]. **3**, Methane-consuming bacteria. **4**, Nitrifying bacteria. **5**, Planctomycete bacteria.

Thauer and Shima, 2006

Microbial methane oxidation

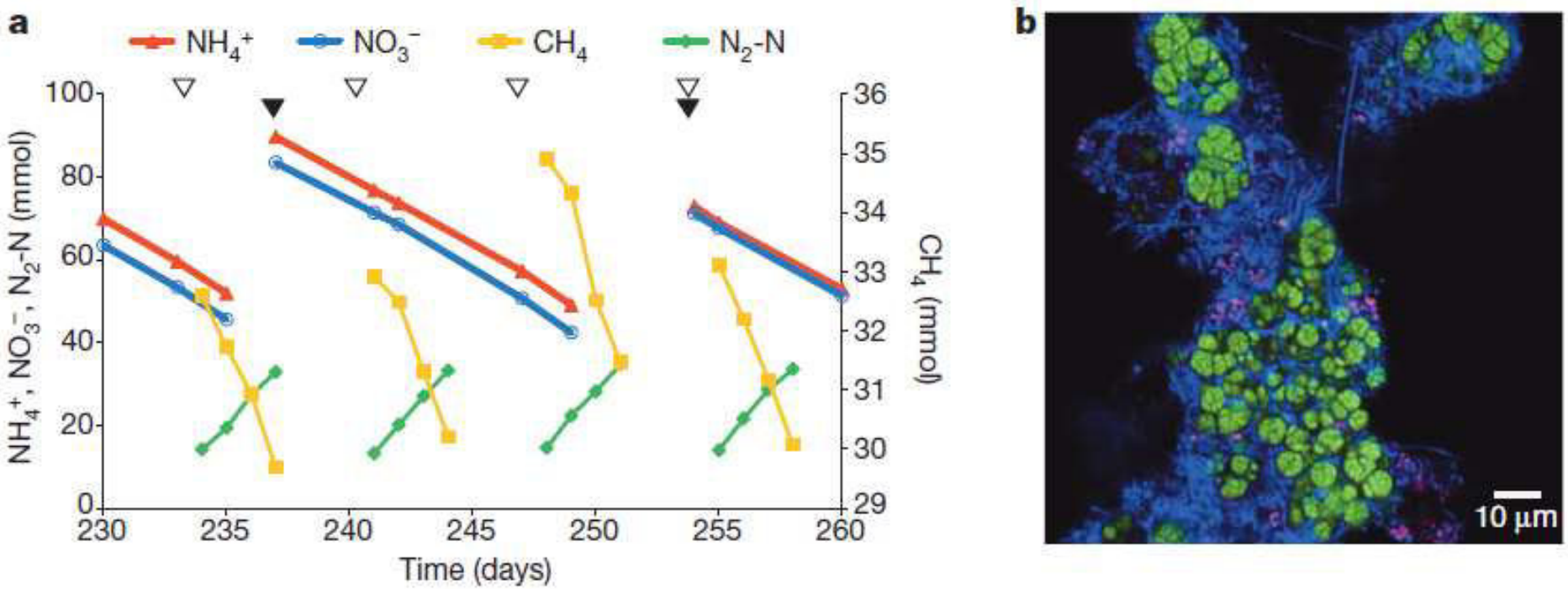

Figure 1 | Bioreactor performance data and microbial community composition. **a**, Key bioreactor performance data during steady-state operation from day 230 to 260 after inoculation. The arrows indicate pulse-feeding events of nitrate and ammonium (black), and methane (white). Nitrate, ammonium and methane consumption, and dinitrogen gas production, can be observed. The concentration of nitrite was negligible throughout the experiment. **b**, Fluorescence *in situ* hybridization micrograph of the bioreactor community showing the dominant '*M. nitroreducens*' population in large, dense clusters (green), smaller flanking *Kuenenia* cells (magenta) and other bacteria (blue).

Haroon et al. , 2013

Microbial methane oxidation

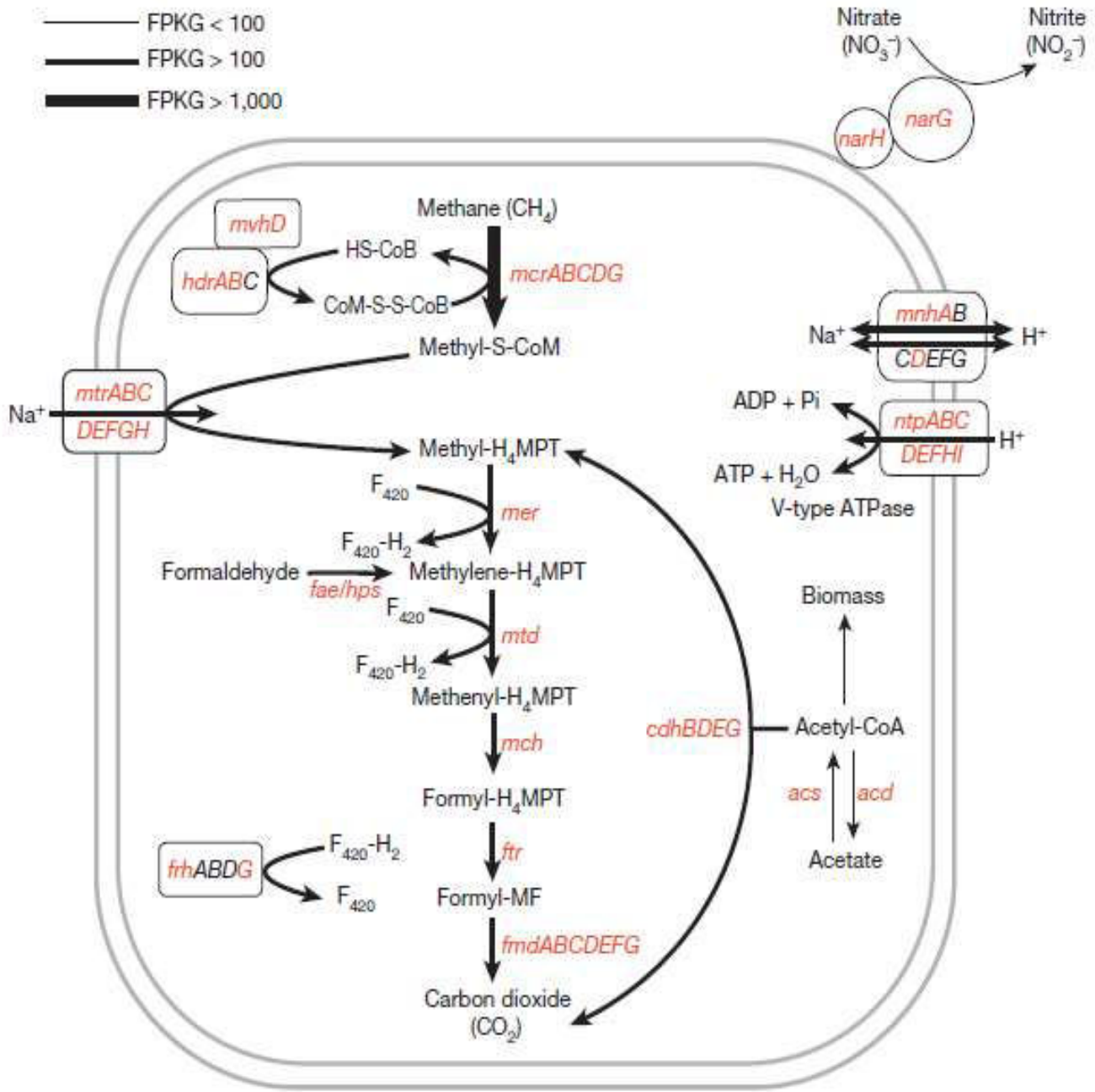

Key carbon and nitrogen transformations in 'Methanoperedens nitroreducens'.
Reverse methanogenesis pathway in *Ca.* 'M. nitroreducens' coupled by an unknown electron carrier to nitrate reduction. Highly expressed genes are shown in red, indicating that the complete reverse methanogenesis pathway and nitrate reduction genes were active in the bioreactor. Increasing line thickness indicates increasing absolute gene expression values. FPKG (fragments mapped per kilobase of gene length) is a measure of normalized gene expression.

Haroon et al. , 2013

universität wien

Microbial methane oxidation

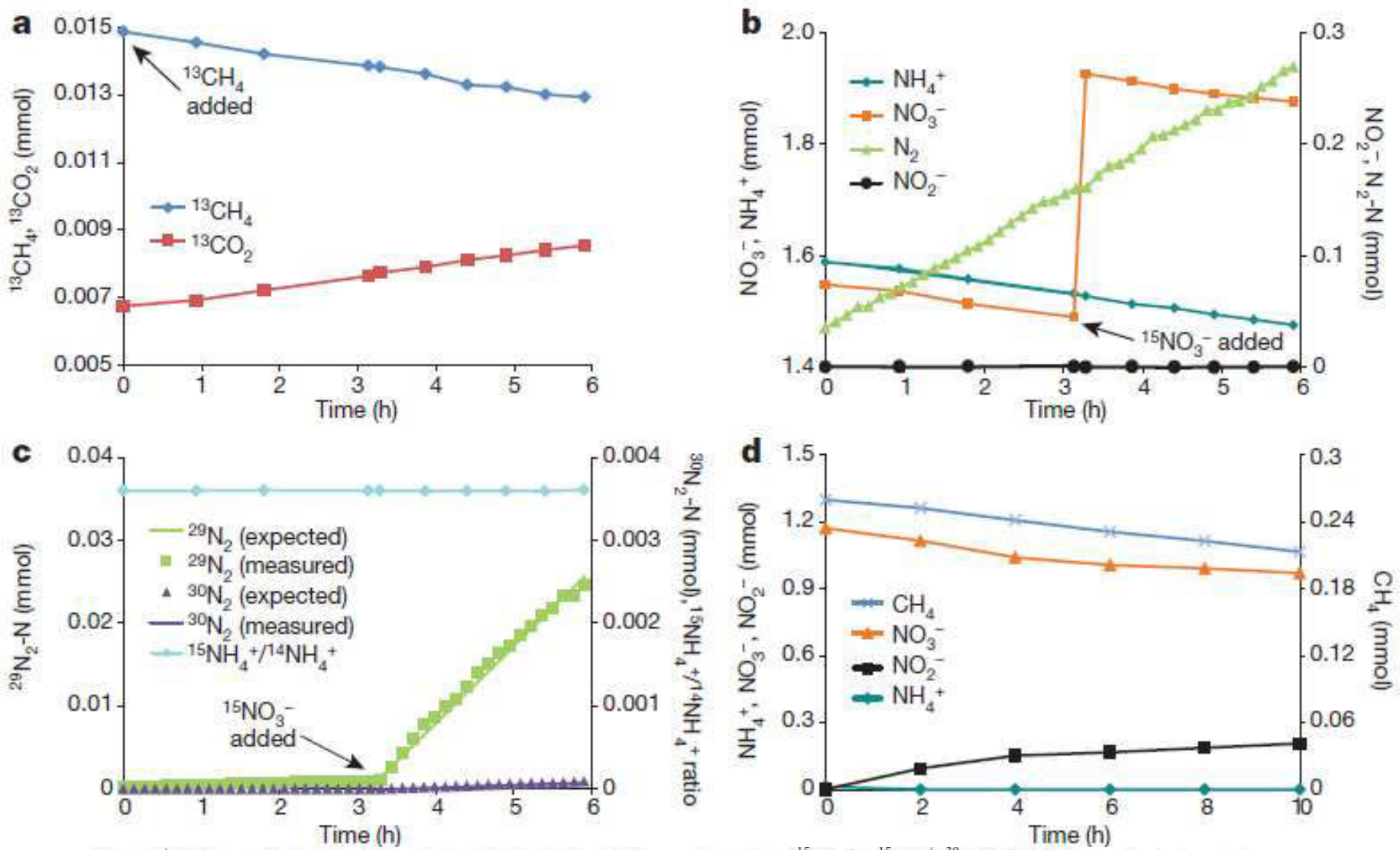

Figure 3 | Methane oxidation coupled to nitrate reduction in the AOM bioreactor. **a**, **b**, Data from isotope labelling batch test demonstrating stoichiometrically balanced conversion of $^{13}CH_4$ to $^{13}CO_2$ (**a**), and NO_3^- and NH_4^+ to N_2 without accumulation of NO_2^- (**b**). **c**, Experimentally measured production of $^{29}N_2$ and $^{30}N_2$ matching predictions (green and purple lines, respectively) based on assumed reactions (see details in Methods). The ratios between $^{15}NH_4^+$ and $^{14}NH_4^+$ are shown to confirm that there was no conversion of $^{15}NO_3^-$ to $^{15}NH_4^+$. ^{30}N-labelled dinitrogen gas also increased as predicted, albeit to a much smaller extent, owing to reaction between $^{15}NO_2^-$ and naturally present $^{15}NH_4^+$. The ratios between $^{15}NO_3^-$ and $^{14}NO_3^-$ in the system before and after $^{15}NO_3^-$ addition were stable (data not shown). **d**, Batch test showing the accumulation of nitrite as a result of nitrate reduction when ammonium was removed from the feed.

Haroon et al. , 2013

Microbial methane oxidation

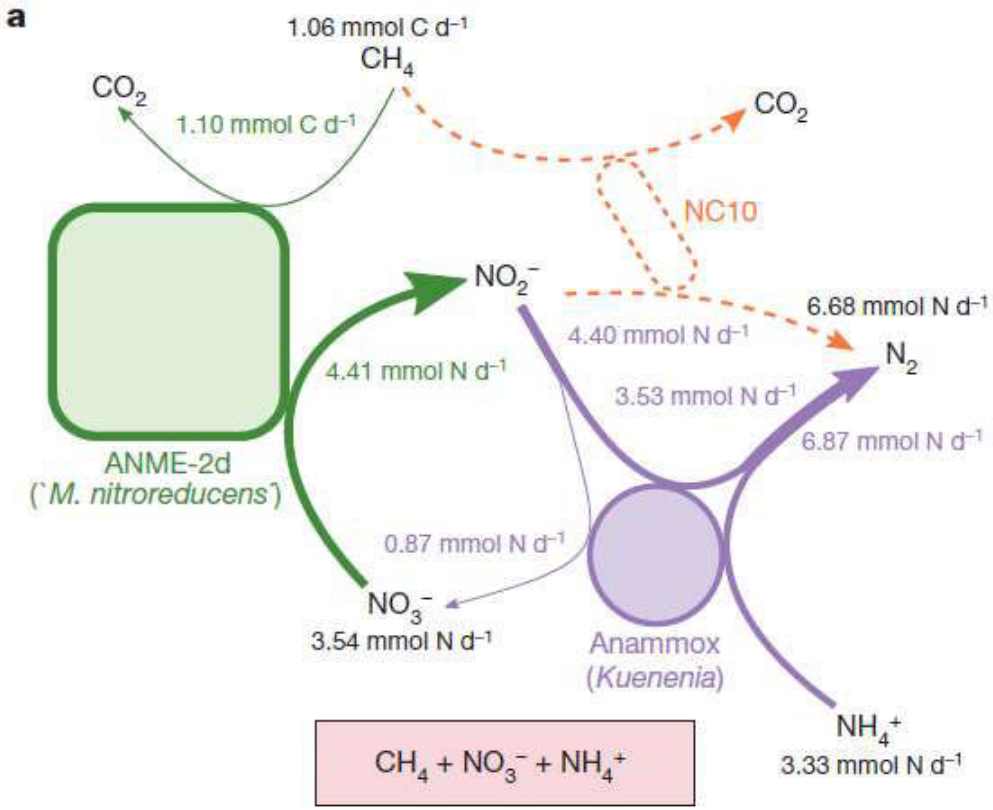

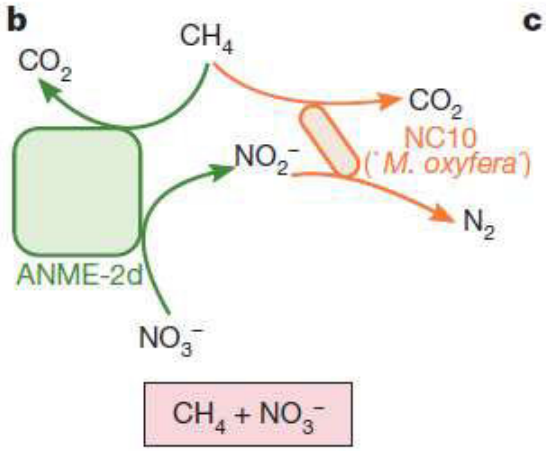

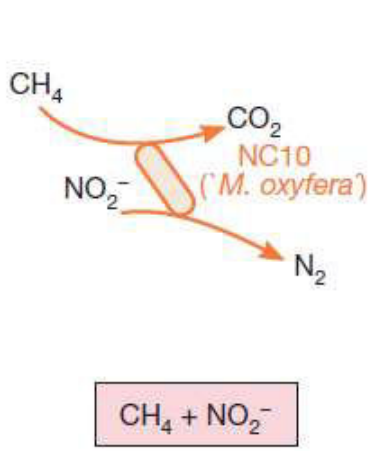

Figure 4 | Observed interactions between key populations in methane-fed bioreactors with differing nitrogen sources. Each population and its associated metabolic activities are colour-coded. **a**, Interactions under methane, nitrate and ammonium conditions in the current study. The thicknesses of arrows indicate reaction flux rates, and dashed arrows represent interactions not occurring under the given conditions (see Supplementary Table 10 for mass balance calculations). The methane consumption (1.10 mmol C d^{-1}) and dinitrogen gas production (6.87 mmol N d^{-1}) rates predicted based on measured ammonium, nitrate and nitrite data closely match their measured rates (1.06 mmol C d^{-1} and 6.68 mmol N d^{-1}) with only 3.8% and 2.8% errors, respectively. Mass and electron balance and molecular data further indicate that all of the methane consumed was used for reduction of nitrate to nitrite by '*M. nitroreducens*', and all of the produced nitrite (4.41 mmol N d^{-1}) was consumed by *Kuenenia* (4.40 mmol N d^{-1}). The outcompeted NC10 population is showed in dashed lines with no shading. **b**, Interactions in a bioreactor fed with methane and nitrate resulting in a co-culture of ANME-2d and '*M. oxyfera*'[4,5,14]. **c**, Interactions in a bioreactor fed with methane and nitrite resulting in a dominant '*M. oxyfera*' population[3,14].

$$CH_4 + 4NO_3^- \rightarrow 4NO_2^- + 2H_2O$$

$$(\Delta G^o = -503\,kJ\,mol^{-1}\,CH_4)$$

Haroon et al. , 2013